DISSERTATION

GREEN COMMUNICATION AND SECURITY IN WIRELESS NETWORKS BASED ON MARKOV DECISION PROCESS AND SEMIVARIANCE OPTIMIZATION

Submitted by

Fateh Elsherif

Department of Electrical and Computer Engineering

In partial fulfillment of the requirements

For the Degree of Doctor of Philosophy

Colorado State University

Fort Collins, Colorado

Summer 2020

Doctoral Committee:

Advisor: Edwin K.P. Chong

Anura P. Jayasumana
J. Rockey Luo
Rebecca Atadero

ABSTRACT

GREEN COMMUNICATION AND SECURITY IN WIRELESS NETWORKS BASED ON MARKOV DECISION PROCESS AND SEMIVARIANCE OPTIMIZATION

Wireless networking has become an integral part of our everyday life. Certainly, wireless technologies have improved many aspects of the way people communicate, interact, and perform tasks, in addition to enabling new use cases, such as massive machine-type communications and industry verticals, among others. While convenient, these technologies impose new challenges and introduce new design problems. In this dissertation, we consider three problems in wireless networking. Specifically, we formulate optimization problems in green communication and security, and develop computationally efficient solutions to these optimization problems.

First, we study the problem of base station (BS) dynamic switching for energy efficient design of fifth generation (5G) cellular networks and beyond. We formulate this problem as a Markov decision process (MDP) and use an approximation method known as policy rollout to solve it. This method employs Monte Carlo sampling to approximate the Q-value. In this work, we introduce a novel approach to design an energy-efficient algorithm based on MDP to control the ON/OFF switching of BSs; we exploit user mobility and location information in the selection of the optimal control actions. We start our formulation with the simple case of one-user one-ON. We then gradually and systematically extend this formulation to the multi-user multi-ON scenario. Simulation results show the potential of our novel approach of exploiting user mobility information within the MDP framework to achieve significant energy savings while providing quality-of-service guarantees.

Second, we study the problem of jamming-aware-multi-path routing in wireless networks. Multipath routing is a technique for transmitting data from one or more source node(s) to one or more destination node(s) over multiple routing paths. We study the problem of wireless jamming-

mitigation multipath routing. To address this problem, we propose a new framework for mitigating jamming risk based on semivariance optimization. Semivariance is a mathematical quantity used originally in finance and economics to measure the dispersion of a portfolio return below a risk-aversion benchmark. We map the problem of jamming-mitigation multipath routing to that of portfolio selection within the semivariance risk framework. Then we use this framework to design a new, and computationally feasible, RF-jamming mitigation algorithm. We use simulation to study the properties of our method and demonstrate its efficacy relative to a competing scheme that optimizes the jamming risk in terms of variance instead of semivariance. To the best of our knowledge, our work is the first to use semivariance as a measure of jamming risk. Directly optimizing objective functions that involve exact semivariance introduces certain computational issues. However, there are approximations to the semivariance that overcome these issues. We study semivariance problems—from the literature of finance and economics—and survey their solutions. Based on one of these solutions, we develop an efficient algorithm for solving semivariance optimization problems. Efficiency is imperative for many telecommunication applications such as tactile Internet and Internet of Things (recall that these types of applications have stringent constraints on latency and computing power). Our algorithm provides a general approach to solving semivariance optimization problems, and can be used in other applications.

Last, we consider the problem of multiple–radio-access technology (multi-RAT) connectivity in heterogeneous networks (HetNets). Recently, multi-RAT connectivity has received significant attention—both from industry and academia—because of its potential as a method to increase throughput, to enhance communication reliability, and to minimize communication latency. We introduce a new approach to the problem of multi-RAT traffic allocation in HetNets. We propose a new risk-averse multi-RAT connectivity (RAM) algorithm. Our RAM algorithm allows trading off expected throughput for risk measured in throughput semivariance. Here we also adopt semivariance as a measure of throughput dispersion below a risk-aversion–throughput benchmark. We then formulate the multi-RAT connectivity problem as a semivariance-optimization problem. However, we tackle a different optimization problem in this part of the research. The objective function of the

optimization problem considered here is different from the objective function of the optimization problem above that also uses semivariance to quantify risk (because the underlying standard form of portfolio selection is different). In addition, the set of constraints is different in this optimization problem: We introduce new capacity constraints to account for the stochastic capacity of the involved wireless links. We also introduce a new performance metric, the risk-adjusted throughput; risk-adjusted throughput is the ratio between the expected throughput and the throughput semideviation, where semideviation is the square root of semivariance. We evaluate the performance of our algorithm through simulation of a system with three radio-access technologies: 4G LTE, 5G NR, and WiFi. Simulation results show the potential gains of using our algorithm.

ACKNOWLEDGEMENTS

First and foremost, I would like to thank God for the strength and perseverance he has given me to complete this research. Without his help and countless blessings, I would not have maintained my focus, patience, and curiosity to pass the many milestones toward my Ph.D.

I would like to express my deepest appreciation to my advisor, Prof. Edwin K. P. Chong, for his guidance and encouragement throughout the process. Under his supervision, I learned how to see the world of wireless communication and networking through the lens of mathematical optimization. He helped me boost my problem-solving skills. He also taught me how to conduct research more efficiently and independently. The years I spent under his supervision were exciting and will continue to inspire me to tackle challenging engineering problems.

My sincere gratitude goes to Prof. Anura P. Jayasumana, Prof. J. Rockey Luo, and Prof. Rebecca Atadero for serving as my committee. They offered me invaluable suggestions and helpful advice to improve my work in many directions. In particular, their questions and feedback during my qualifying exam helped me improve my presentation timing and style. During my preliminary exam, their insightful comments helped me significantly refine my research. I enjoyed all these thrilling and inspiring (also challenging) moments and interactions.

I would also like to thank Prof. Jeong-Ho Kim from Ewha Woman's University-South Korea, who co-authored one of my research papers during his time as a visiting scholar at Colorado State University. I benefited a lot from his wide range of experience in the wireless industry. I would like to thank Prof. George Collins, Prof. Ali Pezeshki, and Prof. Jade Morton. They are great educators and amazing people. They shared their tremendous knowledge and expertise in the areas of MEMS, statistical DSP, and GPS.

I would like to extend my thanks to the former and current members in our group, Dr. Yajing Liu, Dr. Yugandhar Sarkale, Tushar Ganguli, Mahsa Ghorbani, and Apichart Vasutapituks for the support and for the exciting conversations about engineering and life.

I am indebted to my friends Maged Elhemri, Ziyad Arhouma, Siraj Elgawi, Mazin Irfaee, Youssif Elkabaili, Essam Elgandoli, Mansor Hamed, Dr. Fathalla Eldali, Mohamed Elbigetea, Ahmad Buhalfaia, Ahmad Elmahdi, Adam Elawami, Murad Altair, Ahmad Elmarkhi, Jimmy Singh, Dan Cambell, Billy Heckathorn, Sandra Hurtado, Jessica Quinn, and Dave Rasicci. Thank you all for being the most supportive and awesome friends I could ask for.

I gratefully acknowledge the support of the Ministry of Higher Education and Scientific Research, Libya for providing me with a scholarship to undertake my Ph.D. My study would not have been possible without the financial support I got through this scholarship.

This journey would not have been possible without the support of my parents, brothers, and sister. Family, you are the best thing in my life. No words can express how much you mean to me. To my parents, Mohamed Elsherif and Faouzia Omaiesh, thank you for the prayers, and for encouraging me and inspiring me in every way possible to follow my dreams. You are my first teachers and my greatest lifelong influencers. To my brothers, Salah Elsherif, Nasri Elsherif, Gadri Elsherif, Hani Elsherif, Waleed Elsherif, and to my sister, Zamzam Elsherif, thank you for all the unwavering support and unconditional love. I know you always wanted the best for me.

DEDICATION

I dedicate this thesis to my family for their constant support and unconditional love.

TABLE OF CONTENTS

LIST OF TABLES

LIST OF FIGURES

Chapter 1

Introduction

1.1 Scope and Background

Wireless networking has become an integral part of our everyday life. Certainly, wireless technologies have improved many aspects of the way people communicate, interact, and perform tasks, in addition to enabling new use cases, such as massive machine-type communications and industry verticals, among others. While convenient, these technologies impose new challenges and introduce new design problems. In this dissertation, we consider problems in green communication and security in wireless networks. Specifically, we formulate optimization problems in green communication and security, and provide computationally feasible solutions to these optimization problems. First, we introduce Markov decision process as a framework[1] for non-myopic energy-efficient base station control within the context of green communication. In the context of security, we introduce a new optimization framework—the semivariance-optimization framework[2]—and use it to formulate and solve two problems in security: The first semivariance-based problem is developing a scheme for wireless-jamming mitigation in multipath routing networks. The second problem based on semivariance is to devise a risk-averse scheme for multiple radio access technology (multi-RAT) connectivity in heterogeneous networks (HetNets).

[1]We briefly introduce the Markov decision process framework in Section 1.1.2 of this chapter. We study this framework in more detail in Chapter 2. For our purpose here, it is a framework for non-myopic optimization to balance immediate cost and long-term cost.

[2]We briefly discuss semivariance optimization in Section 1.1.3 of this chapter. In Chapter 3 and Chapter 4, we comprehensively study semivariance optimization. For now, it is an optimization framework that facilitates the tradeoff between potential gains and risks.

1.1.1 Requirements and challenges in contemporary and future wireless networks

Here, we discuss requirements, issues, and challenges in wireless networks within the contexts of green communication and security.

Recently, green communication has attracted significant research attention. One way to meet the increasingly pressing demands on network capacity is to deploy more base stations (BSs) with smaller coverage areas. Existing wireless systems, including 4G LTE, is primarily optimized for coverage and capacity and they meet past and current capacity demands. However, to meet the projected future demands, more small BSs (i.e., pico cells and femto cells) need to be added and this trend of adding more small cells is set to continue, leading to ultra-densified networks. While ultra-densification of BSs significantly contributes to meeting capacity requirements during peak periods, it creates a new challenge: Because operators provision capacity to meet demands at peak periods, BSs become underutilized during off-peak periods, leading to a huge waste of energy. This inefficient use of resources has two negative implications: (1) This inefficiency results in unnecessary emissions of CO_2 and contributes to global warming. (2) It unnecessarily increases network operational costs by increasing the electricity bill. Thus, energy consumption is expected to receive more attention in the business models fo future iterations of wireless networks. Just to keep energy consumptions at the same level, energy efficiency needs to improve at least by a hundredfold in 5G networks relative to the efficiency of 4G networks. This requirement of hundredfold improvement in energy efficiency remains the same at least for the foreseeable future (e.g., a hundredfold improvement in energy efficiency is required when transitioning from 5G to 6G systems). Indeed, meeting this requirement is even more challenging in 6G because the baseline is energy efficiency of 5G networks. Current wireless systems are primarily optimized for coverage and capacity. Hence, there is a need to address this issue and provide green communications solutions. Among others, dynamic BS ON/OFF control is a promising technique to achieve the goals of green communication [1], [2], [3].

Another important class of problems in wireless networks, which we consider in this dissertation, is related to RF jamming, which is a form of denial-of-service (DoS) attacks performed at the physical layer. Nowadays, we rely on wireless technologies to perform many of our daily tasks, including tasks that require high network availability. For example, 4G LTE is a strong candidate for safety networks in the United States [4], [5]. However, because of the broadcast nature of the wireless technologies and the availability of relatively cheap and easy-to-program software-defined radio (SDR) products, wireless networks have become more vulnerable to RF jamming [4], [6]. Hence, it is important to detect these attacks and take proper countermeasures. In multipath routing networks, a possible RF-jamming mitigation approach involves first detecting jamming attacks through collecting information about certain traffic metrics (e.g., through collecting information about packet-success rates), then using this information to allocate traffic to the available routing paths according to predefined strategies [7], [8], [9].

The third problem we consider in this dissertation is the problem of optimizing traffic allocation in HetNets, while accounting for stochastic wireless link capacities and risk in the traffic allocation decision making. Because of its potential to increase throughput, enhance communication reliability, and reduce latency, multi-RAT connectivity in HetNets has recently received significant research attention both in academia and industry. Standardizing and development bodies such as the 3rd Generation Partnership Project (3GPP) recognize these potential gains and requires emerging and next generations to co-exist and be more integrative than previous iterations of wireless systems. Hence, there is a need for develop unifying architectures and devise new traffic allocation schemes. Moreover, there are opportunities to leverage the inherent interface diversity offered by multi-RAT connectivity and HetNets to devise traffic allocation schemes that contribute to the development of wireless networks with high security and availability [10], [11], [12], [13], [14].

1.1.2 Markov decision process: Bellman's principle of optimality

An MDP is a mathematical framework for sequential non-myopic optimal control in stochastic environments. It has become a generic optimization framework, spanning a broad spectrum of decision-making problems.

According to the MDP framework, at each decision epoch, a non-myopic optimal control is achieved through solving an optimization problem, trading off immediate cost for expected long-term cost over a time horizon. In contrast, myopic (greedy) strategies seek to minimize only the immediate cost with no regard to the long-term impact of decisions taken at each decision epoch.

In principle, the tradeoff in MDPs is achieved by minimizing an objective function known as the Q-value, which is the sum of two terms: The first term represents the immediate cost incurred at the decision epoch. The second term accounts for the expected long-term cost over the time horizon starting at the next time step. This is known as Bellman's principle of optimality (named after mathematician Richard E. Bellman).

Usually, the first term of the Q-value can be calculated easily. Computing the second term, however, is generally burdensome because of the curse of dimensionality. As a result, finding exact solution for MDPs, by the value iteration or policy iteration algorithms, is impractical for most scenarios in real-world problems.

Hence, in many scenarios, we must resort to approximation methods, even for problems characterized by relatively small action space and state space. Many approximate dynamic programming methods exist to efficiently solve MDPs by replacing the second term of the Q-value (the expected long-term cost) by an approximation known as the cost-to-go [15], [16], [17].

1.1.3 Downside risk: Markowitz's semivariance optimization

Semivariance optimization, first introduced by economist and Nobel laureate Harry Markowitz, is a framework for trading off potential gains (measured in the mean value of return) for risk (expressed by semivariance). Semivariance is a mathematical quantity originally used to measure the dispersion of return below an investor-specified risk-aversion benchmark. While Markowitz

presented this framework within his second of two variations of portfolio selection theory for applications in finance and economics (the first variation of his theory being one that measures risk in terms of return variance), his mathematical model is rich enough to encompass risk-averse resource-allocation problems in a wide range of applications.

The main advantage of semivariance optimization is offering a tool to distinguish between upside and downside volatilities and to deal with each of them differently. In other words, semivariance allows identifying potential gains and losses (in contrast to variance-based optimization that perceives both upside and downside volatilities as losses). Another attractive feature of using semivariance is flexibility, i.e., the possible customization of a given resource allocation strategy by adjusting the risk-aversion benchmark (recall that variance only measures volatility relative to the mean; thus, it is inflexible in this regard) [18], [19], [20], [21].

While Markowitz himself recognized the plausibility of semivariance as a measure of risk, unfamiliarity of semivariance and computational problems led Markowitz to develop his first variation of portfolio selection based on variance instead. However, later efforts introduced a number of approximation methods (e.g., [20], [21]) that overcome the computational problems associated with using semivariance.

1.2 Aim and Motivation

In this section, we introduce the issues, needs, and opportunities that trigger our motivation to study problems in wireless communication and networking, and explore the potential to develop effective solutions. In this dissertation, we are interested in the three problems stated below.

1.2.1 Green communication: Non-myopic ON/OFF base station control

Recently, dynamic BS ON/OFF switching has received significant research attention because of its potential to reduce unnecessary energy consumption during off-peak periods. For example, the efforts in [22], [23], [24], [25], and [26] consider the problem of BS ON/OFF switching by adapting to the fluctuations to network traffic loads. However, none of these papers take the ON/OFF

transition energy cost into account. In highly fluctuating environments such as that of cellular networks, it is important to account for this factor when designing an ON/OFF control scheme because the transition cost can significantly reduce the efficiency of a given ON/OFF scheme. In certain scenarios when fluctuations of traffic loads are extremely high, the performance of an ON/OFF scheme can become even worse than an always-ON scheme; results of such scenarios are reported in [27].

The efforts in [28–30] consider switching energy cost. According to [30], the most effective method to minimize energy consumption in cellular networks is ON/OFF switching of BSs in real-time using information about user locations. However, similar to the efforts in [22], [23], [24], [25], and [26] the efforts in [28–30] suggest heuristics and algorithms that are greedy in nature (i.e., myopic methods that do not account for the expected long-term cost of the control decisions taken at each decision epoch).

Energy savings exploiting user location information has been studied in many papers. For example, the work in [31] highlights the possibility to use the available support in 4G LTE networks for user location predication via a dedicated GPS protocol. However, the authors only focused on the feasibility of the employment of model predictive control using this location prediction support. Another example is the work in [27]. The authors of this paper suggest using a basic user mobility model to design an energy saving algorithm and reported energy savings of up to 36%.

A number of localization and positioning methods have been applied to 2G, 3G, and 4G LTE [32]. Information about user locations is used for decision making regarding capacity planning, emergency response (E911), network security, identification of coverage holes, and supporting location-based services (LBS) [33]. The state-of-the-art of location measurement precision is deployed in 4G LTE. Typically, in 4G LTE, the collected data is sent to a central entity, e.g., mobility management entity (MME), for processing. The frequency at which updates are collected is operator specific [32]. The authors of [32] suggest parsing some data and processing it at the edge. The amount of information needed is the same as that in 4G LTE, and following an approach similar to that in [32], the processing could be done at the edge to reduce the amount of data oth-

erwise needed to be sent to the MME. With the availability of vast computational power and the maturity of big data analytics, there is an increasing tendency towards adopting data-driven decision making techniques in wireless networks. Thus, using mobility and user location information is no additional burden.

The myopic nature of suggested schemes in the literature, the potential of the MDP framework, and the availability of location information motivate us to investigate the possibility of developing a non-myopic energy-efficient BS control to achieve the goals of green communication without disrupting quality-of-service (QoS) in terms of minimum received power.

1.2.2 Mitigating RF-jamming by multipath routing

There is a vast literature on RF-jamming attacks and mitigation (e.g., see [34], [35], [36], [37], [38], [39], [40], [41], [9]).

The efforts in [37], [38], [39] consider the problem of RF jamming in multipath routing networks. However, there are some problems with the underlying assumptions in these papers. First, these efforts assume node-disjoint and link-disjoint paths guarantee to failure-independent paths; having node-disjointness and/or link-disjointness does not guarantee uncorrelatedness of the effects of jamming in wireless networks (e.g., a jammer geographically located between two or more node/link-disjoint paths can concurrently impact some or all of them and renders these paths failure-correlated). Second, these efforts assume that disjointness at the network layer guarantees failure-independent paths; disjointness at the network layer does not guarantee uncorrelated failures at the physical layer because of the topological independence between the two layers [42], [40]. For example, given a number of paths, regarded of IP-layer disjointness, an RF jammer (at the physical layer) can concurrently disrupt the services over these paths because network layer protocols are virtual networks built on top of possibly common physical infrastructure (underlay network(s)).

Because of issues with the assumptions mentioned above, some efforts use on historical data to predict the impact of jamming instead of relying on these assumptions (see [42], [40], and

[41]). These predictions of the impact of jamming are used to control traffic allocation over the available routing paths. However, these efforts use thresholding to determine link availability. This can severely reduce the efficiency of path selection. While these efforts overcome the problems associated with measuring path correlation, thresholding-based schemes can be sub-optimal from communication resource allocation point of view.

The efforts in [9] map the problem of jamming-aware multipath routing to portfolio selection to overcome the issues with correlation and thresholding. Specifically, the authors of [9] suggest using mean-variance optimization, hence trading off trading off mean for risk in the form of throughput throughput variance. Formulating the problem as a mean-variance optimization problem the issues with path correlation and thresholding. However, the main problem with this framework is that it measures risk as the throughput variance, hence treating upside and downside throughput dispersion in the sane way. Another issue is that this framework assumes symmetric distribution of throughput [43] and can either underestimate or overestimate risk if the distribution of throughput is asymmetric.

Motivated by the issues mentioned above and the advantages of using the semivariance-optimization framework, we explore the possibility of developing a computationally feasible algorithm for RF-jamming mitigation in multipath routing networks that overcomes the problems resulting from thresholding-based traffic allocation strategies and underlying path correlation assumptions in the literature, in addition to properly quantifying risk in terms of throughout semivariance instead of variance.

1.2.3 Risk-aversion in multi-RAT HetNet environments

Co-existence between technologies from different cellular generations and WLAN has been emphasized in recent 3GPP releases. Because of its potential to increase throughput, improve communication reliability, and reduce latency, the problem of multi-RAT connectivity in HetNets has recently received significant research attention both in academia and industry (e.g., see [10], [44], [45], [12], [13], [14], [46], [47]). While these papers consider the problem of throughput max-

imization using concurrent transmissions across the available multiple radio interfaces in HetNet environments, none of these papers view the problem from the perspective of risk. Additionally, none of the papers above explicitly show how to account for the capacities of the involved RATs and how to calculate the total throughput from the involved air interfaces. Also, none of these papers explicitly account for the correlation between the throughput of the radio interfaces involved in the considered multi-RAT connectivity problems.

The availability of multi-RAT connectivity architectures creates new opportunities for innovation when combined with complementary concepts such as network slicing and edge computing. Network slicing enables dynamic resource allocation and can adapt to varying user preferences over time and space. The maturity of edge computing platforms allows implementing decentralized algorithms at the BSs. The combination of these concepts enables agile provisioning and computation-oriented communications instead of the static/semi-static provisioning for target QoS [1], [10], [11], [44], [45].

Motivated by the problems and opportunities discussed above, we investigate the possibility of implementing an algorithm for multi-RAT connectivity that allows users to specify different throughput requirements and accounts for correlation and risk in the traffic allocation problem. Moreover, we explore the feasibility of developing a systematic method to quantify the total throughput that involves different capacities of wireless links and varying number of involved interfaces, and defining a metric that simultaneously captures potential gains and risks.

1.3 Thesis Outline and Contributions

In this section, we outline this dissertation, highlighting the contributions within each chapter.

In Chapter 2, we consider the problem of BS dynamic switching for energy efficient design of 5G cellular networks and beyond. We formulate this problem as an MDP and use an approximation method to solve it. In this Chapter 2, we introduce a novel approach to design an energy efficient BS control algorithm exploiting user mobility and location information in the optimization of action selection. We develop a scalable solution by starting from the one-user one-ON scenario and

extending this formulation to the multi-user multi-ON case. We test the performance of our algorithm in comparison to three different schemes from the literature through extensive simulation scenarios and under different parameter values. Simulation results show the potential of our approach of exploiting user mobility information within the MDP framework to achieve significant energy savings without sacrificing QoS. We summarize our contributions in Chapter 2 as follows:

First, the main contribution in Chapter 2 is the formulation of the problem as an MDP. All the efforts introduced in the literature consider optimizing energy consumption in a single time step (myopic strategies). In contrast, by formulating the problem as an MDP, we introduce a new non-myopic framework. To the best of our knowledge, this is the first work that considers user mobility within the MDP framework for the design of green cellular networks.

Second, we develop a new rollout algorithm to solve the MDP problem, together with a specific choice of a suitable base policy. Note that the rollout method does not specify anything about the choice of the base policy; it is here our responsibility as the algorithm designers to make an appropriate choice of the heuristic according to wireless communication domain knowledge. We also introduce an approach to modifying the action space to make the method amenable to practical implementation.

Third, our work is the first to handle the problem of decoupled uplink/downlink traffic in the context of energy-efficient BS control.

Fourth, our work is among the few efforts to consider BS switching energy in the formulation of the problem. However, in contrast to the work in the literature, we seamlessly incorporate the switching energy into one cost function to be minimized.

Fifth, compared to existing efforts in the literature, our work considers user state dynamics in the service area. Our work employs the available information about user location to facilitate QoS guarantees. The existing research efforts consider the statistics of the aggregated users and traffic distribution, and thus do not employ user dynamics and lack QoS in this sense.

Sixth, our simulation results show that the designed algorithm achieves very significant energy savings compared to the benchmarking schemes.

In Chapter 3, we describe our work on RF-jamming mitigation. We consider the problem of network security. More specifically, we consider the problem of jamming-aware-multi-path routing in wireless networks. To address this problem, we propose a new framework based on semivariance optimization. We map the problem of jamming-aware-multi-path routing to the portfolio-selection problem within the semivariance risk framework. We use this framework to design a new RF-jamming mitigation algorithm. We study methods to measure RF jamming without the need of information about the actual jammer location, number of jammers, or jamming power. We provide simulation performance analysis to evaluate our algorithm in comparison to a benchmarking scheme based on mean-variance optimization. We summarize our main contributions in Chapter 3 as follows:

First, we formulate the problem of jamming mitigation as a portfolio-selection problem. Together with [9] and [48], our work here is among the few efforts to apply a portfolio-selection treatment to the problem of jamming.

Second, in our problem formulation, we use a downside-risk cost function. Specifically, we use semivariance as a measure of risk. Our work is the first to exploit semivariance as a measure of risk in the context of security against jamming, and communication-network security in general. To the best of our knowledge, our work is also the first to introduce downside risk and semivariance to the lexicon of telecommunications.

Third, we study semivariance problems and survey their solutions.

Fourth, we adopt and modify a semivariance approximation method, from economics and finance, and use it to develop our new scheme to solve semivariance problems in the context of RF jamming mitigation.

Fifth, we develop an efficient scheme for solving semivariance optimization problems. Efficiency is an essential feature for telecommunication applications, considering low latency and low computing power constraints (e.g., tactile Internet and Internet of Things).

Sixth, our scheme provides a general approach to solving semivariance optimization problems, and can be used in other applications.

In Chapter 4, we introduce a new approach to the problem of multi-RAT traffic allocation in HetNets. We propose a new risk-averse multi-RAT connectivity (RAM) algorithm that allows trading off expected throughput for risk measured in throughput semivariance. In this approach, we also adopt semivariance as a measure of throughput dispersion below a risk-aversion–throughput benchmark and formulate the multi-RAT connectivity problem as a semivariance-optimization problem. The optimization problem in this chapter has a different objective function and set of constraints from that in Chapter 3. In addition, in Chapter 4, we define a new performance metric—the risk-adjusted throughput— and use it to evaluate the performance of our algorithm through simulation of a system with three radio-access technologies: 4G LTE, 5G NR, and WiFi. We also study 3GPP and 802.11n specifications of throughput calculations in 4G LTE, 5G NR, and WiFi 4. We design and conduct different simulation experiments guided by these specifications to realistically reflect HetNet environments. Simulation results show the potential gains of using our algorithm. In Chapter 4, our main contributions are as follows:

First, our work contributes to the efforts that aim at throughput maximization without retransmission requests (which lead to latency that can violate the quality of service (QoS) for delay-sensitive applications).

Second, by formulating the problem as a semivariance optimization problem, we introduce a unified framework for the multi-RAT connectivity problem.

Third, our work is the first to take a risk-averse view of the source-data fragmentation decision making in the context of multi-RAT connectivity.

Fourth, we introduce a new traffic allocation performance metric, the risk-adjusted throughput.

Fifth, we define new stochastic capacity constraints to account for wireless link capacities of 4G LTE, 5G NR, and WiFi links.

Last, following 3GPP and 802.11n specifications for throughput calculation in our simulation, we develop an algorithm that is amenable to practical implementation in real scenarios of network control and provisioning, with only minor modifications to match deployment specificities.

We conclude this dissertation and introduce future research directions in Chapter 5.

Chapter 2

Energy-Efficient Base Station Control Framework for 5G Cellular Networks Based on Markov Decision Process

2.1 Introduction

Green communication is one of the main defining terms of the emerging fifth generation (5G) cellular networks and beyond [49], [50]. Existing cellular networks, including 4G LTE, are primarily optimized for coverage and capacity. Yet, global warming and CO_2 emissions caused by existing wireless networks amount to 2%. In addition, 70–80% of the energy consumption of the current cellular networks is caused by radio access networks and base station (BS) operational cost [51]. Added to the environmental concerns, the electricity bill due to network energy consumption is expected to receive more attention in the cellular business models [52]. With the surge in data traffic envisioned in the near future, hundredfold increase in cellular network traffic is expected by 2020. Consequently, energy consumption will drastically increase. Thus, just to keep the energy consumption at the current level, a reduction in the (J/bit) by a factor of $1/100$ is needed in future cellular networks [3].

To meet the explosive demand on data traffic, cell deployment will reach unprecedented levels of densification. Cellular networks are designed to meet the traffic demand at peak times. However, during low-traffic periods, there is a huge waste of energy when the cells are underutilized [53], [54]. To achieve the goal of green communication, a new dimension should be added to the problem of network optimization. Specifically, energy consumption needs to be incorporated into the objective function in the network optimization problem. It seems natural to think about switching off the underutilized BS in low-traffic periods. One of the promising techniques to implement the efficient communication networks of tomorrow is the dynamic BS ON/OFF control.

Referring to Fig. 2.1, in this chapter we present our work on small-cell ON/OFF control of the 5G cellular networks exploiting user mobility. We limit the scope of our algorithm to small-cell control for 5G networks. As 5G networks focus more on capacity enhancement than coverage extension, one of the main 5G design themes is to use ultra-cell-densification with small-cell technology to provide the required system-capacity enhancement [3]. This inevitably incurs too many unoccupied cells owing to uneven traffic distributions. Under this situation, the proposed algorithm can provide significant gains over the conventional systems. As a result, the dynamic ON/OFF control of the cells can achieve efficient use of the available power. We emphasize that the effectiveness of our algorithm is sound for small-cell capacity networks. However, in case of coverage networks, which deal with sparse traffic distributions of mobile users, each BS should be turned on with high probability since it will have more users per BS to accommodate in its coverage area than of capacity networks. Hence, its merit in coverage networks would be marginal.

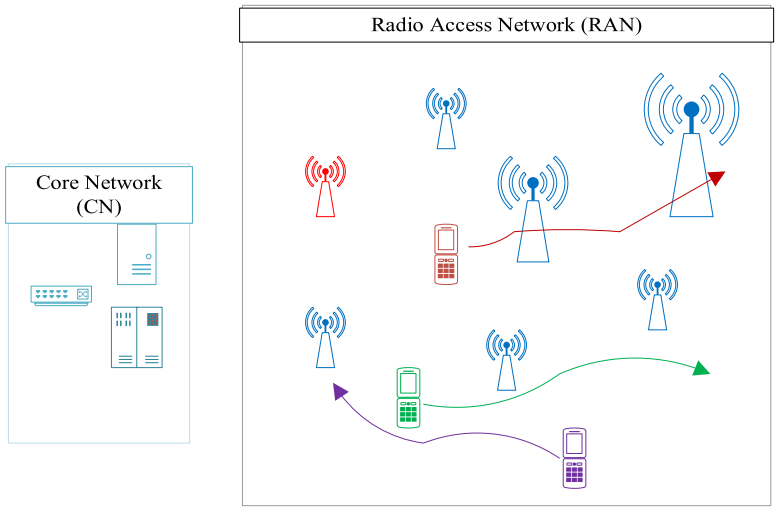

Figure 2.1: Green communication exploiting user mobility.

In this work, we introduce our design of a real-time control algorithm for BS ON/OFF switching. The problem of dynamic ON/OFF BS switching has recently received a lot of research attention. The research in [22–26,55,56] consider the problem of dynamically optimizing the switching

of BSs according to the fluctuations of network traffic load, and many algorithms and heuristics have been suggested to solve this problem. In [22], a swarm intelligence algorithm was proposed to solve the optimization problem of determining the BSs to be switched off. The authors of [23] proved the NP hardness of the problem of BS switching, and a decentralized heuristic was proposed as a solution that can be integrated within existing 4G networks. In [24], the problem of energy saving was formulated as a set cover problem to minimize the number of active BSs, and three cell-sorting criteria were investigated to optimize the ordering of cell switch-off. In [25], the energy-delay trade-off was considered. Two theoretical heuristics, one for user association and the other for BS control, were introduced. A third heuristic for practical implementation was also proposed, with no additional signaling overhead. In [55], the traffic was modeled as sinusoidal. The provided results from the first-order analysis of the network showed that the amount of energy saving depends on the traffic ratio of mean and variance and the BS density. The work in [55] is extended in [56] by introducing a notion of network-impact, to account for the increase in network load brought by turning off a BS. The work in [26] follows a game-theoretic approach. Based on the traffic load, neighboring BSs cooperate to optimize BS switching strategies, with the goal of maximizing the energy saving while providing quality-of-service (QoS) guarantees in terms of minimum received power to provide the signal to interference plus noise ratio (SINR) required for the specified bit rate.

In contrast to the efforts above, our current work explicitly accounts for the ON/OFF transition energy costs. Energy costs due to BS switching can greatly impact the total energy consumption. In highly fluctuating environments such as that of cellular networks, it is important to account for this factor in the formulation of this type of problems. There are some efforts that consider transition costs [28–30]. However, most of the existing research considers the assumption of fixed transmission power when solving the BS ON/OFF problem. In reality, energy consumption also depends on path-loss and attenuation (this dependency becomes more apparent in scenarios like outdoor to indoor communication links), and continuous update of transmitted power levels via power control is necessary for reliable communication links. Among the efforts that consider

switching energy costs, [30] considers power adjustment as well. According to [30], the most efficient way to minimize energy consumption in cellular networks is to control the ON/OFF state of BSs in real-time utilizing the information about user locations. While the work in [30] considers the control of BSs over a time period (which is divided into time units), in real-time, it assumes the availability of static location information in advance for each time unit and over the entirety of the time period, specifically a day. This leads to formulating the energy minimization problem as a deterministic optimization problem and for an entire day, with no QoS guarantees.

Furthermore, the work in [30] suggests that it is hard to solve the problem of minimizing energy consumption directly because of two difficulties: (1) When the switching energy cost is considered in the ON/OFF BS control, the action selection in adjacent time units is correlated. (2) In each time unit, the working states and transmission power of neighboring BSs are also coupled. Thus, the work in [30] breaks the energy saving problem into two subproblems. The first subproblem is that of independently determining the ON/OFF states of the BSs, and the transmission power of all BSs in each time unit. The second subproblem is that of minimizing the switching energy consumption of all BSs over the entire time period (a day), given the solution of the first subproblem.

Now, to solve the first subproblem, the work in [30] suggests using one of two heuristics, which are both greedy in nature. The authors of [30] call the first heuristic Efficiency First Strategy (EFS), and call the second heuristic Closest Distance Strategy (CDS). To solve the second subproblem, the authors of [30] suggest another heuristic, which they call Minimum Switching Cost (MSC), and is based on Dijkstra's algorithm.

While our work considers the same problem as that in [30], there are major differences in the way we handle the energy saving problem. First, we formulate the problem as a Markov Decision Process (MDP). Thus, we offer a non-myopic treatment of the problem, in contrast with the myopic approach followed in [30], and in all other efforts mentioned in the literature. Another major difference in our work is seamlessly incorporating the ON/OFF switching energy costs with the operational cost in one objective function. Thus, solving the problem of minimizing the operational energy cost and the switching cost in one step rather than splitting the problem into two subprob-

lems, as opposed to the work in [30]. This allows an explicit trade-off between the operational and the switching energy cost.

Additionally, our cost function introduces a new perspective on handling the ON/OFF switching energy by explicitly representing the ON and the OFF energy transition costs. This allows our algorithm to compare and select the action as to which BS(s) to turn ON for BSs with different hardware.

Another difference is that the work in [30] introduces CDS to solve the problem of minimizing the operational cost, yet it does not include an important part of the energy consumption, namely the non-radiation power consumption. It also introduces EFS, which on the other hand does not consider the radiation energy, and requires a very strict assumption. It requires that each BS in the network to have different energy efficiency and says nothing about the case if some BSs are equally efficient (EFS is already outperformed by CDS, and in the simulation part we will use CDS as one of the benchmarking schemes). On the other hand, our algorithm considers all the parts that constitute the total energy consumption, including both the radiation and the non-radiation power consumptions.

Last but not least, our algorithm considers the state dynamics and provides QoS guarantees while the work in [30] considers static information about the user locations. This can result in coverage holes and sacrificing QoS. Recall that self-driving cars and tactile Internet are two of the major anticipated use cases of 5G; both of these use cases require a very high network availability.

In this chapter, we design a real-time control algorithm based on an MDP formulation to minimize energy consumption by optimizing the switching of BSs. We provide a systematic approach amenable to practical implementation. We account for the ON and the OFF switching energy costs separately in our formulation of the problem (as opposed to the mentioned papers which account for the transition energy cost as a whole). Separation of the ON and the OFF switching energy costs allows more flexibility to handle scenarios related to different BS hardware. We also consider power control at the BS side of the communication link. Our approach provides energy saving and QoS guarantees exploiting user mobility in the optimization of decision making. According

to [57], user location can be predicted with high probability. The potential of energy saving exploiting the available support in the existing LTE networks for user location predication via a dedicated GPS protocol is highlighted in [31]. However, the authors only focused on the feasibility of the employment of model predictive control using this location prediction support. A basic mobility model for user movement between home and work is employed in the design of an energy saving algorithm, and a saving of up to 36% was reported in [27].

To handle asymmetric downlink/uplink traffic, some network operators adopt decoupled downlink/uplink access [58], [59]. None of the papers mentioned above consider this implementation issue in the formulation of the BS control problem. For two reasons, our formulation of the problem is a natural framework for decoupled downlink/uplink access: First, our algorithm is based on location information. Second, our algorithm considers adaptive power control. That being said, however, the framework is equally relevant in the case of coupled downlink/uplink access.

For the sake of completeness and fair comparison with existing cellular systems, we believe that an estimate of the signaling (control) overhead associated with the implementation of our proposed algorithm would be necessary. A number of localization and positioning methods have been applied to 2G, 3G, and 4G LTE [32]. These pieces of information about user locations are used to optimize decisions regarding capacity planning, emergency response (E911), network security, identification of coverage holes, and supporting location-based services (LBS) [33]. All of the cellular systems mentioned above would need to acquire updates of locations of mobile users in their coverage areas via the employment of time-of-arrival, angle-of-arrival, cell ID, and received signal strength, with the state-of-the-art of location measurement precision being deployed in 4G LTE. Typically, in 4G LTE, the collected data is sent to a central entity, e.g., mobility management entity (MME), for processing. The frequency at which updates are collected is operator specific [32]. The authors of [32] suggest parsing some data and processing it at the edge (fog computing). Our proposed algorithm needs to acquire location updates of network users and currently serving cell IDs, in addition to statistical model(s) for user mobility based on the mobility behavior of users. With 4G LTE as the baseline, we claim that our algorithm introduces little to no additional signaling

overhead. The amount of information needed is the same as that in 4G LTE, and following an approach similar to that in [32], the processing could be done at the edge to reduce the amount of data otherwise needed to be sent to the MME. With the availability of vast computational power and the maturity of big data analytics, there is an increasing tendency towards the application of data-driven intelligence in wireless networks. Thus, requirement of statistical models is no additional burden.

Our contribution is multifold:

- First, the main contribution of in this chapter is the formulation of the problem as an MDP. All the efforts introduced in the literature consider optimizing energy consumption in a single time step (myopic optimization approach). In contrast, by formulating the problem as an MDP, we introduce a new non-myopic framework to approach the problem of ON/OFF BS control. To the best of our knowledge, this is the first work that considers user mobility within the MDP framework for the design of green cellular networks.

- Second, we develop a new rollout algorithm to solve the MDP problem, together with a specific choice of a suitable base policy. Note that the rollout method *per se* does not specify anything about the choice of the base policy; it is here our responsibility as the algorithm designers to make an appropriate choice of the heuristic according to wireless communication domain knowledge. In this chapter, we also introduce an approach to modifying the action space to make the method amenable to practical implementation.

- Third, our work is the first to handle the problem of decoupled uplink/downlink traffic.

- Fourth, our work is among the few efforts to consider BS switching energy in the formulation of the problem. However, in contrast to the work in the literature, we seamlessly incorporate the switching energy into one cost function to be minimized.

- Fifth, compared to existing efforts in the literature, our work considers user state dynamics in the service area. Our work employs the available information about user location to facilitate

QoS guarantees. The existing research efforts consider the statistics of the aggregated users and traffic distribution, and thus do not employ user dynamics and lack QoS in this sense.

- Last but not least, our simulation results show that the designed algorithm achieves very significant energy savings and outperforms the benchmarking schemes.

The rest of this chapter is organized as follows. In Section 2.2, we review the MDP framework. In Section 2.3, we introduce our formulation of dynamic BS control as an MDP. In Section 2.4, we briefly discuss the rollout algorithm, which is an approximation method to solve MDPs. We also show how we modify the rolluot algorithm and use it for our application. We then introduce our simulation results in Section 2.5. We conclude this chapter in Section 2.6.

2.2 Review of Markov Decision Processes

As our design of the control algorithm is based on MDPs, we first introduce MDPs following the treatment in [15]. For our purpose, an MDP is a discrete-time stochastic process partly under control of an action selector. It can be represented by a 4-tuple that contains the following elements:

- A set of states and a distribution that determine the random initial state.
- An action space representing the set of feasible actions.
- A state-transition law specifying the conditional distribution of the next-state given an action taken at a current state.
- A cost function for evaluating the cost of an action taken at a state.

Moreover, an MDP starts with an initial state at time $k = 0$. At this state, an action is selected by the action selector, and a cost is incurred. As per the definition of the cost given above, the cost incurred depends on the action and the state. The state of the system then moves to some random next state, according to the dynamics given by the state-transition law. The process continues to evolve randomly over time, responding to the actions; at each time, the process is at some state, and the selected action at that state determines the cost and next state.

Now, MDPs provide a framework for optimal control in a stochastic environment. Note that in the context of stochastic optimization, the control actions are only optimal in the sense of the expected cost. More specifically, the objective function here is the expected cumulative cost over a time horizon H. The optimality of an MDP solution is based on Bellman's principle and the idea of lookahead. Bellman's principle of optimality can be written as

$$J_H^*(s_0) = \min_b (g(s_0, b) + E[J_{H-1}^*(s_1)|s_0, b]), \tag{2.1}$$

where $J_H^*(s_0)$ is the optimal cost starting at a state s_0 and acting optimally over a horizon H, g is the immediate cost, and $E[J_{H-1}^*(s_1)|s_0, b])$ is defined as the expected cumulative cost over the time interval $1, \ldots, H-1$, starting at the next (random) state s_1. Moreover,

$$\mu_0^*(s_0) = \arg\min_b (g(s_0, b) + E[J_{H-1}^*(s_1)|s_0, b]) \tag{2.2}$$

defines an optimal policy. Defining the Q-value of taking an action b at a state s_0 as

$$Q_H^*(s_0, b) = g(s_0, b) + E[J_{H-1}^*(s_1)|s_0, b]. \tag{2.3}$$

We can rewrite Bellman's principle of optimality as

$$\mu_0^*(s_0) = \arg\min_b Q_H^*(s_0, b). \tag{2.4}$$

Equation (2.4) states that according to Bellman's principle, knowing the Q-values is all we need to make optimal control decisions. In other words, if we are currently at state s_0, we only need to find the action b that minimizes $Q_H(s_0, b)$.

The MDP control framework, shown in Fig. 2.2, is built on this principle. Referring to the figure, the system we seek to control is the wireless cellular network. The system receives as its input actions given by the action selector. Specifically, the actions in our problem are the subsets of BSs in the ON state, subject to the input power levels meeting the QoS constraints. The output of

the wireless network system is the observed states. As shown in Fig. 2.3, the action selector consists of two parts, an optimization algorithm and a Q-value calculator. The optimization algorithm minimizes the Q-value. The Q-value calculator receives the candidate actions and approximates the value of the Q-function [15].

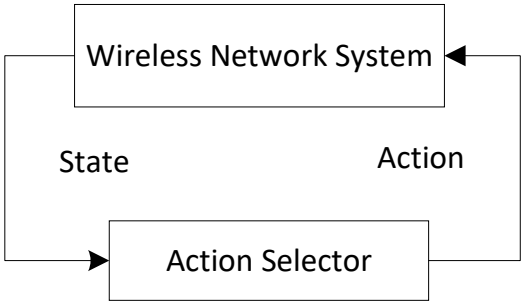

Figure 2.2: Basic lookahead.

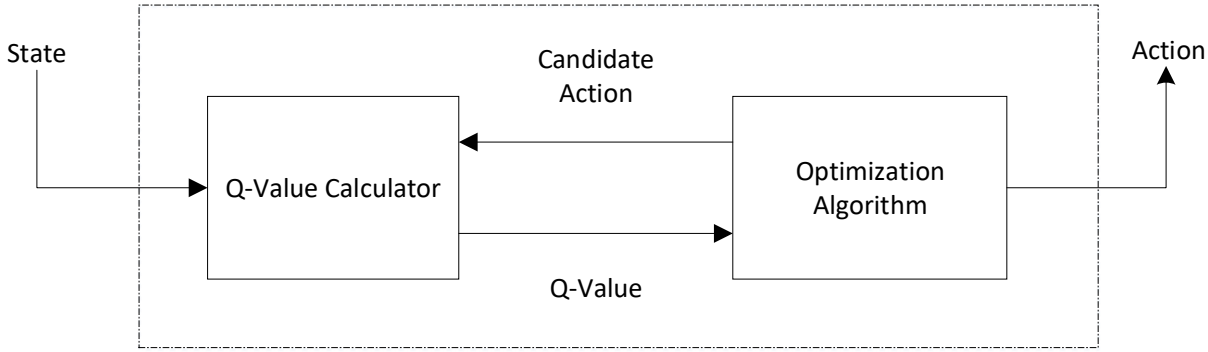

Figure 2.3: Action selector.

2.3 Problem Formulation

We formulate the problem as an MDP. For the sake of clarity, we start by introducing the problem formulation for the one-user scenario with only one-BS in ON status; for short, we will refer to this scenario as one-user one-ON from now on. We then show how we extended our formulation to the case of multi-user with only one BS allowed to be in ON status; we refer to this

arrangement as multi-user one-ON. Finally, we introduce our approach to extend this formulation to the multi-user with the possibility to turn ON as much BSs as needed; we refer to this case as multi-user multi-ON.

To formulate the problem as an MDP for a network of M BSs, we need to define the MDP ingredients for this specific problem for the three different scenarios.

2.3.1 One-user one-ON formulation

System States

The state at each time step is the 2D user position, velocity, and the ON/OFF status of the BSs. Mathematically, this can be written as

$$s_k = [x_k, \dot{x}_k, y_k, \dot{y}_k, a_{k,1}, \ldots, a_{k,M}]^T \tag{2.5}$$

where x_k and y_k are the 2D coordinates of the user position, $\dot{x}_k$ and $\dot{y}_k$ are the 2D coordinates of the user velocity, and $a_{k,m} \in \{0, 1\}$ is the ON/OFF status of BS m, $m = 1, \ldots, M$.

Actions

At each time step, the action is the ON/OFF BS control for each BS. Recall that in this simple case, we only turn ON one BS at a time. Thus, the action space is $B = \{1, \ldots, M\}$, and $b_k \in B$ is the action at time k, where M is the number of BSs as defined above. The decision is based on the user position and velocity, in addition to the current status of the BSs. The outcome of this process is the ID of the BS that is turned ON at time k. In this scenario, only one among $a_{k,1}, \ldots, a_{k,M}$ can be nonzero.

State-transition law

We assume that the vector $u_k = [x_k, \dot{x}_k, y_k, \dot{y}_k]^T$ transitions in a Markovian fashion. Specifically, we can write the next state of the system as

$$s_{k+1} = f(s_k, b_k, v_k) = [f^u(u_k, v_k^u), f^a(b_k)]^T, \tag{2.6}$$

where f^u is the state dynamics of user mobility, and f^a is the ON/OFF status of the BSs; all its components are zero except for the one that corresponds to the BS in the ON status. In other words,

$$f^a(b_k) = \begin{bmatrix} a_{k,1} \\ \vdots \\ a_{k,M} \end{bmatrix} \text{ and } a_{k,i} = 1 \iff b_k = i. \tag{2.7}$$

To represent f^u, or more particularly $f^u(u_k, v_k^u) = u_{k+1}$, we use the mobility model given in [60]:

$$u_{k+1} = \begin{bmatrix} x_{k+1} \\ \dot{x}_{k+1} \\ y_{k+1} \\ \dot{y}_{k+1} \end{bmatrix} = \begin{bmatrix} 1 & T_s & 0 & 0 \\ 0 & 1 & 0 & 0 \\ 0 & 0 & 1 & T_s \\ 0 & 0 & 0 & 1 \end{bmatrix} \begin{bmatrix} x_k \\ \dot{x}_k \\ y_k \\ \dot{y}_k \end{bmatrix} + \begin{bmatrix} \frac{T_s^2}{2} & 0 \\ T_s & 0 \\ 0 & \frac{T_s^2}{2} \\ 0 & T_s \end{bmatrix} \begin{bmatrix} v_k^x \\ v_k^y \end{bmatrix}, \tag{2.8}$$

where T_s is the duration of each discrete time step (sampling time), v_k^x and v_k^y are independent noise processes with zero mean and variances σ_x^2 and σ_y^2, representing the 2D components of user acceleration.

Cost per time-step

We define the cost at each time step k as the input energy (E_{in}), in Joules, required to meet the QoS constraints in terms of the minimum power level $P_{\min}(dBm)$[3] at the receiver (to provide the SINR required for the specified bit rate). Let m_k be the BS that is active[4] at time k, i.e., the index m such that $a_{k,m} = 1$. Then we can define the per-time-step cost E_{in} as

[3]Note that the minimum power level at the receiver is calculated as the minimum power level to provide the required (SINR), where, SINR= $\frac{P_{\min}}{I+N_0B}$, and the required value of the SINR for a specified bit rate and bandwidth B is calculated using this equation:
bit rate= $B \log_2(1 + \text{SINR})$.

[4]There is only one exception to this definition of m_k. In the initial state of the system at time $k = 0$, there might be more than one BS in the ON state. However, for all other time steps $k \geq 1$, m_k follows the definition given above.

$$E_{\text{in}} = \{E^{\text{nr}}_{b_k} + E^{r}_{b_k}\} + \begin{cases} 0, & \text{if } b_k = m_k \\ E^{\text{ON}}_{b_k} + E^{\text{OFF}}_{m_k}, & \text{otherwise} \end{cases}, \tag{2.9}$$

where E_{in} consists of two parts, an operation cost and a transition cost. The operation cost is comprised of $E^{\text{nr}}_{b_k}$, which is the non-radiation energy consumption by BS b_k, and $E^{r}_{b_k}$, which is the radiation energy by BS b_k. Here $E^{r}_{b_k}$ is calculated as $E^{r}_{b_k} = p^{r}_{b_k}.T_s = \frac{4\pi p_{\min}.d^{\alpha}_{b_k}.\text{Loss}_m.\text{Loss}_{\text{BS}}}{G_m.G_{BS}}.T_s$, where $p^{r}_{b_k}$ is the average radiation power by BS b_k, d_{b_k} is the distance between BS b_k and the mobile user location, α is the path-loss exponent, Loss_m and Loss_{BS} are the mobile and BS RF chain losses, and G_m and G_{BS} are the mobile and BS antenna gains. In the case where $b_k \neq m_k$, the transition cost equals the sum of $E^{\text{ON}}_{b_k}$ and $E^{\text{OFF}}_{m_k}$, which denote (in this special case where $b_k \neq m_k$) the transition cost to ON status (for the BS chosen to be ON at time k) and the transition cost to OFF status (for the BS turned OFF at time k), respectively.

2.3.2 Multi-user one-ON formulation

For the multi-user one-ON case, we need to make two changes. First, we modify the system states, and the state-transition law to accommodate more than one user. Second, the total energy consumption is now the sum of energy spent by the system to provide QoS coverage to all the active users considered in the network.

System States

To go from one-user to multi-user, we modify the system states in our formulation. For $L \geq 2$ users in the network, we express the system states as

$$s_k = [x^k_1, \dot{x}^k_1, y^k_1, \dot{y}^k_1 \ldots, x^k_L, \dot{x}^k_L, y^k_L, \dot{y}^k_L, a_{k,1}, \ldots, a_{k,M}]^T, \tag{2.10}$$

where x^k_i and y^k_i are the 2D coordinates of user i position, $\dot{x}^k_i$ and $\dot{y}^k_i$ are the 2D coordinates of user i velocity, where $i \in \{1 \ldots, L\}$. Similar to the previous case, $a_{k,m} \in \{0, 1\}$ is the ON/OFF status of BS m, $m = 1, \ldots, M$.

Actions

The definition of the actions here follows the same as that of the previous scenario with only one difference. In addition to the current status of the BSs, the decision in this case depends on the positions and velocities of more than one user (all users in the network).

State-transition law

The state-transition law is modified to match the changes made to the system states. The state dynamics of all users in the network is given by

$$u^{k+1} = [u_i^{k+1}]_{(i=1,\dots,L)}^T = [f^u(u_1^k, v_1^k), \dots, f^u(u_L^k, v_L^k)]^T. \tag{2.11}$$

As we assume that the users are moving independently, we can write the state dynamics of each user as

$$u_i^{k+1} = \begin{bmatrix} x_i^{k+1} \\ \dot{x}_i^{k+1} \\ y_i^{k+1} \\ \dot{y}_i^{k+1} \end{bmatrix} = \begin{bmatrix} 1 & T_s & 0 & 0 \\ 0 & 1 & 0 & 0 \\ 0 & 0 & 1 & T_s \\ 0 & 0 & 0 & 1 \end{bmatrix} \begin{bmatrix} x_i^k \\ \dot{x}_i^k \\ y_i^k \\ \dot{y}_i^k \end{bmatrix} + \begin{bmatrix} \frac{T_s^2}{2} & 0 \\ T_s & 0 \\ 0 & \frac{T_s^2}{2} \\ 0 & T_s \end{bmatrix} \begin{bmatrix} v_i^{x_k} \\ v_i^{y_k} \end{bmatrix}, \tag{2.12}$$

where $i \in \{1, \dots, L\}$. Equation (2.11) together with equation (2.12) give a detailed description of the part of state dynamics that represents all users in the network. To formulate the complete state-transition law, we add the part that represents the BS dynamics:

$$S^{k+1} = [u_i^{k+1}, f^a(b^k)]_{(i=1,\dots,L)}^T = [f^u(u_1^k, v_1^k), \dots, f^u(u_L^k, v_L^k), f^a(b^k)]^T. \tag{2.13}$$

Since we consider the scenario where only one BS in the ON status, $f^a(u^k)$ is still a vector of all zeros, except in the position corresponding to the BS in the ON status.

Cost per time-step

The cost at each time step is defined here as the total energy consumption required to provide the minimum power level to each of the mobile users in the network by the BS in ON status.

Denoting the total energy consumption as $E_{\text{in}}^{\text{total}}$, we write

$$E_{\text{in}}^{\text{total}} = \{E_{b_k}^{\text{nr}} + \sum_{i=1}^{L} E_{b_k,i}^{r}\} + \begin{cases} 0, & \text{if } b_k = m_k \\ E_{b_k}^{\text{ON}} + E_{m_k}^{\text{OFF}}, & \text{otherwise} \end{cases}, \tag{2.14}$$

where $E_{b_k,i}^{r}$ is the radiation energy consumed by the active BS b_k to serve user i.

2.3.3 Multi-user multi-ON formulation

In this scenario, we need to modify the system states and energy consumption. In addition, the actions as well need to be modified because now more than one BS can be turned ON at each time step k.

System states

Because a multi-user scenario is considered in this section too, the user dynamics segment of system states (u^{k+1}) remains the same as that of the previous case. However, the part of system states that represents BS status is now different as we consider more than one BS in ON state. Thus, the vector f^a now contains more than one nonzero component. At each time step, the nonzero components correspond to the activated BSs.

Actions

Because we consider that more than one BS can be turned on at each time step, we modify the definition of actions accordingly. Notice that so far nothing has been explicitly said about BS and network capacities (because, for simplicity of formulation, we only allowed one BS to be in the ON status). However, now we need to determine how many BSs are required to be turned on to have enough capacity. One way to take capacity into account (which is what we do in our simulations) is to predetermine a maximum number of users that each BS can accommodate. So, for example, if there are 20 users, and the maximum number of users that each BS can serve is 5, then we need to turn on at least 4 BSs. In this case, we say that the capacity of each BS is 5 users. The decision to

turn on each BS still depends on the positions and velocities of the active users in the network, in addition to the current state of the BSs. The definition of the capacity of any communication system is firmly tied to the multiple access (MA) technique employed in the system. Because 5G has a number of MA candidates, we choose to define the capacity in terms of space division multiple access (SDMA). This allows the definition of the capacity to be easily extended by "plugging in" any of the MA candidates. For example, we can extend our definition of the capacity to include orthogonal frequency multiple access (OFDMA), which is one of the MA techniques adopted in many modern wireless systems, like WiFi and 4G LTE (combined with time slices to form the 4G LTE resource blocks). In 5G, the MA technique is most likely to be a combination of SDMA with other MA candidates [3], [30]. The need for high directivity to compensate for the high energy losses associated with millimeter waves and the promised performance of massive multiple-input-multiple-output (MIMO) technology highlights the choice of SDMA.

State-transition law

For consistency with the changes we made to the system states, we append the term $f^a(u^k)$ as redefined in the system states for this scenario, to the u^{k+1} part of the state-transition law defined by equation (2.11).

Cost per time-step

The cost per time-step here is the total energy consumption required to provide the minimum power level at each of the mobile users in the network by all the active BSs in the network Thus, we can write the total energy consumption ($E_{\text{in}}^{\text{total}}$) as

$$E_{\text{in}}^{\text{total}} = \{\sum_{m=1}^{M} I_{ON}(m) E_{\text{in}}^{\text{total}}(m)\} + E_{b_k \setminus m_k}^{\text{ON}} + E_{m_k \setminus b_k}^{\text{OFF}}, \tag{2.15}$$

and,

$$E_{\text{in}}^{\text{total}}(m) = E_m^{\text{nr}} + \sum_{i=1}^{l_m} E_{m,i}^{r}, \tag{2.16}$$

where $I_{ON}(m)$ is the indicator function that determines the ON/OFF status of BS m, $E_{\text{in}}^{\text{total}}(m)$ is the "operational" energy consumption by BS m, which is comprised of two parts: the non-radiation energy cost E_m^{nr} and the radiation energy cost $\sum_{i=1}^{l_m} E_{m,i}^r$, where $l_m \leq$ maximum BS capacity (in number of users as defined above) is the number of users served by BS m and $E_{m,i}^r$ is the radiation energy required by BS m to serve user i. Note that at each time k, $I_{ON}(m) = 1$ if and only if $m \in b_k$. As now more than one BS can be either turned ON or OFF at each time step k, we use the terms $E_{b_k \setminus m_k}^{\text{ON}}$ and $E_{m_k \setminus b_k}^{\text{OFF}}$ to account for the transition costs for both subsets of BSs from the OFF to the ON states and vice versa; $E_{b_k \setminus m_k}^{\text{ON}}$ denotes the transition energy to the ON states consumed by the subset of BSs $b_k \setminus m_k$ at time step k, and $E_{m_k \setminus b_k}^{\text{OFF}}$ refers to the transition energy to the OFF states consumed by the subset of BSs $m_k \setminus b_k$ that were ON and now turned OFF at time step k.

2.4 MDP Solution

Many algorithms exist to solve MDP problems, such as value iteration and policy iteration. However, in this work, we limit our attention to a brief introduction of policy rollout as an approximation method to the policy iteration solution of our MDP.

2.4.1 Policy rollout algorithm with modified action space

Policy iteration is one of the widely studied algorithms to solve MDP problems. The algorithm works by alternating between two steps, policy evaluation and policy improvement [16], [17]. For our type of problem, the state space is naturally very large. Representing and then iterating on a policy generate a huge computational burden for problems with large state spaces. This makes policy iteration very difficult to implement, especially for real-time control problems. To overcome this problem, an approximation method known as policy rollout is utilized. In this section of the chapter, we introduce our implementation of the rollout algorithm. We start by presenting a typical implementation in the first part of this section. In the second part, we introduce a modified version of the algorithm. We modify the action space to improve the efficiency of the algorithm and make it feasible and beneficial from a practicality perspective.

Policy rollout algorithm

This approximation method was introduced in [61], and further explained among other approximations in [16], [17], and [15]. In rollout, a policy is not explicitly constructed as in policy iteration. Instead, a base (candidate) policy according to some reasonable heuristic is defined. We call this policy μ_{base}. Now referring to equation (2.3), the optimal cost-to-go J^*_{H-1} is replaced by $J^{\mu_{\text{base}}}_{H-1}$ (note that g and J are the standard notation for immediate cost and cost-to-go, respectively, in MDPs, but keep in mind that our cost function is defined in terms of energy). Thus, the resulting equation incorporating the base policy can be written as,

$$Q^{\mu_{\text{base}}}_H(s_0, b) = g(s_0, b) + E[J^{\mu_{\text{base}}}_{H-1}(s_1)|s_0, b], \tag{2.17}$$

where the rollout policy μ is defined by

$$\mu(s_0) = \arg\min_{b \in U} Q^{\mu_{\text{base}}}_H(s_0, b). \tag{2.18}$$

To implement the rollout algorithm, we compute the output of the policy at each time step. To approximate the Q-value, we use Monte Carlo sampling. Fig. 2.4 illustrates the action selection process in rollout. Comparing the left block of Fig. 2.4 to that of Fig. 2.3, we can see that in rollout, the Q-value calculator is replaced by a Monte Carlo sampling block. The approximation of the Q-value produced by Monte Carlo sampling is fed to the optimization algorithm. The selected action is then fed back to the Monte Carlo sampling block as the system evolves. We can dismantle the process of computing the Q-value into two parts: the first part is the computation of the immediate cost (which, in general, can be easily computed in a straightforward manner), and the second part is the calculation of the expected cost-to-go (which is generally more challenging and computationally demanding). Thus, it is sufficient, in general, to approximate the second part in order to be able to approximately calculate the Q-value. In rollout, this approximation of the Q-value is based on Monte Carlo sampling of the base policy. More specifically, we generate multiple independent sampling runs of the base policy (starting at the current state and for a given

candidate action) and use the averaged sampling output as the approximation of the expected cost-to-go. Rollout dramatically reduces the computational complexity of policy iteration by employing "a one-step lookahead." This is crucial for the implementation of real-time control. It has been established that the policy defined by equation (2.18) performs at least as good as its underlying base policy [16], [15]. This result is due to the fact that rollout leverages the policy improvement feature of policy iteration.

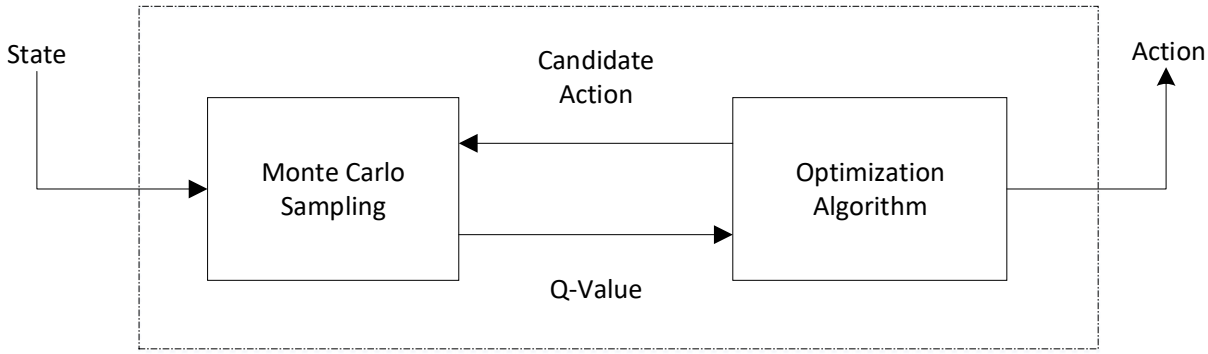

Figure 2.4: Action selector in rollout algorithm.

As mentioned above, the rollout algorithm involves incorporating a base policy, typically a heuristic based on domain knowledge. The base policy is used as a surrogate to evaluate the one-step cost at each time step in the Monte Carlo simulation described above. In our work, the base policy heuristic that we use is the greedy (myopic) heuristic, i.e., the base station selected is simply the one with the lowest immediate (one-step) energy consumption, given by equations (2.9), (2.14), (2.15), and (2.16) (it is worth mentioning that the rollout method *per se* does not specify anything about the choice of the base policy; it is here our responsibility as the algorithm designers to make an appropriate choice of the heuristic according to wireless communication domain knowledge). We use the base policy above in our rollout algorithm to approximate the cost-to-go by approximating the Q-value over the sample paths produced by the Monte Carlo simulation. The reader should be careful not to confuse the base policy with the rollout policy. The

base policy is greedy, but the policy resulting from our rollout algorithm is *not* greedy—it accounts for the impact of each action on the future. The rollout algorithm is summarized in Algorithm 1.

Algorithm 1: Rollout algorithm

Input: Current state s_k
Output: Selected base station b_k
Set base station $b_k = \arg\min_b Q_{rollout}(s_k, b)$
Output b_k
end algorithm
function $q = Q_{rollout}(s, b)$
Input: s, b
Output: q
Total_Cumulative_Cost = 0
for sample = 1, . . . , maxSample
Simulate system under base policy starting at state s for H time steps with initial base station selection b
Record E_{in} at each time step, where E_{in} = one-step cost (equations (2.9), (2.14), (2.15), and (2.16))
Set Total_Cost(sample) = cumulative E_{in} over H time steps
Total_Cumulative_Cost = Total_Cumulative_Cost + Total_Cost(sample)
end for
Output $q = \frac{\text{Total\_Cumulative\_Cost}}{\text{maxSamples}}$
end function

Modification of action space

5G networks will have an extreme level of small cell densification that has never been seen before in all previous generations of cellular networks. This is a crucial part of 5G networks to address the demand on capacity, especially in hot-spot areas, with unseen use cases. The typical implementation of rollout introduced in the previous part is often not practically feasible with this level of densification. It takes a prohibitively long time to select an optimal action at each time step due to the huge action space. Hence, we deviate from this typical implementation by modifying the action space. We accelerate the algorithm utilizing a heuristic to shrink the action space. This tremendously improves the performance of the algorithm, while still provides significant energy savings, as we will see. To this end, we suggest the following heuristics.

First, at each time step, we consider only the most promising actions by restricting the action search space to the second tier of neighboring BSs. Of course the more tiers of neighbors we include in the candidate action space, the higher the energy savings, but the longer the run time will be. In our situation, we argue that the two-tier neighbor level is a good choice as a balanced trade-off between energy savings and run time.

Recall that the action space is defined as $B = \{1, \ldots, M\}$, and $b_k \in B$ is the action at state S_k for M BSs. If we define the action space as the available controls at state S_k (available as heuristically modified above), then we can write it in the form $b_k \in B(S_k)$: $B(S_k) = \bar{B} \subseteq B$. Thus, according to our modification, equation (2.18) can be replaced by

$$\mu(s_0) = \arg\min_{b \in \bar{B}} Q_H^{\mu_{\text{base}}}(s_0, b). \tag{2.19}$$

In our experimentation, the number of elements in $\bar{B}$ is only 25 (second-tier neighbors plus the BS in ON status, replacing the whole number of BSs in the network).

Second, to cut down on the number of computations even more, we cluster users at the beginning of a multiple of the sampling times and examine combinations of the least number of BSs sufficient to accommodate the active users in the network. For example, if we assume that all BSs have equal capacity of 5 users each, it is not worth examining a situation in which 50% out of, say, 600 BSs are turned ON to accommodate 10 users. Alternatively in this case, it makes more sense to try two-BS combinations to provide the required capacity to this number of active users.

2.5 Simulation

2.5.1 Simulation setup

A number of mobile users is assumed to be moving in the cellular network coverage area according to the mobility models given by equation (2.8), equation (2.11), and equation (2.12). We employed a wrap-around technique in our simulation. So whenever a user reaches any of the borders of the simulation area at one side, the user enters the simulation area from the opposite

side. This allows for a longer simulation run. We assume that power control is active on the BS side of the communication link, while no power control is assumed on the user side. Thus, a BS is capable of (and responsible for) extending its coverage to provide a QoS signal level. In our simulation, all mobile phones are assumed to have antennas with gains of 0 dBi, and all BSs are assumed to have antennas with gains of 5.5 dBi. On the other hand, all mobile phones are assumed to have RF chain losses of 40%, whereas all BSs are assumed to have RF chain losses of 55%; RF chain losses here are due to antenna and amplifier losses in both the mobile phone and the BS sides of the communication link.

We examine the performance of our proposed rollout algorithm in comparison to algorithms from the literature under different combinations of parameters. The benchmarking schemes are: the no-switching scheme, CDS, and CDS + MSC (introduced earlier and explained again below). The energy savings achieved by the no-switching scheme represents an upper bound on the energy savings achievable by the algorithms and schemes that do not include switching energy cost in BS control. These schemes are introduced in Section 2.1. The other two benchmarking schemes are taken from reference [30]. The no-switching scheme here refers to a scheme that includes the non-radiation and the radiation energy consumptions of the BSs in the selection of BS control actions, while not considering ON/OFF BS switching energy costs. We briefly introduced CDS and CDS + MSC in Section 2.1. Closest Distance Strategy (CDS) selects the BSs based on the distances between BSs and mobile users. The BSs that are closer to the mobile users are turned ON. This scheme excludes both the non-radiation energy consumption and the switching energy cost from the action selection. Minimum Switching Cost (MSC) then solves the problem of minimizing switching energy cost given the solution attained by CDS. We compare the performance of our algorithm with the performance of the mentioned schemes under the effects of different parameters: path-loss exponents, different mobile speeds and different BS ON/OFF costs (the later two parameters together affect the energy cost incurred due to BS switching), and different non-radiation energy costs. A summary of the examined simulation parameters and their values is given by Table 2.1.

Table 2.1: Simulation Parameters

Parameter	Value
Mobile Antenna Gain G_m	0 dBi
BS Antenna Gain G_{BS}	5.5 dBi
Mobile phone RF chain losses Loss_m	40%
BS RF chain losses Loss_{BS}	55%
Horizon H	100 T_s
Path-loss Exponent α	3, 3.5, 4
$E_{m_k}^{\text{ON}}$	$(10, 8, 5, 2)J$
$E_{m_k}^{\text{OFF}}$	1 $(10, 8, 7)J$
Non-radiation (static) energy E_m^{nr}	1 $T_s \times (10, 15, 20, 25, 35)W$
Number of BSs M	121
BS Capacity	5 users
Network Capacity	605 users
BS Dimensions	$100m \times 100m$
Maximum interference temperature	-60 dBm
Noise power spectral density (N_0)	- 174 dBm/Hz
Bandwidth for each user (B)	180 KHz
Minimum data rate per user	512 Kbps

We investigate the performance of the algorithm under three different path-loss values: α = 3, 3.5, and 4. Our goal here is to examine the impact of the propagation environment (urban, suburban, foliage, etc.) on our algorithm. It is well known that many factors contribute to the overall path-loss: T_x-R_x separation distance, diffraction, refraction, and absorption, to name a few. Some propagation-destructive mechanisms, such as absorption, become even more amplified at higher frequencies (millimeter waves will form a significant part of the overall 5G spectrum). The sampling time T_s can be fraction or a multiple of a minute, depending on the scenario. We also consider a horizon H of $10T_s$.

We implemented the rollout algorithm, which is a sampling-based algorithm. To approximate the Q-value, we employed Monte Carlo sampling; our sampling was driven by the models described in the problem formulation subsection of this chapter.

2.5.2 Preliminary illustrations and the one-user case

Fig. 2.5 illustrates the sequential BS control of our algorithm. At each time step, a BS is turned ON to provide the required coverage to the user. To facilitate visualization, in Fig. 2.5 we only show the one-user one-ON scenario, with only four user trajectories, and without showing the sample paths. In our simulation, however, we considered the multi-user multi-ON scenario and used a large number of trajectories and sample paths (although the rollout algorithm only requires enough number of samples to reflect the adequate ranking of decisions [15]). Fig. 2.6

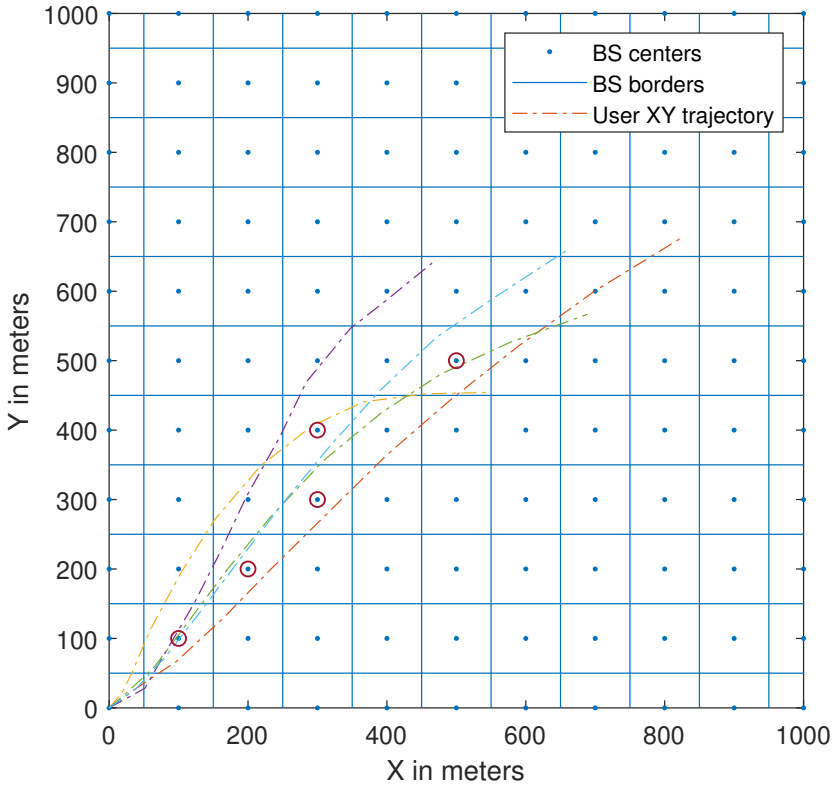

Figure 2.5: Sequential BS control (circles indicate BSs in ON status at each time step).

shows the average energy consumption for the one-user one-ON case, comparing our scheme with the always-ON scheme (i.e., no ON/OFF control, following the method adopted in the literature to calculate percentage energy savings [24], [30], and [27]). Notice that this figure is not intended

to be an evaluation of our algorithm. Indeed, Fig. 2.6 is only an illustration of energy savings quantification and optimization over a specified finite time horizon. From the figure, we see that the largest amount of energy consumption occurs at the initial state of the system. This is due to the fact that a user can be anywhere relative to the BS(s) in the ON status (also notice here that initially there can be more BSs in the ON status than what is optimally needed considering energy saving). Consequently, this can lead to unnecessary energy consumption. The figure shows how our algorithm optimizes the energy consumption and provides significant energy savings over the horizon.

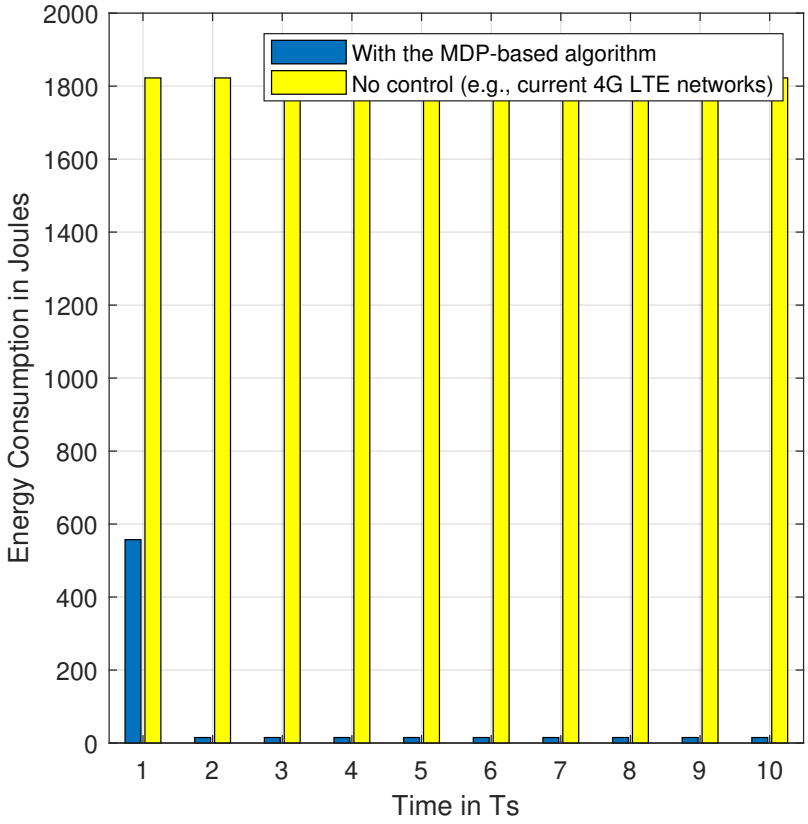

Figure 2.6: Expected energy consumption over the horizon.

While it might seem somewhat trivial to compare an ON/OFF switching scheme with an always-ON scheme, things are not as simple as they appear. In particular, in certain situations,

an ON/OFF switching scheme might have even worse energy consumption than an always-ON scheme. We will explain this by considering [62]. The work in [62] investigates energy efficiency in vehicular networks by cooperative BS sleep scheduling. The authors of this paper introduce a scheme for energy savings in 1-D based wireless networks formed by vehicles on a highway. Energy savings in the proposed scheme is achieved by switching between active and sleep states depending on the density of vehicles measured in $vehicle/Km$ and the distance between vehicles. The model is rather simple and its applicability is limited to 1-D based networks. However, an interesting result (which applies to any ON/OFF switching scheme) is that when designing ON/OFF switching schemes there is always a threshold of switching beyond which no further savings is possible. Moreover, a scheme not only becomes useless but can become harmful by introducing more energy consumption than an always-ON scheme. This can happen when the number of ON/OFF switchings becomes excessively large. As we will see in the next subsections, when we evaluate the performance of our algorithm and the other schemes, the energy savings can decrease and even hit zero. In this case, we suggest temporarily pausing the control schemes when savings go down to zero, thus avoiding useless computations and/or excessive ON/OFF BS switchings.

Now we take a "microscopic" look at the action selection to explain the importance of considering energy costs in our proposed way (i.e., separating the ON and the OFF BS energy consumption) and how it improves the action selection. It is easier to visualize the behavior of our algorithm versus the benchmarking schemes in the the one-user one-ON environment (the results of the multi-user multi-ON case are presented in the next section). To this end, we run the following experiment. Referring to Fig. 2.5, assume that the non-radiation component of the power consumption is equal for all BSs in the neighborhood of the BS centered at $(100, 100)$ and that $E_{m_k}^{\text{OFF}}$ for the mentioned BS is $2J$. Now assume that $E_{m_k}^{\text{ON}}$ for the BS centered at $(100, 200)$ is $5J$ and that of the BS centered at $(200, 200)$ is $2J$. Also assume that a mobile user was at the XY coordinates $(190, 140)$ in the previous time step and was served by the BS centered at $(100, 100)$. Further assume that the user is at the XY coordinates $(190, 200)$ in the current time step. The no-switching scheme will select the BS centered at $(100, 200)$, whereas according to the heuristic

driving our rollout algorithm, the BS centered at $(200, 200)$ is selected because it is less "expensive" to turn ON when switching energy consumption is considered. For the same experiment, the CDS scheme selects $(100, 200)$ and later minimizes the consumption by MSC. However, even MSC does not take the information about the $E_{u_k}^{\mathrm{ON}}$ into consideration when selecting the BS (recall that the first step of the CDS + MSC, myopically selects the BS depending on the distance between the mobile and the BS; thus, there is no explicit trade-off between the switching cost and the operational cost of the BS as the optimization is done in two steps).

The work in [27] considers exploiting user movement patterns to maximize energy savings; the authors of [27] reported maximum savings in energy consumption of 36%. Obviously, our algorithm (and the benchmarking algorithms too) offers (offer) more savings than 36%. We exclude [27] from further direct comparison with our work in the simulation section. The next subsections are devoted to the evaluation of our algorithm in comparison with other schemes under the effects of different parameters.

2.5.3 Multiuser case

We now turn to the case of multiple users (multi-user multi-ON). We will consider the effects of three important system parameters: path-loss exponent, ON/OFF switching costs, and non-radiation power.

We analyze the performance of our algorithm in light of equations (2.9), (2.14), (2.15), and (2.16). Recall that these equations summarize the trade-offs that are automatically and systematically performed by the base policy in our rollout algorithm. It is clear from Fig. 2.7 through Fig. 2.12 that our algorithm outperforms the three benchmarking algorithms under all the scenarios and parameter combinations explored here and presented by these figures. In the next subsections, we introduce our simulation results and performance analysis of our algorithm against the benchmarking schemes for various parameters. We study the effects of these parameters: the path-loss, the ON/OFF BS switching energy costs, and the non-radiation energy costs.

Effect of path-loss exponent

The path-loss exponent (α) is an important parameter that can change energy consumption profile in a wireless network environment. The role of the path-loss exponent is to represent the behavior of the RF signal as it propagates through different environments, ranging from the theoretical free space environment to the most obstructed environments. Table 2.2 below shows typical α values for different environments [63].

Table 2.2: Path-loss exponent for different environments

Environment	Path-loss exponent (α)
Free space	2
Urban area cellular radio	2.7 to 3.5
Shadowed urban cellular radio T_s	3 to 5
In building line-of-sight	1.6 to 1.8
Obstructed in building	4 to 6
Obstructed in factories	2 to 3

Fig. 2.7, Fig. 2.8, and Fig. 2.9 show energy savings for different numbers of users in the network under three different values of the path-loss (α), namely, $\alpha = 3$, $\alpha = 3.5$, and $\alpha = 4$. In these three figures, all parameters other than α are kept at fixed values taken from Table 2.1 (this allows us to focus on the performance analysis of our algorithm and evaluate the energy savings under the effect of different α values). As we can see, the percentage energy savings goes down as the number of users increases. This is unsurprising. Perhaps more unexpected is the result that the percentage energy savings goes down as the path-loss exponent goes up. Nonetheless, we can see that our algorithm offers a significant amount of energy savings even under aggressive propagation environments. Notice that for a given $T_x - R_x$ separation, as the path-loss exponent increases the radiation energy consumption goes up. Thus, the contribution of the radiation energy to the overall cost function increases. As mentioned above, for Fig. 2.7, Fig. 2.8, and Fig. 2.9, all parameters other than path-loss are equal. Under these conditions, this results in more frequent BS switchings,

when $\alpha = 4$, as the mobile users now traverse less distance to trigger BS switching as compared to the case when $\alpha = 3.5$ and the case when $\alpha = 3$.

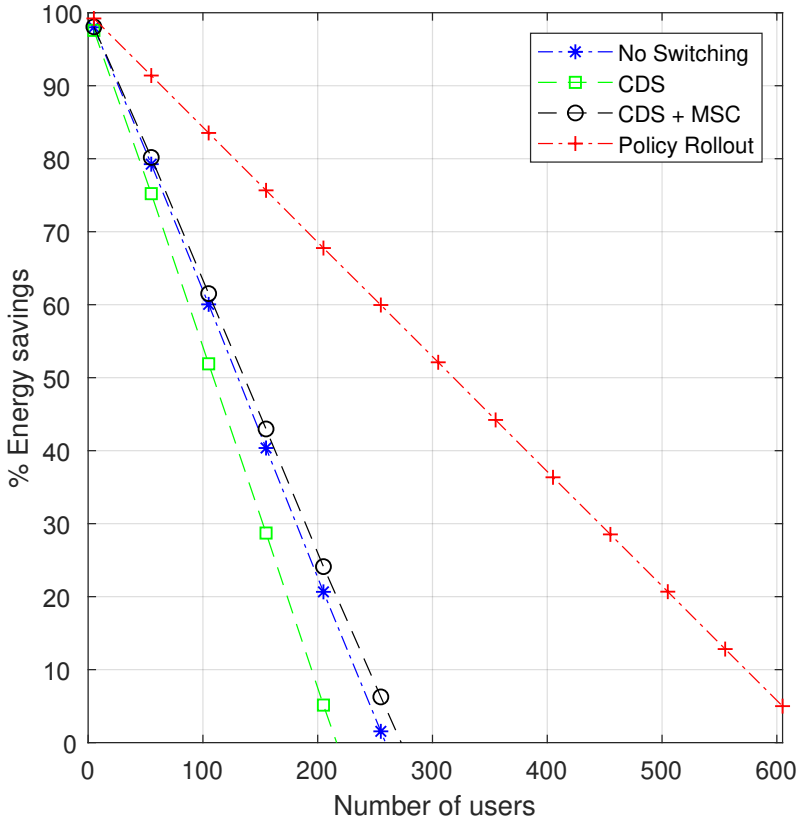

Figure 2.7: Expected energy savings as a function of the number of users for $\alpha = 3$.

Effect of ON/OFF switching energy cost

Here, we examine the performance of our algorithm by varying ON/OFF switching energy costs. To this end, we indirectly alter the frequentness of BS switchings by controlling the speeds of the mobile users and keeping all other parameters equal among the different scenarios. By controlling the speeds, we can either increase or decrease how often ON/OFF BS switchings happen. Fig. 2.10 and Fig. 2.11 show the performance of our algorithm and the benchmarking schemes under the same parameter values as that of Fig. 2.9, except with different speeds of the mobile users. On average, the speeds in Fig. 2.9 are double that in Fig. 2.10 and four times that in Fig. 2.11. Ac-

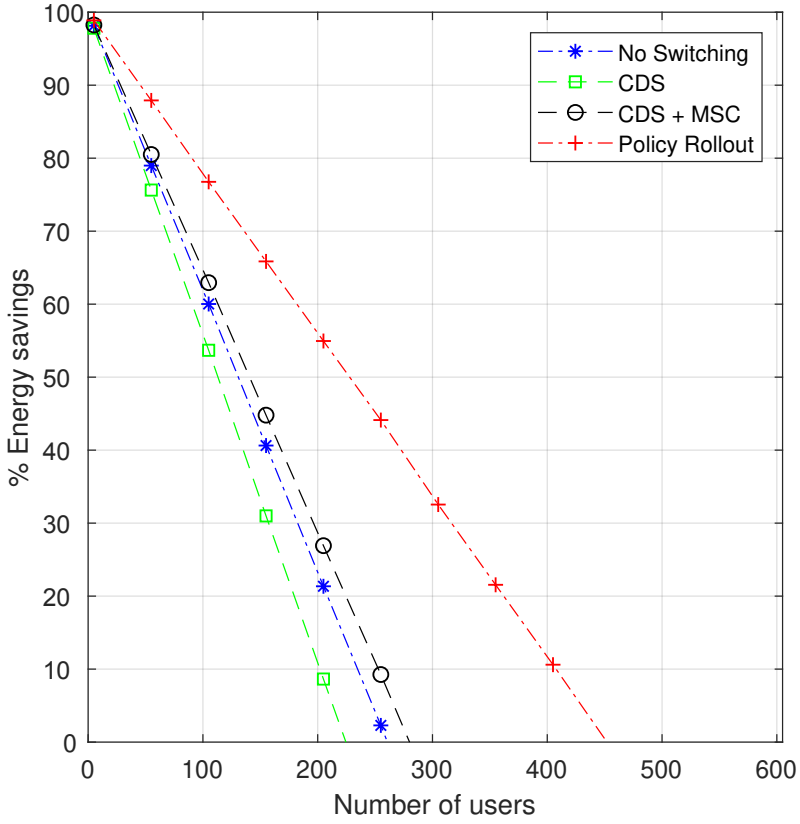

Figure 2.8: Expected energy savings as a function of the number of users for $\alpha = 3.5$.

cordingly, this results in more frequent number of ON/OFF BS switchings in Fig. 2.9, less frequent ON/OFF BS switchings in Fig. 2.10, and the least frequent ON/OFF BS switchings is for the scenario in Fig. 2.11. We can see that for the three figures, there is a decrease in energy savings as the speed increases (i.e., more frequent ON/OFF BS switchings). To highlight the significance of explicitly considering the ON/OFF energy consumption, we specifically compare our algorithm with the no-switching algorithm and the CDS algorithm. Obviously, the worst performance is for CDS for the three different speeds (recall that CDS does not consider switching cost beside the fact that it does not consider the non-radiation energy consumption in minimizing energy consumption). At the highest speeds, the second worst performance is for the no-switching algorithm. The best performance is achieved by our algorithm as it takes the switching energy into consideration when performing the trade-off between energy consumption due to BS switching and the other sources

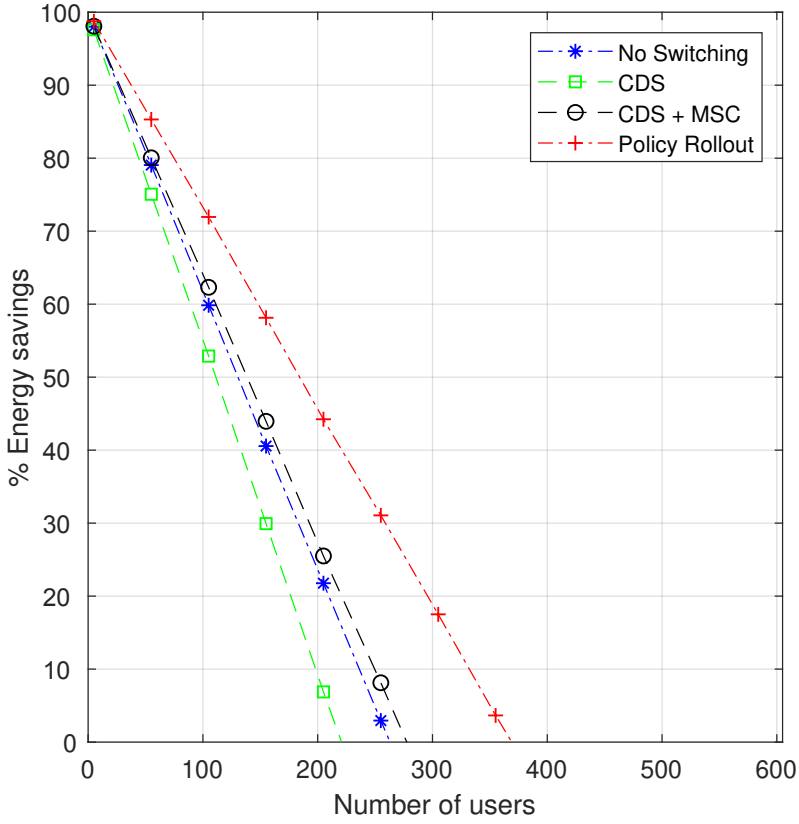

Figure 2.9: Expected energy savings as a function of the number of users for $\alpha = 4$.

of energy consumptions as described by equations (2.9), (2.14), (2.15), and (2.16). Notice that for Fig. 2.11, the no-switching scheme outperforms CDS + MSC as the contribution from BS ON/OFF switchings becomes less significant for lower speeds.

Effect of the non-radiation power

To examine the effect of this parameter on the performance of our algorithm, we replace twenty BSs in the network with BSs that have higher non-radiation power consumptions. The purpose of this experiment is to amplify the effect of the non-radiation power to be able to examine the impact caused by this parameter. We randomly place the less-efficient BSs. Recall that the non-radiation power consumption (together with the switching energy costs considered in the previous subsection) are unavoidable BS hardware imperfections. These energy consumption values can be reported by the vendors or measured during the commissioning and testing stages when new BSs

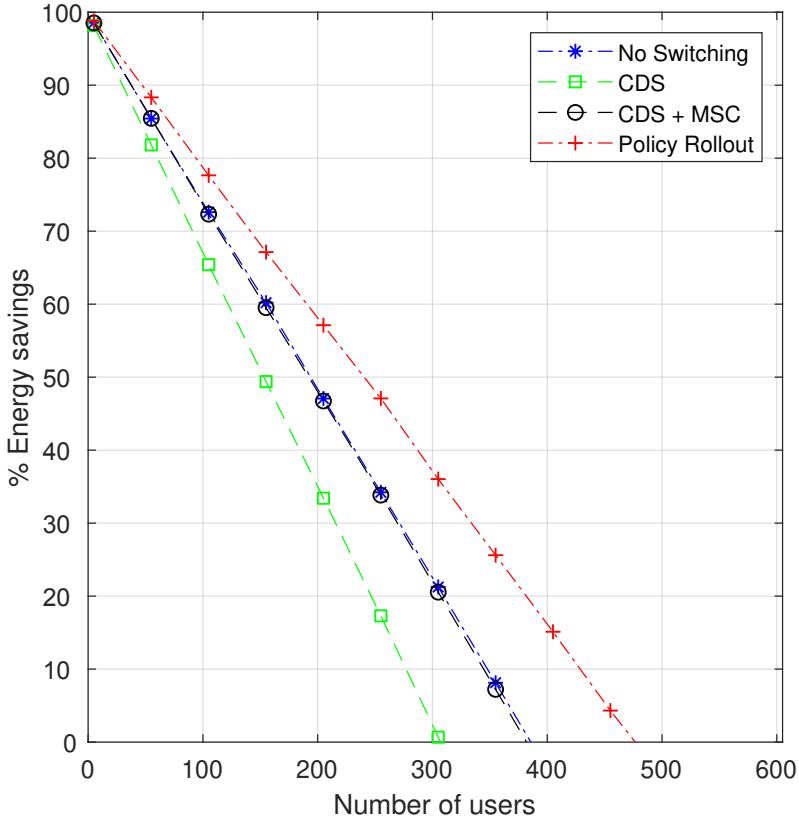

Figure 2.10: Expected energy savings as a function of the number of users for $\alpha = 4$ and medium mobile speeds (speeds here are half that in Fig. 2.9).

are added to an existing wireless network (or when deploying a new wireless network). Recall that CDS and CDS + MSC do not consider the non-radiation power in the action selection. On the other hand, our algorithm and the no-switching scheme both consider the non-radiation power consumptions in action selection. Fig. 2.12 depicts the performance of the different schemes when we introduce the twenty less-efficient BSs. Fig. 2.9, on the other hand, shows the performance of the different schemes under the same conditions but without the replacement of the twenty original BSs. We can see from both figures that when the twenty less-efficient BSs are inserted into the scenario, the no-switching scheme outperforms the other two benchmarking schemes. At the same time, we can see that the energy savings of our algorithm have significantly improved. In both arrangements, our algorithm outperforms all the benchmarking schemes.

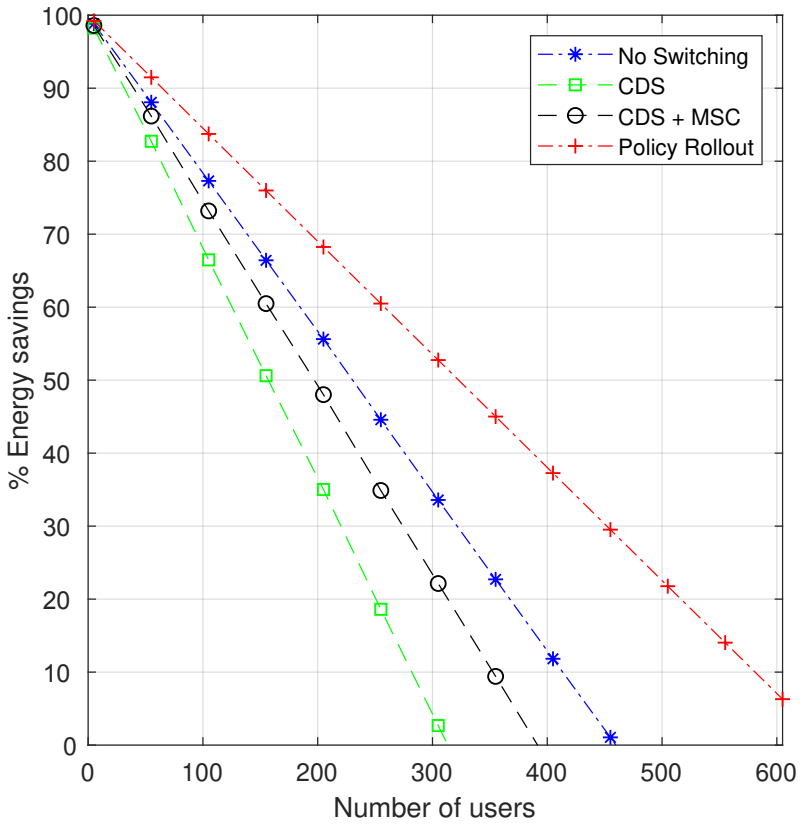

Figure 2.11: Expected energy savings as a function of the number of users for $\alpha = 4$ and slow mobile speeds (speeds here are one fourth that in Fig. 2.9).

Effect of computing and cooling

For the sake of completeness, we consider the effect of computing and cooling on the total BS energy consumption in 5G. Compared to current non-5G commercial cellular systems, the cell densification in 5G will reduce the energy cost of communication, but increase the computing cost because of the massive MIMO and beamforming techniques. Therefore, the computing and cooling costs will increase, and the associated equipment might be hard to switch ON and OFF frequently. Note that in the literature, it is common to assume that energy consumption is negligible (zero) when the BS transitions to the OFF/sleep state. However, the additional consideration that the computing and cooling equipment might be hard to switch ON/OFF frequently would apply to any BS ON/OFF scheme, and thus would reduce the upper bound on the achievable energy savings for all schemes, including the benchmarking schemes.

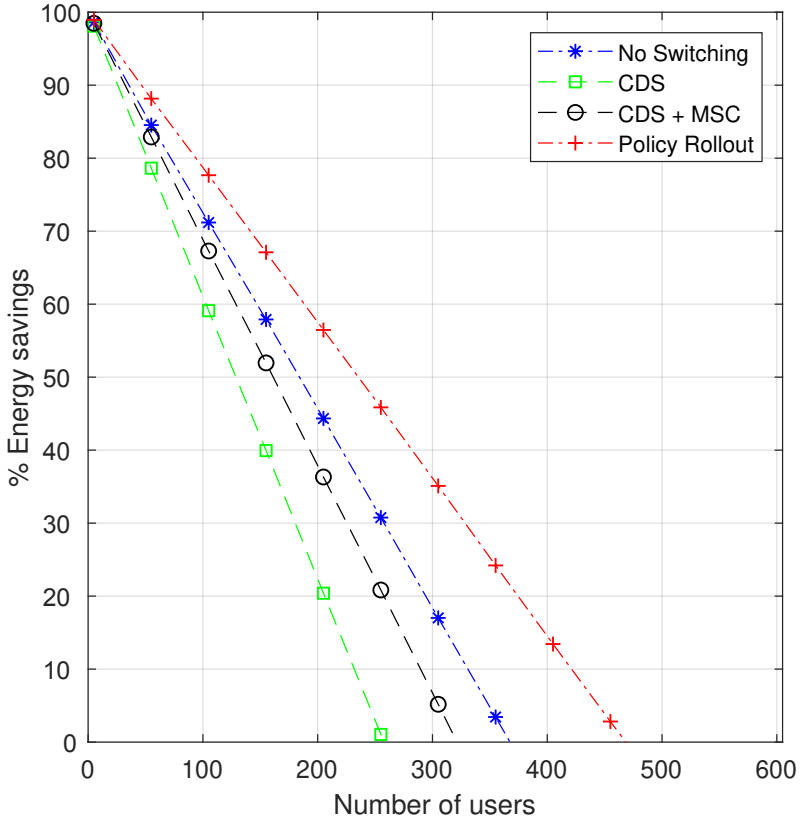

Figure 2.12: Expected energy savings as a function of the number of users for $\alpha = 4$. Twenty BSs are randomly replaced by less-efficient BSs that have higher non-radiation power consumptions.

Here we quantitatively account for the computing and cooling energy costs as parts of the non-radiation energy cost. We assume that the equipment for computing and cooling cannot be switched OFF. We evaluate two scenarios for the contribution of these two energy-consumption sources to the total non-radiation energy: 15% and 30%. Fig. 2.13 shows the performance of our algorithm and the top-performing benchmarking scheme (CDS + MSC) for $\alpha = 3$ when 15% and 30% of the equipment cannot be switched OFF. Obviously, our algorithm outperforms the benchmarking scheme. However, the energy savings are naturally lower than the ones in Fig. 2.7.

2.6 Conclusion

In this chapter, we introduced our design of an MDP-based algorithm for BS control. We designed a fast algorithm to facilitate real-time control of the BSs. This allows fast adaptation to user

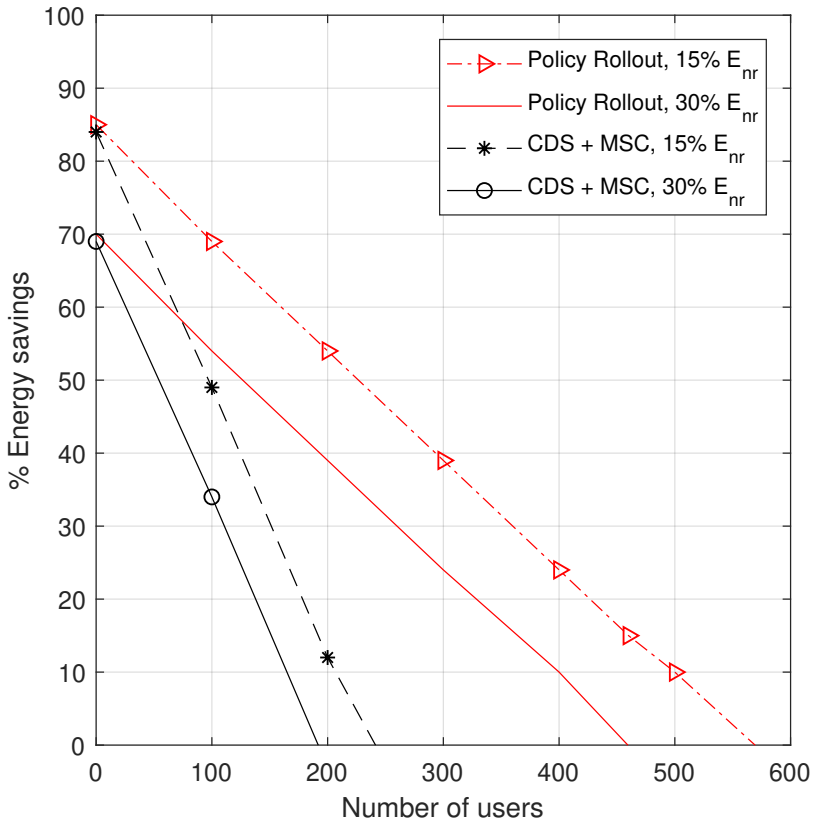

Figure 2.13: Expected energy savings as a function of the number of users for $\alpha = 3$. A percentage, as shown in the legend, of the equipment producing the non-radiation energy cannot be switched OFF.

location in the network to provide more energy savings, while providing QoS guarantees. For efficient implementation, we employed the rollout algorithm as an approximation method for MDP. The simulation results show the potential of our proposed solution by fostering significant energy savings without sacrificing QoS. An important feature of the suggested solution is scalability (for multi-user multi-ON scenarios). We started by introducing our solution to the smallest version of this problem (one-user one-ON). We presented a systematic and modular algorithm design that allows "plugging in" new models and features. We then scaled up our proposed solution to solve the problem for the multi-user multi-ON scenario. Possible future extensions are to consider information about user destination, and to use our algorithm with maps of real roads and highways. This increases the potential of using the algorithm and allows customizing its design. The performance of the algorithm can also be augmented by the utilization of the available support of location pre-

diction in LTE networks. As there is a growing interest in implanting sensor fusion in 5G networks, we envision the possibility of incorporating sensor fusion in our BS control action selection, with location information coming from different sources. It is possible to borrow some best practices form fleet management in location-based services as well.

Chapter 3

Wireless Jamming Mitigation for Multipath Routing Using Semivariance Risk Measures

3.1 Introduction

Jamming attacks represent a major threat to wireless communication networks. The ubiquity of wireless technologies has provided unparalleled levels of convenience to our everyday lives. While convenient, these technologies raise new concerns and impose new challenges on wireless network design. Because of the broadcast nature of wireless communication, combined with the availability of relatively cheap off-the-shelf software-defined radio (SDR) products, wireless networks have become more susceptible to attacks initiated at the physical layer of the network protocol stack [6], [4].

Jamming at the physical layer is a form of denial-of-service (DoS) attack in which the attacker interferes with the network operation by intentionally inducing radio-frequency (RF) interference in the wireless link, thus "jamming" the communication channel [6]. To be sure, there are other jamming attacks that can take place in the upper layers as well. For example, a router can be bombarded by a large number of packets to cause buffer overflow, resulting in a DoS in the forms of excessive delay or packet drop. We limit the scope of this chapter to jamming at the physical layer, i.e., RF jamming.

Network availability remains to be one of the main security requirements in virtually all modern wireless networks. Even the most sophisticated and the most prominent and widely accepted wireless cellular standards like 4G LTE Advanced Pro are still susceptible to security threats like jamming. Moreover, with the ever increasing adoption of cell phones and wireless-enabled gadgets, we will continue to be dependent on wireless technologies like Wi-Fi, ad-hoc networks, 4G LTE, and the emerging 5G NR to perform our daily tasks. Conceivably, the problem may become

more serious if these technologies are used for mission-critical communications. For example, in the United States, 4G LTE is proposed for a nationwide wireless broadband public safety network [4], [5].

Considering the threats mentioned above, and driven by the contemporary need for secure communication networks, there has been a flurry of research on jamming attacks and possible defensive strategies. The research on RF jamming spans various wireless standards, from Wi-Fi, WiMaX, and cellular networks (e.g., 4G LTE and 5G) to multipath ad-hoc networks, among others. The common concern is, although there are security improvements in today's wireless standards as compared to the older ones, today's wireless networks are still vulnerable to jamming attacks. Section 3.2 of this chapter is dedicated to describing these research efforts in more details.

The focus of research conducted in this area varies from revealing the vulnerabilities in available wireless networks, to introducing different solutions to counteract RF jamming. A straightforward way of defending a wireless network against jamming is implemented in the physical layer via spread spectrum and beamforming. The goal of these defensive techniques is to force the jammer to spend more energy to reach the same impact of the jamming attack. However, recent papers have shown the feasibility to perform intelligent jamming by incorporating cross-layer protocol error detection and correction.

In this chapter, we introduce our contribution to mitigating RF jamming. Specifically, we consider the problem of jamming-aware-multipath routing. Fig. 3.1 depicts a multipath routing network, with one source node and one destination node, in presence of an RF jammer. We propose a new security framework and use it to design a new optimal anti-jamming scheme. To the best of our knowledge, this is the first work to apply semivariance-based treatment to the problem of jamming, but also to security risks in general.

In this chapter, we lay out our new security framework based on semivariance as a measure of risk. To test the performance of our scheme based on this framework, we adopt the threat and network models from [9], [48]. We map the problem of jamming mitigation to that of the portfolio selection within the semivariance risk framework [21].

We summarize our main contributions as follows:

- We formulate the problem of jamming mitigation as a portfolio-selection problem. Together with [9] and [48], our work here is among the few efforts to apply a portfolio-selection treatment to the problem of jamming.
- In our problem formulation, we use a downside-risk cost function. Specifically, we use semivariance as a measure of risk. Our work is the first to exploit semivariance as a measure of risk in the context of security against jamming, and communication-network security in general.
- To the best of our knowledge, our work is the first to introduce downside risk and semivariance to the lexicon of telecommunications.
- We study semivariance problems and survey their solutions.
- We adopt and modify a semivariance approximation method—from economics and finance—and use it to develop our new scheme to solve semivariance problems in the context of RF jamming mitigation.
- We develop an efficient scheme for solving semivariance optimization problems. Efficiency is an essential feature for telecommunication applications, considering low latency and low computing power constraints (e.g., tactile Internet and Internet of Things).
- Our scheme provides a general approach to solving semivariance optimization problems, and can be used in other applications.
- Last but not least, we provide a useful survey of jamming problems and their solutions.

The rest of this chapter is organized as follows: In Section 3.2, we review research efforts on RF jamming, and highlight the similarities and differences relative to our work. In Section 3.3, we introduce some needed preliminaries. We review portfolio selection[5] within the variance and

[5]We use the terms portfolio selection and portfolio optimization interchangeably.

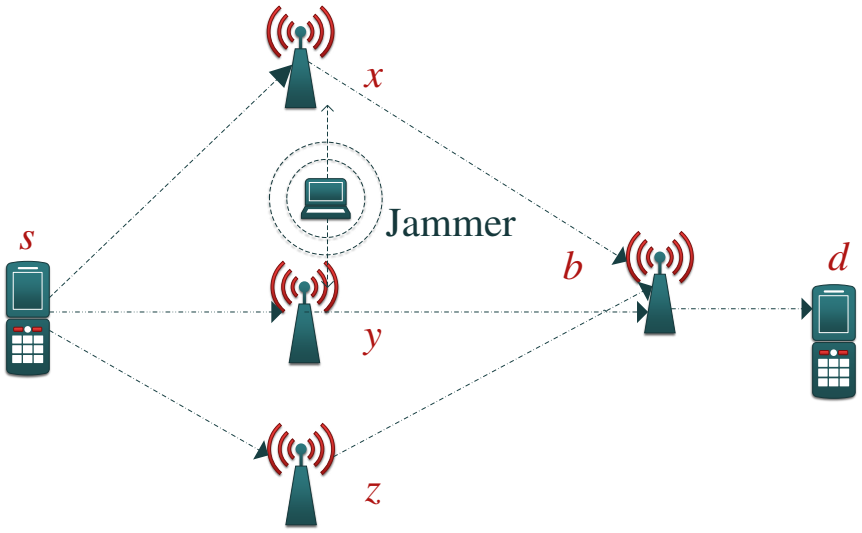

Figure 3.1: Pictorial representation of a multipath routing network, with one source node and one destination node, in presence of an RF jammer.

semivariance risk frameworks, summarizing the advantages and disadvantages of each approach. In Section 3.4, we introduce the threat and network model, and formulation of the jamming-mitigation problem within the semivariance risk framework. In Section 3.5, we describe our jamming-mitigation scheme based on approximating the problem by a quadratic program. Section 3.6 is dedicated to the simulation setup and results. We conclude the chapter in Section 3.7.

3.2 Survey of Related Work

Recently, there has been an increasing awareness of the risk of RF jamming owing to the increased reliance on wireless technologies as a last-mile connectivity solution. There is a vast literature on RF-jamming attacks and mitigation. In this section, we survey efforts in the literature to provide insights into the potential threats and defense techniques for this type of DoS attacks. Recently, there has been an increasing awareness of the risk of RF jamming, owing to the increased reliance on wireless technologies as a last-mile solution. Many research papers have been introduced in the literature that provide insights into the potential threats and mitigations of this type of DoS attacks.

3.2.1 Protocol-specific jamming attacks and mitigation

In this section we introduce efforts that consider RF jamming problems for specific wireless protocols.

The authors of [34] consider the problem of RF jamming of an IEEE 802.15.4-based wireless sensor network. The authors suggest a four-mechanism defensive MAC-layer protocol to mitigate stealthy jammers. They assume that jammers collect information about the network and adapt the RF jamming accordingly. The goal of the defensive mechanisms is to reduce the impact of the attack by hiding communication and misleading the search of the jammer. Despite its good performance, which is shown through experimentation with special-purpose hardware, this defensive solution has high implementation overhead.

In [35], two protocol-aware energy-efficient jamming mechanisms for IEEE 802.11 networks are proposed: Low data rate random jamming and adaptive data rate shot-noise jamming. By producing shot-noise pulses during tuned time intervals, both mechanisms reportedly achieve high energy efficiency and low probability of detection. The purpose of inducing shot-noise like interference by the jammer in [35] is to resemble the naturally produced shot noise,[6] and hence hide anomalies and reduce the probability of being detected.

The authors of [64] extend the work in [35] by modifying the proposed attacks in [35] to target GSM and WiMaX networks. The results show that GSM and WiMaX have better jamming resilience than IEEE 802.11. This is because both GSM and WiMAX use frequency-hopping spread spectrum to mitigate jammer-induced shot noise.

The work in [4] is one of the pioneering efforts in the identification of vulnerabilities in the PHY and MAC layers in 4G LTE. The authors comprehensively describe different uplink and downlink channels, and identify vulnerabilities in these 4G LTE channels. Additionally, the work in [4] suggests some metrics to evaluate the performance of jamming attacks on the control channels in the 4G LTE standard. These metrics are jamming-to-signal ratio on the level of the LTE resource

[6]Shot noise is a type of noise induced in electronics and RF devices due to the flow of charge carriers (electrons and holes) across semiconductors.

element and jamming-to-signal ratio on the frame level. The authors conclude their paper with recommendations for anti-jamming techniques as research directions. Additionally, the authors give some exemplary use cases. The authors of [5] conduct a study on 5G NR similar to that in [4]. They provide a detailed description of the 3GPP release 15, which is the defining document of the first and only accepted 5G standard at the time of press, namely, the 5G NR standard. There are many similarities between 4G LTE/LTE-A and 5G NR air interfaces. There are of course some modifications; nevertheless, 4G LTE and 5G NR will continue to coexist and inter-work for quite some time. RF jamming, and security concerns in general, will be equivalently relevant for both types of networks, at least for the coming few years.

Rao et al. [65] introduce an open-source SDR platform as a testbed for research and experimentation of RF jamming attacks and mitigation in 4G LTE networks. The authors reported the results of their experiments on jamming of 4G LTE downlink control signaling. Similar to the work in [4], the objective is to identify susceptibilities in this standard to RF jamming. Moreover, the authors of [65] introduce an additional metric to evaluate jamming attacks: The ratio between jamming power and the downlink shared-channel power.

The work in [36] investigates vulnerabilities of the 4G LTE uplink control channel to RF protocol-aware jamming. The authors suggest two defensive methods to detect RF jamming. The first method is RF-jamming detection by monitoring for excess physical uplink control channel energy. The second method is detecting an abnormal amount of physical uplink control channel errors. The authors of [36] also suggest some possibilities for RF-jamming mitigation. For example, the authors suggest using more robust modulation and coding at the cost of throughput when RF jamming is detected. Another example is a mitigation strategy based on dynamic physical uplink control channel sizing. Because the size of the physical uplink control channel is a parameter of the eNodeB, the physical uplink control channel can be expanded to use more resource blocks if an RF jamming attack is detected.

The authors of [66] provide an interesting perspective of jamming in 4G LTE networks in their proof-of-concept paper. The authors overview a series of local and effective jamming attacks

that strengthen basic jamming. The authors conclude their paper with recommendations for anti-jamming techniques as research directions. Below, we provide two interesting examples from [66].

The authors of [66] emphasize that in many scenarios, jamming a larger area/size is not the most important factor. Rather, achieving a very specific and localized goal for economic or military advantage is the key element; a local jamming attack targeting a cell serving the New York Stock Exchange is a very relevant scenario in this context.

Another interesting example from [66] showcases the importance of localized impact of jamming regardless of how large or small the attacked area/size is. Often in cyber attacks, the purpose is to steal private information. If RF jamming is used in such scenarios, the main goal is not complete denial of service. Instead, RF jamming is used as a tool to knock a connected device off a secure network and force it down to an insecure radio access network to pursue further attacks and data theft.

The recent work in [5] builds on that of [4] and applies a similar treatment of jamming evaluation to the emerging 5G NR networks. The authors of [5] provide a detailed description of 3GPP release 15, which is a defining document of the first and only accepted 5G standard at the time of [5]; namely, the 5G NR standard. They use information about 5G NR control channels to gain insights into the vulnerability of this wireless standard to RF jamming.

There are many similarities between the 4G LTE and 5G NR air interfaces. There are of course some modifications; nevertheless, 4G LTE and 5G NR will continue to coexist and interoperate for quite some time. RF jamming, and security concerns in general, will be equally relevant for both types of networks, at least for the coming few years.

The work in [67] considers jamming in wireless sensor networks. A fully distributed network protocol is designed based on mutually orthogonal Latin squares to mitigate jamming. When a jamming attack is detected in the network, data transmission is rapidly rescheduled around jammed regions using multiple communication channels.

3.2.2 Jamming in multipath routing: Uncorrelated path failures

We now describe the efforts in [37], [38], [39], and [68], which consider the problem of jamming and network availability in multipath routing networks. However, for the sake of clarity, we start this section by explaining some important terminology related to assumptions in these papers.

Given a source node s and destination node d, two paths through the network from s to d are said to be *node-disjoint* (or *link-disjoint*) if these paths do not have common nodes (or links) [42], [40]. Referring to Fig. 3.1, we can see that the paths $p_1 = \{(s,x),(x,b),(b,d)\}$, $p_2 = \{(s,y),(y,b),(b,d)\}$, and $p_3 = \{(s,z),(z,b),(b,d)\}$ are neither node-disjoint nor link-disjoint because they all share the node b and the link (b,d).

The authors of [40] define IP-layer "disjoint" paths as those that are disjoint with respect to the logical topology (i.e., topology at Layer 3 of the OSI mode) of their network, regardless of its physical topology (i.e., topology at Layer 1 of the OSI model). A clear example of IP-layer "disjointness" is two end-to-end virtual circuits "dedicated" to two users and/or applications.

Also according to [42] and [40], given the availability/failure history of two paths, these paths are said to be *failure-correlated* if their historical data show concurrent failures, otherwise they are said to be *failure-independent*.

As mentioned above, the efforts in [37], [38], [39], and [68] consider the problem of jamming and network availability in multipath routing networks. These papers share the assumptions that node-disjoint and link-disjoint paths lead to failure-independent paths. Moreover, some of these efforts assume that disjointness at the network layer *guarantees* failure-independent paths.

There are two problems with these assumptions. First, having node-disjointness and/or link-disjointness does not guarantee uncorrelatedness of the effects of jamming in wireless networks. An example is a jammer geographically located between two or more node/link-disjoint paths, and can concurrently impact some or all of them; consequently these paths will be failure-correlated. Second, disjointness at the network layer does not guarantee uncorrelatedness of failures at the physical layer because of the topological differences between the two layers [42], [40]. Recall that network layer protocols—e.g., TCP/IP—are virtual networks (overlay networks) built on top

of physical layer infrastructure (underlay network(s)). Hence, given a number of paths, regarded of IP-layer disjointness, a jammer at the physical layer can concurrently disrupt the services over these paths.

3.2.3 Jamming-mitigation routing with path correlations

The efforts in [42], [40], and [41] also consider the problem of jamming-aware multipath routing. However, in contrast to the papers in Section 3.2.2 above, these efforts consider path correlations. These efforts rely on historical data to predict the impact of jamming, and these predictions are used to control traffic allocation.

In [42], a jamming-mitigation approach using path availability statistics is proposed; link availability is decided with respect to a specified packet-delivery rate threshold. Link availability information is then stored in a binary-valued vector. Logical "AND" operations between the elements of these vectors are performed to determine path availability/failure. The problem is formulated as a binary integer program and solved using a greedy heuristic.

The work in [40] extends the initial work in [42], which is further extended in [41]. In these papers, thresholding is used to determine link availability. This can severely reduce the efficiency of path selection. Consider a situation in which a wireless link is right below some threshold of availability, thus can be restored using, e.g., power control instead of being deemed a failed link. As a result, the corresponding path is considered to be unavailable. This can unnecessarily squeeze the scarce wireless network resources, which are already squeezed under the pressure of the ever increasing number of users with data-hungry applications.

3.2.4 Jamming mitigation: Portfolio-selection approach

Now we show the differences between our work and the efforts mentioned in Sections 3.2.2 and 3.2.3. Indeed, the main difference between our work and the efforts discussed there is that we approach the problem as a portfolio-selection problem. Other specific differences with respect to the efforts in each of these two sections are explained below.

A key difference between our work and the efforts mentioned in Section 3.2.2 is that the latter assume disjointness between the routing paths lead to failure-independent paths, while our work does not make these assumptions. We discussed the issues with these assumptions above. We base our work on modern portfolio theory, which does not require asset returns to have zero covariances (or semicovariances). In fact, portfolio selection achieves diversification through measuring either portfolio variance or portfolio semivariance, which in turn implies calculating covariances or semicovariances between individual assets (which can be nonzero in general).

A key difference between our work and the efforts mentioned in Section 3.2.3 is that—in contrast to the efforts there—we avoid thresholding. Thresholding can reduce the efficiency of an applied scheme from a perspective of resource allocation (by resources here we mean routing paths).

Now we discuss the similarities and differences between our work and the efforts in [9] and [48]. Similar to our work, the efforts in [9] and [48] apply a portfolio-selection treatment to the problem of jamming mitigation in multipath networks.

Tange, Nabar, Ritcey, and Poovendran [9] introduce a new scheme for traffic allocation based on mean-variance optimization as introduced by *modern portfolio theory*. Henceforth, we refer to the scheme introduced in [9] as the TNRP algorithm.

In the TNRP algorithm, historical records of link packet-success rate samples are used to estimate the mean and the variance of the end-to-end packet-success rates. These estimates are used to optimize the allocation of source-data rate over the multiple routing paths, trading off mean and variance.

The authors of [48] conduct an empirical study via an NS2 implementation of the TNRP algorithm. The efforts in both [9] and [48] employ mean-variance optimization, which in turn employs variance as a measure of risk.

Referring to Fig 3.2 (a and b), the issue with the mean-variance optimization framework is that both upside and downside volatilities (above and below the mean deviations) are treated equally. In other words, over-performance is penalized in the same way as under-performance. Moreover, this

framework is built on the assumption of a symmetrical distribution of risk. In case of asymmetrical distributions, this approach can lead to faulty estimation of risk. That is, if downside dispersion is greater than upside volatility, risk will be underestimated. In contrast, semivariance only penalizes volatility below a specified risk-aversion benchmark (where investors can set the benchmark equals to the mean as a special case) [43].

Our work is different from the efforts in [9] and [48] in a crucial way. We address the issues associated with the mean-variance optimization framework by using semivariance instead of variance in the optimization problem. To the best of our knowledge, our work is the first to use semivariance as a measure of risk in the context of security against jamming, and in telecommunication applications in general.

3.3 Preliminaries

In this part, we review variance and semivariance portfolio optimization frameworks, following the treatments in [21], [18], and [19]. We also introduce the advantages and disadvantages of each approach.

3.3.1 Review of mean-variance portfolio optimization

Portfolio optimization problem can be posed in four standard forms:

- Minimizing the risk of a portfolio;
- Minimizing the risk of a portfolio subject to a target return;
- Maximizing the return of a portfolio subject to a target level of risk;
- Maximizing the risk-adjusted return of a portfolio.

In this review, we consider the second form of the problem: Minimizing the risk of a portfolio, subject to a target return. For now, we will measure the portfolio performance in terms of its variance V (later to be replaced by its semivariance, a term that will be defined precisely soon). Let E be the portfolio return and R^T the target return. Consider a collection of n assets, indexed

by $i = 1, \ldots, n$. Let μ_i be the expected value of return from asset i. Let $x_i \in \mathbb{R}, i = 1, \ldots, n$ be the relative amount to be invested in asset i (x_i is the decision variable of the optimization problem). Denote the covariance between assets i and j by σ_{ij}. The portfolio optimization problem can be written as

$$\begin{aligned} V^* &= \min_{x_1,\ldots,x_n} \sum_{i=1}^{n} \sum_{j=1}^{n} x_i x_j \sigma_{ij}, \\ \text{subject to} \quad E &\triangleq \sum_{i=1}^{n} x_i \mu_i = R^T, \quad \sum_{i=1}^{n} x_i = 1, \end{aligned} \tag{3.1}$$

where the superscript $*$ signifies the minimum value. Note that the variables x_i can take negative numbers in general because of the possibility of short sales. This problem has a closed-form solution, which follows from the fact that it is a quadratic-optimization problem with only equality constraints.

Having a closed-form solution is arguably the chief advantage of the variance-based optimization framework when compared to its semivariance-based counterpart. Nevertheless, semivariance-based optimization has an edge on variance-based optimization because it employs semivariance as a measure of risk (recall that variance-based optimization adopts portfolio variance as a measure of risk). The variance-based approach treats and penalizes upside and downside volatilities in the same way. Obviously, this often does not properly reflect the notion of risk from the perspective of a reasonable investor. For this reason, semivariance is commonly accepted as a better measure of risk; it treats upside and downside volatilities differently. Intuitively, a reasonable investor would feel satisfied with unexpectedly-high returns (upside volatility), but will never be appeased by losses (downside volatility). In other words, an investor is concerned about underperformance but not unexpected overperformance. Therefore, semivariance is more plausible as a measure of risk and is more reflective of a reasonable investor's preferences and behavior in risky investment environments. This observation was first made by Markowitz in his seminal work [18]. Markowitz himself preferred semivariance as a measure of risk. However, due to the computational complexity associated with semivariance, in addition to the popularity of variance among researchers and

practitioners, Markowitz developed his modern portfolio theory on the mean-variance optimization framework [18], [19].

3.3.2 Semivariance optimization: Definitions, issues, and solutions

On one hand, posing the problem of portfolio selection as a semivariance-based optimization problem is as easy as replacing variance in equation (3.1) with semivariance. On the other hand, solving the semivariance-based problem is not as straightforward. This part is dedicated to introducing basic definitions, explaining the issues that arise with the use of semivariance, and discussing some solutions from the literature.

Definitions—Markowitz semivariance and semicovariance

In his celebrated work [18], Markowitz introduced modern portfolio theory based on mean-variance optimization. Part of his book [18] was dedicated to introducing the notion of semivariance (Markowitz defined the semivariance and discussed—in contrast to variance—the pros and cons of measuring portfolio risk in terms of semivariance). Here, we use the terms *Markowitz semivariance* and *Markowitz semivariance* to distinguish the original definitions—by Markowitz—from other notions of semivariance and semicovariance, such as the notion of *symmetric semivariance* defined later in this section. The *Markowitz semivariance* Σ^2_{pB} is defined as

$$\begin{aligned} \Sigma^2_{pB} &= E\left[(R(x) - B)^2 \cdot \mathbb{1}_{\{R(x) < B\}}\right] \\ &= \sum_{i=1}^{n} \sum_{j=1}^{n} x_i x_j S_{ijB}(x), \end{aligned} \tag{3.2}$$

where $x = (x_1, \ldots, x_n)$, R_i is a random variable representing return of asset i, $R(x) = \sum_{i=1}^{n} x_i R_i$, B is an investor-specified parameter called the *benchmark*, $\mathbb{1}_{\{R(x) < B\}}$ is the indicator function of the event $\{R(x) < B\}$, and $S_{ijB}(x)$ is called the *Markowitz semicovariance* between R_i and R_j. The definition of the *Markowitz semicovariance* $S_{ijB}(x)$ is

$$
\begin{aligned}
S_{ijB}(x) &= E[(R_i - B)(R_j - B) \cdot \mathbb{1}_{\{R(x) < B\}}] \\
&\approx \frac{1}{T} \sum_{t=1}^{T} (R_{it} - B)(R_{jt} - B) \cdot \mathbb{1}_{\{R_t(x) < B\}},
\end{aligned}
\tag{3.3}
$$

where T is the total number of data samples, $\{R_{it} : t = 1, \ldots, T\}$ are samples of R_i, and $R_t(x) = \sum_{i=1}^{n} x_i R_{it}$. Note that in general $S_{ijB}(x)$ depends on the vector x. The benchmark parameter B specifies the level of *risk aversion*. A larger value of B reflects a higher level of risk aversion (or, correspondingly, a lower level of risk tolerance). In the context of wireless networks, we suggest that with the emergence of the network slicing architecture (e.g., in 3GPP Release 15 and 16), users can subscribe to "slices of the network" for user-specified levels of security. In such scenarios, higher values of B might require a prime subscription and probably users would be charged more because service providers would spend more to provide the required (higher) data rates.

Issues using Markowitz semivariance

The empirical formula in (4.3) has one main disadvantage. The problem is that to compute the semicovariance, one needs to know the time periods in which the portfolio underperforms the benchmark (i.e., those t such that $R_t(x) < B$). This limits the practicality of this empirical calculation; it has elements that economists call "endogenous" [21]. The term endogenous in this context means the following: The values of the semicovariance depend on the allocation vector x. This makes the Markowitz semivariance difficult to calculate and even more difficult to optimize.

Portfolio semivariance approximations

To overcome the issue mentioned above, many solutions have been proposed, with varying levels of complexity and applicability [21]. Many researchers have introduced solutions to these problems from different points of view. For example, the work in [20] presents a method to approximate the semicovariance $S_{ijB}(x)$ between asset returns R_i and R_j. This approximation $\Sigma_{ijB}^{\text{asym}} \approx S_{ijB}(x)$ is given by

$$
\Sigma_{ijB}^{\text{asym}} = E[(R_i - B) \cdot \min(R_j - B, 0)], \tag{3.4}
$$

We use the superscript *asym* in equation (3.4) to indicate that this definition of the semicovariance is asymmetric: In general, $\Sigma^{\text{asym}}_{ijB} \neq \Sigma^{\text{asym}}_{jiB}$. This can be disadvantageous: It is not clear how assets i and j contribute to the risk of the portfolio. Another disadvantage of the definition of $\Sigma^{\text{asym}}_{ijB}$ in [20] is that it was limited to the case where $B = R_f$, and R_f is the risk-free rate (the return of a risk-free asset, such as U.S. treasury bills). In this case, the approach does not account for individual investor's perception of risk [21]. The work in [69] suggests a non-parametric approach to calculate and optimize the semivariance. The work in [70] proposes a definition of the semivariance that lends the problem of mean-semivariance optimization to parametric-quadratic programming. However, [70] limits the benchmark to the mean. Thus, this approach does not express individual investors' preferences regarding the measure of risk. To cope with the problems mentioned above, Estrada [21] suggests yet another approximation to the semicovariance. Denoting this approximation by $\Sigma^{\text{sym}}_{ijB} \approx S_{ijB}(x)$, it is defined by

$$\begin{aligned} \Sigma^{\text{sym}}_{ijB} &= E\left[\min(R_i - B, 0) \cdot \min(R_j - B, 0)\right] \\ &\approx \frac{1}{T}\sum_{t=1}^{T}\left[\min(R_{it} - B, 0) \cdot \min(R_{jt} - B, 0)\right]. \end{aligned} \tag{3.5}$$

The approximation of the semicovariance $\Sigma^{\text{sym}}_{ijB}$ in (3.5) is symmetric and *exogenous*: It does not depend on x. We use the superscript *sym* to signify that this approximation is symmetric. Plugging Σ^{sym}_{ij} into equation (3.2), we get the following approximation of the portfolio semivariance:

$$\hat{\Sigma}^2_{pB} = \sum_{i=1}^{n}\sum_{j=1}^{n} x_i x_j \Sigma^{\text{sym}}_{ijB}. \tag{3.6}$$

The approximation $\hat{\Sigma}^2_{pB}$ in (3.6) using $\Sigma^{\text{sym}}_{ijB}$ overcomes the problems associated with S_{ijB} and $\Sigma^{\text{asym}}_{ijB}$. Last but not least, it is worth mentioning here that, as a by-product, the benchmark B, introduced by Markowitz [18] and modified by Estrada [21], allows individual investors to express their preferences regarding risk. Now, the complete semivariance-based optimization problem can be approximated as

$$\hat{\Sigma}_{pB}^{2*} = \min_{x_1,\ldots,x_n} \sum_{i=1}^{n}\sum_{j=1}^{n} x_i x_j \Sigma_{ijB}^{\text{sym}},$$
$$\text{subject to} \quad E \triangleq \sum_{i=1}^{n} x_i \mu_i = R^T, \quad \sum_{i=1}^{n} x_i = 1. \tag{3.7}$$

3.4 Jamming-Mitigation Problem Formulation

Referring to Fig. 3.1, we assume that a jamming device is located (and possibly moving) close to nodes x and y. As in [9] and [48], we assume that the source node has no direct information about the jammer mobility, location, or the jamming power. Rather, what the source can measure is the number of lost packets over time, and the impact of jamming is measured in terms of *packet-success rate* (we use the same definition of packet-success rate as in [9]). Due to the randomness induced by the jammer, the packet losses across the routing paths, as a result, are random. There are n possible routing paths that connect the source s to the destination d through unicast links. Fig. 3.1 illustrates a network with $n = 3$ possible routing paths: Path $p_1 = \{(s,x),(x,b),(b,d)\}$, path $p_2 = \{(s,y),(y,b),(b,d)\}$, and path $p_3 = \{(s,z),(z,b),(b,d)\}$. We assume that the capacity of the links are sufficient to accommodate all the possible allocations of data to the paths. If no jammer is present, assuming all three paths have the same behavior, traffic can be assigned evenly over the n paths. In the presence of the jammer described above, the end-to-end packet-success rates across the links will vary along the routing paths between the values of 0 and 1. More specifically, for a fixed jamming power, if the jammer moves towards node x, the local packet-success rates over the links connecting (s,x) and (x,b) go down, hence reducing the end-to-end packet-success rate over the path p_1. At the same time, as the jammer moves away from the other nodes, the end-to-end packet-success rates over the other two paths p_2 and p_3 go up. Thus, evenly allocating traffic to the three paths will be suboptimal in general.

In our scheme, the source node is assumed to periodically estimate the end-to-end-packet-success rate across the n paths prior to traffic allocation. Similar to the assumptions in [9] and [48], the end-to-end-packet-success rate is estimated by the source node after collecting feedback from the intermediate nodes about local packet-success rates of the individual links. With the assumption

of independent local packet-success rates at each of the intermediate nodes constructing each path, the end-to-end packet-success rate at each of the routing path equals the multiplication of the local packet-success rates across the corresponding links. In our work we assume that the end-to-end packet-success rates are available at the source node. Thus, the notion of local packet-success rate at the individual nodes is no longer needed in the rest of our work. For convenience, we henceforth drop "end-to-end" when referring to "end-to-end packet-success rate."

Having introduced the threat and network model, now we can map this problem to the portfolio-selection problem within the semivariance risk framework. We seek to minimize the *RF-jamming risk* J_r of the multipath traffic allocation—measured in terms of semivariance of the total packet-success rate—subject to a *minimum-acceptable net-packet rate* R_m. As a first step, we express this problem in a form that is identical in form to the portfolio-selection problem:

$$\begin{aligned} J_r^* = \Sigma_{pB}^{2*} &= \min_{x_1,\ldots,x_n} \sum_{i=1}^{n}\sum_{j=1}^{n} x_i x_j S_{ijB}(x), \\ \text{subject to} \quad E &\triangleq \sum_{i=1}^{n} x_i \mu_i = R_m, \quad \sum_{i=1}^{n} x_i = 1, \end{aligned} \tag{3.8}$$

where $x_i \in \mathbb{R}, i = 1, \ldots, n$, is the *relative* source-data rate to be allocated to path p_i, and μ_i is the expected value of the data rate over the path p_i. Recall that the Markowitz semicovariance between paths i and j with respect to a benchmark B is denoted by $S_{ijB}(x)$. This is the standard (Markowitz) form of the semivariance-based allocation problem. Table 3.1 shows how we map elements of the problem of traffic allocation under jamming to the portfolio-selection problem.

While this standard formalism works well for many applications in finance and economics, it does not exactly serve our purpose. Thus, we must deviate from this standard formalism of the problem. For instance, when short sales are allowed in portfolio optimization, the decision variables can have negative values. In our application, we need to impose the non-negativity constraint $x_i \geq 0 \; \forall \; i$ on the decision variables because a negative allocation of source-data rate is not feasible.

In addition to the non-negativity constraint imposed on the decision variables, we introduce an inequality to the constraint of the minimum-acceptable net-packet rate (total from all paths)

R_m. Introducing these constraints, and changing the meaning of some of the variables in the problem, the jamming-aware multipath routing problem based on semivariance risk framework can be written as

$$\begin{aligned} J_r^* = \Sigma_{pB}^{2*} &= \min_{x_1,x_2,\ldots,x_n} \sum_{i=1}^{n}\sum_{j=1}^{n} x_i x_j S_{ijB}(x), \\ \text{subject to } &\sum_{i=1}^{n} x_i\mu_i \geq R_m, \quad x_i \geq 0, i = 1,\ldots,n, \end{aligned} \tag{3.9}$$

where x_i is now the *actual* traffic allocation decision variable (not the *relative* decision variable in the Markowitz problem), $S_{ijB}(x)$ is the semicovariance between packet-success rates of paths i and j, and μ_i is the expected packet-success rate for path p_i. In the optimization problem defined by (3.9), the inequality constraint $\sum_{i=1}^{n} x_i\mu_i \geq R_m$ indicates that the net-packet rate (or throughput) needs *at least* to meet a specified minimum. Notice that the meaning of the variables x_i and μ_i here are different from those in (3.8). However, the objective function is still based on the Markowitz semivariance. Moreover, the benchmark parameter B in the jamming problem still reflects risk aversion: A large value of B reflects a high level of risk aversion to jamming (e.g., because of the desire to communicate mission-critical data).

3.5 Problem Solution: The EQS Scheme

We now introduce our approximation method, based on [21], to solve the jamming problem by replacing the Markowitz semivariance risk measure J_r with its symmetric-semivariance approximation $\hat{J}_r$ as shown below:

$$\begin{aligned} \hat{J}_r^* = \hat{\Sigma}_{pB}^{2*} &= \min_{x_1,\ldots,x_n} \sum_{i=1}^{n}\sum_{j=1}^{n} x_i x_j \Sigma_{ijB}^{\text{sym}}, \\ \text{subject to } &\sum_{i=1}^{n} x_i\mu_i = R_m, \quad x_i \geq 0, i = 1,\ldots,n. \end{aligned} \tag{3.10}$$

Notice that the problem in (3.10) is the same as in (3.9) with only two changes:

- We replace J_r^* with the approximation $\hat{J}_r^*$—it is much easier to optimize the objective function $\hat{J}_r$ in (3.10) (i.e., easier to find $\hat{J}_r^*$ than to find J_r^*), as we discussed in Section 3.3.

- We replace the inequality constraint $\sum_{i=1}^{n} x_i \mu_i \geq R_m$ in (3.9) by the equality constraint $\sum_{i=1}^{n} x_i \mu_i = R_m$. Both optimization problems have the same solution, because the constraint involving R_m is always active at the optimal solution (as the reader can readily show). However, it is clearly easier to solve the problem in (3.10) because it involves a smaller feasible space.

To sum up, in this chapter, we adopt and modify the approximation developed by Estrada [21]. Fig. 3.3 is a schematic of the main steps of our approach. We refer to our proposed algorithm as the EQS scheme (we adopt this as an acronym for "exogenous-quadratic semivariance" because our scheme is built on the exogenous and quadratic approximation of the semivariance introduced in [21]).

We start by specifying the input parameters, providing the packet-success rate samples, and defining the objective function J_r for our problem; to define J_r we need to define $S_{ijB}(x)$. Then, we map the problem of traffic allocation to portfolio selection. Recall that the original portfolio-selection problem—built on the Markowitz semivariance—has some issues. The main issue is that the Markowitz semicovariance $S_{ijB}(x)$ depends on the allocation vector x. As we can see in Fig. 3.3, x is the output of the overall process. This clearly exposes the problem of $S_{ijB}(x)$ being endogenous as discussed before.

To address these issues, we transform the problem of jamming-aware-traffic-allocation within the semivariance framework to a quadratic-programming problem: We replace the original endogenous semicovariance by an approximate and exogenous semicovariance (Estrada's approximation [21], which is much easier to compute because it depends on the input parameter B but not the output allocation vector x). The result is a quadratic-semivariance problem with equality constraints. This problem has a closed-form solution. However, our problem differs from Estrada's because ours involves introducing inequality constraints.

The closed-form solution for equality-constrained quadratic programs no longer applies in our case. Hence, we use numerical optimization to solve our optimization problem. The output of the numerical-optimization step is the traffic allocation decision variables across the routing paths.

Table 3.1: Mapping Traffic Allocation to Portfolio Selection

Portfolio selection	Jamming-aware traffic allocation	Mathematical representation in the jamming problem
Assets	Routing paths	$p_i, i = 1, \ldots, n$
Investment portfolio decision variable	Traffic allocation decision variable	$x_i, i = 1, \ldots, n$ $x_i, i = 1, \ldots, n$
Target portfolio return	Minimum-acceptable net-packet rate (total)	R_m
Portfolio risk-aversion benchmark	Jamming risk-aversion benchmark	B
Expected value of return from asset i	Expected packet-success rate for path i	μ_i
Expected portfolio return	Expected net-packet rate (total)	$E \stackrel{\triangle}{=} \sum_{i=1}^{n} x_i \mu_i$
Portfolio return	Total net-packet rate	$\sum_{i=1}^{n} x_i R_i$
Exact semicovariance between returns of assets i and j	Exact semicovariance between packet-success rates of paths i and j	$S_{ijB}(x)$
Approximate semicovariance between returns of assets i and j	Approximate semicovariance between packet-success rates of paths i and j	$\Sigma_{ijB}^{\text{sym}}$
Portfolio return semivariance	RF-jamming risk	J_r

3.6 Simulation

Referring to the network shown in Fig. 3.1, we consider the simple scenario of one source node, one destination node, and two end-to-end routing paths. We assume that the jammer location coordinates and jamming power are unknown. As mentioned in Section 3.4, we employ the packet-success rates as proxies to evaluate the effect of the stealthy jammer on the network. These packet success rates are obtained (estimated) using the empirical mean of a set of packet-success samples, as we will detail below. Note that our scheme works in the same exact way in the presence of

multiple jammers in the network; the source node can still optimize traffic allocation through the routing paths using empirical records of the packet-success rates.

To simulate the impact of the jammer on the network, we model the packet-success rate samples over the two routing paths in our simulation by two truncated Gaussian distributions. By truncation, we mean that we apply a hard limit to Gaussian samples so that our empirical packet-success rate samples lie between 0 and 1. Specifically, in our simulation, we create a set of samples $\{R_{it} : t = 1, \ldots, T\}$ to represent the packet-success rate samples over time across path p_i at time instants $t = 1, \ldots, T$. Each sample R_{it} (with mean μ_i, the packet success rate over path i) is generated as follows:

$$\begin{aligned} R_{it} &= \min(1, (\max(0, \bar{R}_{it}))), \quad \bar{R}_{it} \sim \mathcal{N}(\bar{\mu}_i, \bar{\sigma}_i^2), \\ & i = 1, \ldots, n, \quad t = 1, \ldots, T, \end{aligned} \tag{3.11}$$

where $\bar{R}_{it}$ is the sample from the underlying Gaussian distribution that corresponds to R_{it}, and $\bar{\mu}_i$ and $\bar{\sigma}_i$ are the mean and standard deviation of this underlying Gaussian distribution of the packet-success rate samples across path p_i. As mentioned above, in this simulation, we consider a scenario of two routing paths, i.e., $n = 2$. We created 1000 samples of R_{it} ($T = 1000$).

We set mean and variance values at $\bar{\mu}_1 = 0.6$ and $\bar{\sigma}_1 = 0.2$ for path p_1, and at $\bar{\mu}_2 = 0.3$ and $\bar{\sigma}_2 = 0.1$ for path p_2, respectively. The different values of μ_i simulate a scenario in which a jammer with a fixed jamming power is located at closer distances to one of the routing path nodes, thus reducing the SINR at the nodes in this path; consequently, the packet-success rate across this path will be smaller than the packet-success rate across the other path. The values of σ_i simulate the randomness in the packet-success samples.

Fig. 3.4 shows histograms of the packet-success rate samples across the two paths. We can see that the values of the packet-success rates across the two paths are confined in the interval $[0, 1]$. Moreover, we can see that path p_1 in Fig. 3.4 is more secure than path p_2; hence, it is natural that p_1 is allocated higher source-data rate when the impact of RF jamming is taken into account.

We evaluate the performance of two jamming-mitigation techniques—our EQS scheme and the TNRP algorithm. We study the difference in performance of the TNRP algorithm and the EQS scheme through quantification of the RF-jamming risk J_r achieved by each of the jamming-mitigation techniques subject to a predefined minimum net-packet rate (throughput) R_m (in Gbits/s, say). We present the results under different values of the benchmark B. Note that our EQS scheme, which uses Estrada's approximation of the semivariance, results in a quadratic program (QP). Once we have a QP, we can use OTC QP solvers, e.g, for our numerical optimization, we used MATLAB's `quadprog`. The original Markowitzian formulation does not yield to these OTC solvers. One would have to write specialized optimization code for it, and then we cannot exploit or take advantage of the advanced developments in QP algorithms (e.g., for efficiency, speed). Even general optimization tools, like MATLAB's `fmincon`, is unsuitable, because it assumes continuity of the objective function.

We use different values of B to reflect the diverse preferences of network users (equivalently, distinct security requirements for a variety of applications). In other words, we vary B to simulate the risk preferences of different users who require network availability tailored to their specific use case(s). For a given of R_m, we expect higher B values for mission-critical applications that require extremely-high network availability. On the other hand, non-mission-critical applications can be provided at lower values of B. Similarly, we also use different values of R_m in our simulations. This is to reflect different throughput requirements..

In Figs. 3.5–3.8, we show the *RF-jamming risk* J_r achieved by the EQS scheme and the TNRP algorithm versus the minimum-acceptable net-packet rate R_m. Each of these figures presents the results for a different value of the benchmark B. As expected, we see that higher jamming risks J_r are associated with higher R_m values. However, we can see that the EQS scheme offers, for a given R_m, a much lower jamming risk for all values of the benchmark B considered in the simulations.

In Fig. 3.5, the scenario mimics low risk applications, where the value of $B = 0.2$. In this scenario, the gap in performance between the EQS scheme and the TNRP algorithm is approximately a factor of 3, though the absolute numbers involved are relatively small in this specific case. The

significance of the performance gap becomes even more noteworthy if we recall that billions of low-rate devices are connected in the era of the Internet of Things.

As for larger values of B, the differences in performance are obviously amplified (see Figs. 3.6–3.8).

Now if we take a closer look at Fig. 3.7 for instance, we can see that for the TNRP algorithm to achieve the same level of security achieved by the EQS scheme, it has to sacrifice a significant amount of throughput. For example, consider that a user or an application seeks an RF-jamming risk of 0.05. The EQS scheme can achieve this targeted security at 0.9 Gbits/s net-packet rate, whereas for the TNRP algorithm to reach the same level of security, it has to sacrifice more than 0.5 Gbits/s.

For the sake of completeness, we include the results of a very specific but interesting experiment. In this experiment, we simulate a peculiar scenario in which the jammer impacts each of the two routing paths in an identical manner. This specific scenario is a most-favorable case for the TNRP scheme, and so in this experiment, the performance of TNRP raises to the same level as that of EQS. This is shown in Fig 3.9 and is unsurprising because in this speical case $R(x)$ does not depend on x, which means any feasible x is equally optimal. This peculiar scenario is unlikely in typical use cases because: 1) It is very demanding—jammers need to have precise location information and mobility control, in addition to perfect power control and antenna beamforming. 2) This peculiar scenario is disadvantageous to jammers because using exactly the same power to jam both paths identically gives the TNRP anit-jammer an advantage against the jammer. Thus this scenario is unlikely in practice.

Now we turn our attention back to the effect of B. Fig. 3.10 plots the RF-jamming risk J_r achieved by the EQS scheme and the TNRP algorithm for different benchmark values at R_m = 0.5 and 0.8. Indeed, higher values of B cause a notable increase in J_r for a given value of R_m (recall that higher B values reflect higher levels of risk aversion). We can see that lower jamming risks are achieved by our EQS scheme at both values of R_m shown in the legend. This is because our scheme aims specifically at minimizing the part of volatility below B. On the other hand, the TNRP

algorithm has no apparatus to directly minimize the part below B. Thus, the TNRP algorithm cuts off parts of the potential net-packet rate gains when trying to minimize the RF-jamming risk.

3.7 Conclusion

In this chapter, we considered the problem of RF-jamming mitigation for multipath routing. We formulated the problem as a portfolio-selection problem. We introduced the Markowitz semivariance as a new and appropriate cost function to measure RF-jamming risk. Because the original Markowitz semivariance has some issues, we adopted an approximation method from economics and finance: This approximation method resolves these semivariance issues. We developed a new jamming-mitigation scheme based on this semivariance approximation.

We evaluated the performance of our algorithm by considering multiple scenarios for different user-specified risk aversion and packet rate requirements. The simulation results show the potential gains of using our proposed jamming-mitigation solution. In some cases, the performance of our solution is multiple times that of TNRP.

This work leads to several future research directions. We plan to extend our work to the 4G LTE and 5G NR technologies. In particular, we plan to apply this approach in tandem with carrier aggregation in 4G LTE and 5G NR networks. We also plan to consider the problem of efficient traffic routing in a full-fledged 5G user equipment (UE) with multiple radio interfaces capable of connecting to various radio access technologies (RAT) to achieve diversification across the multi-RAT environment. Jamming mitigation in this setting has yet to be explored widely.

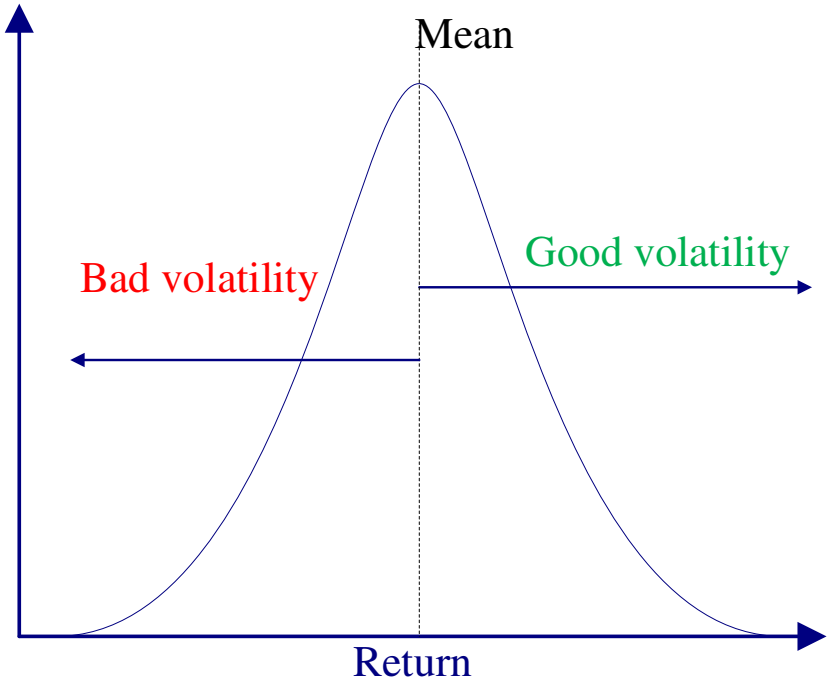

(a)

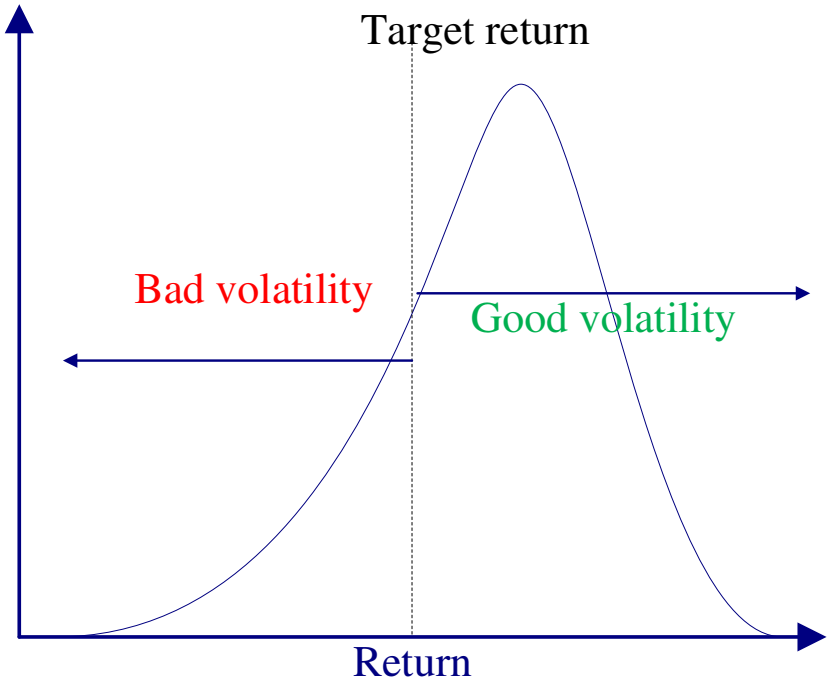

(b)

Figure 3.2: Good and bad volatility: (a) Return with symmetric distribution. (b) Return with skewed distribution. In general target return can be different from the mean.

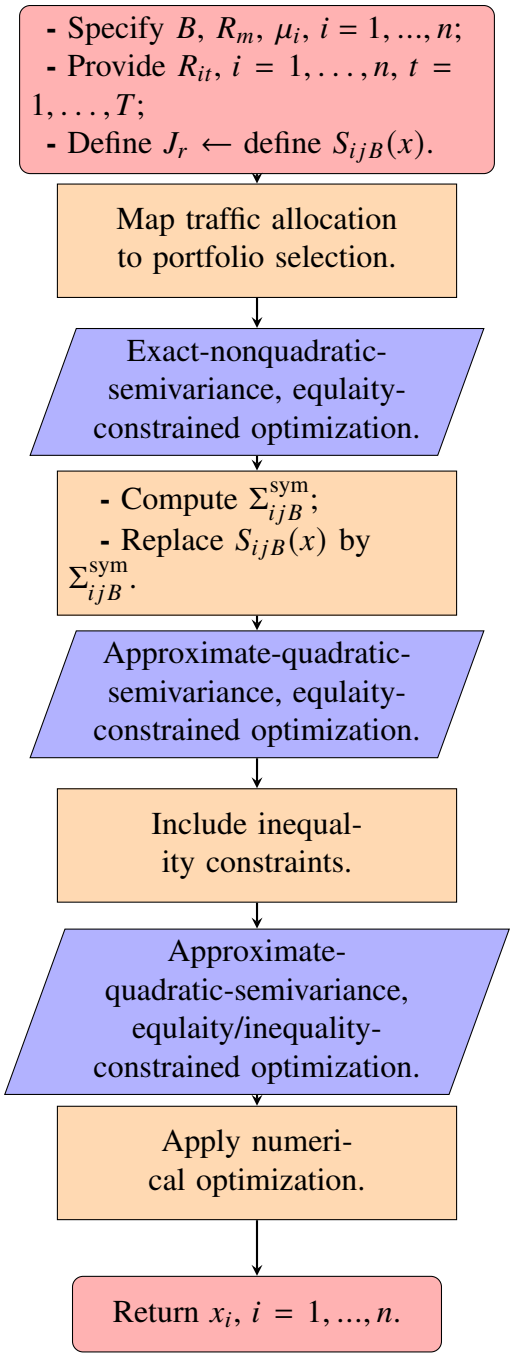

Figure 3.3: Schematic of the EQS-algorithm design and implementation procedure.

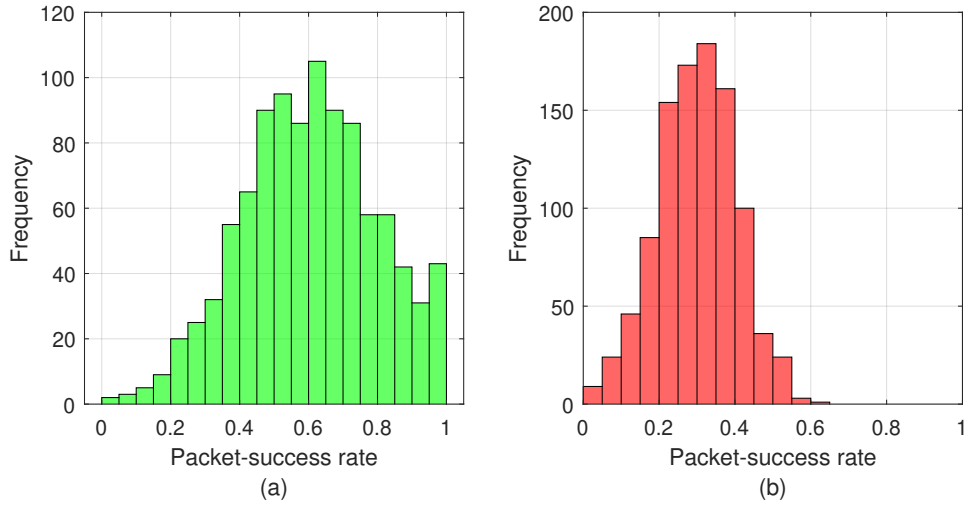

Figure 3.4: Histograms of 1000 packet-success rate samples across the two routing paths: a) Histogram of packet-success rate sample values for path p_1. b) Histogram of packet-success rate sample values for path p_2.

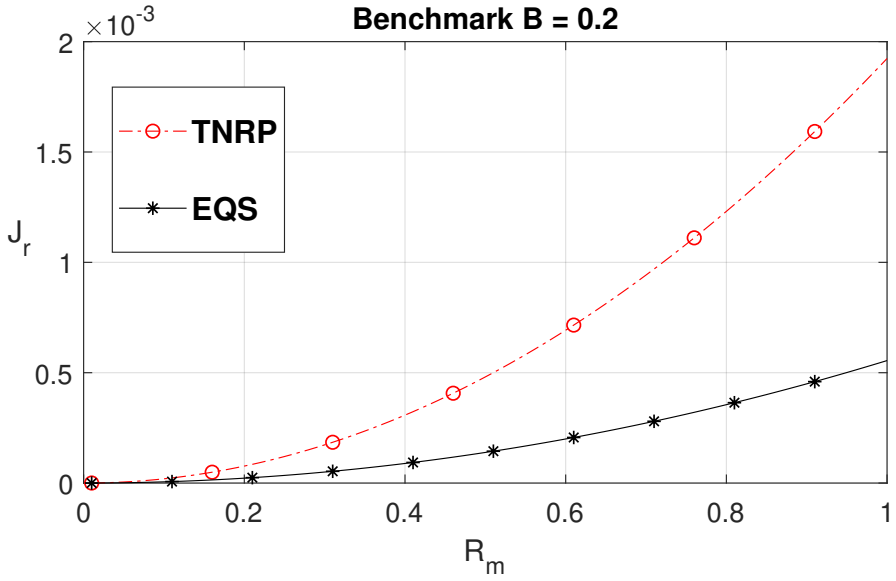

Figure 3.5: RF-jamming risk J_r achieved by the EQS scheme and the TNRP algorithm versus the minimum-acceptable net-packet rate R_m at benchmark $B = 0.2$.

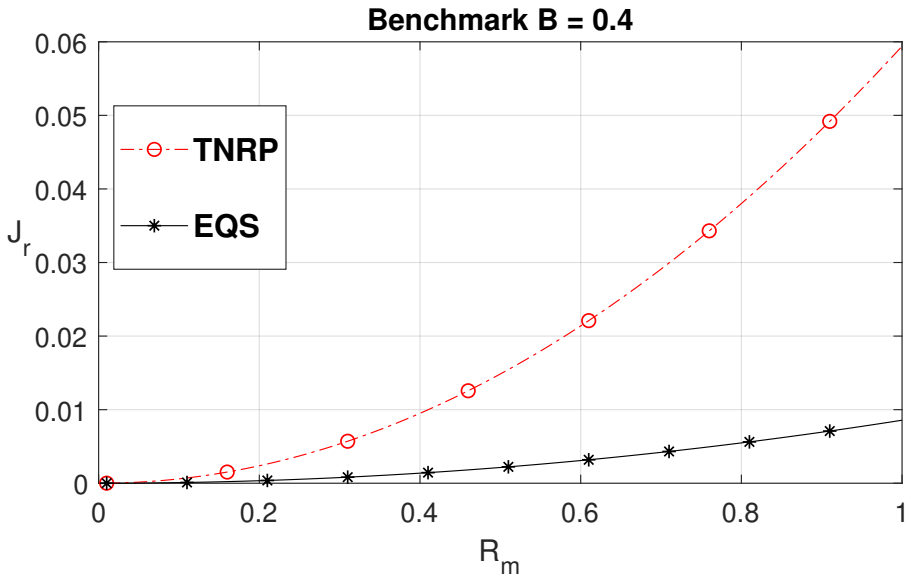

Figure 3.6: RF-jamming risk J_r achieved by the EQS scheme and the TNRP algorithm versus the minimum-acceptable net-packet rate R_m at benchmark $B = 0.4$.

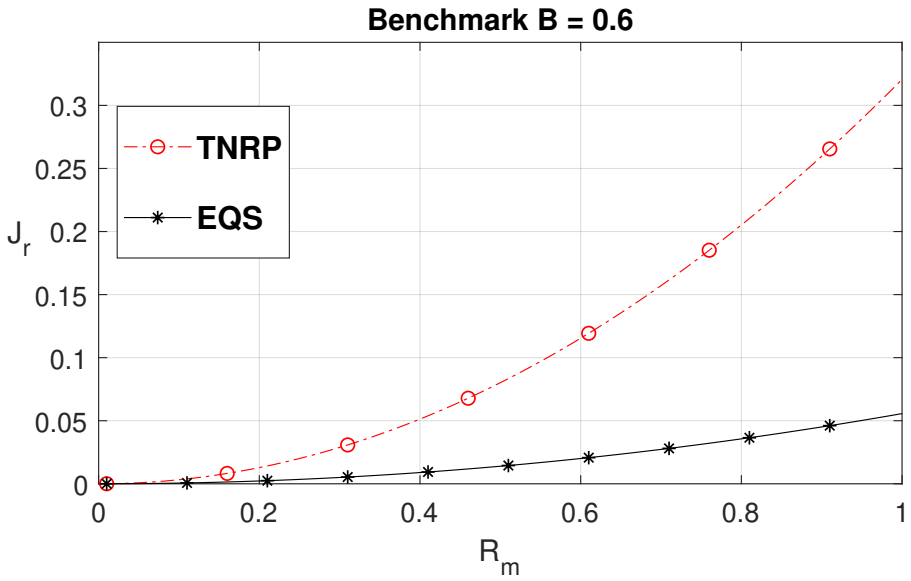

Figure 3.7: RF-jamming risk J_r achieved by the EQS scheme and the TNRP algorithm versus the minimum-acceptable net-packet rate R_m at benchmark $B = 0.6$.

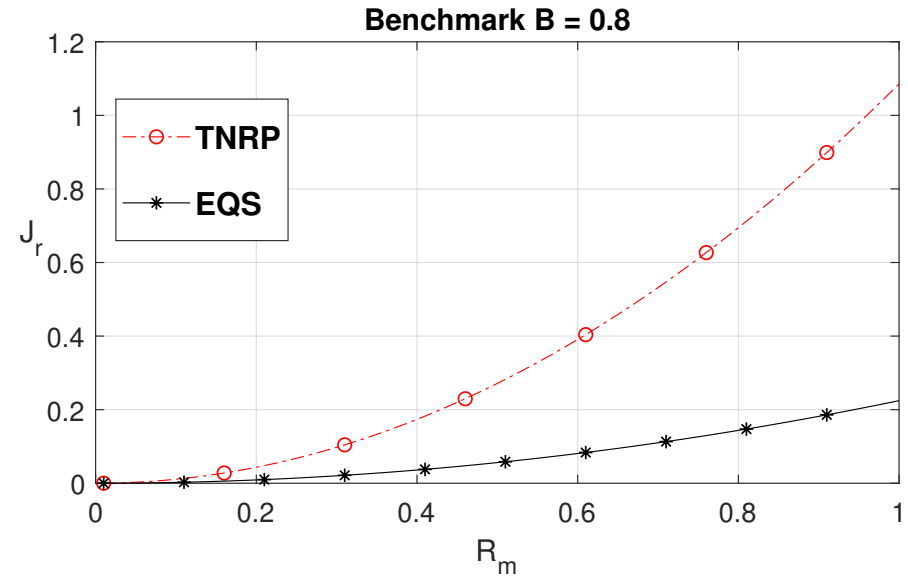

Figure 3.8: RF-jamming risk J_r achieved by the EQS scheme and the TNRP algorithm versus the minimum-acceptable net-packet rate R_m at benchmark $B = 0.8$.

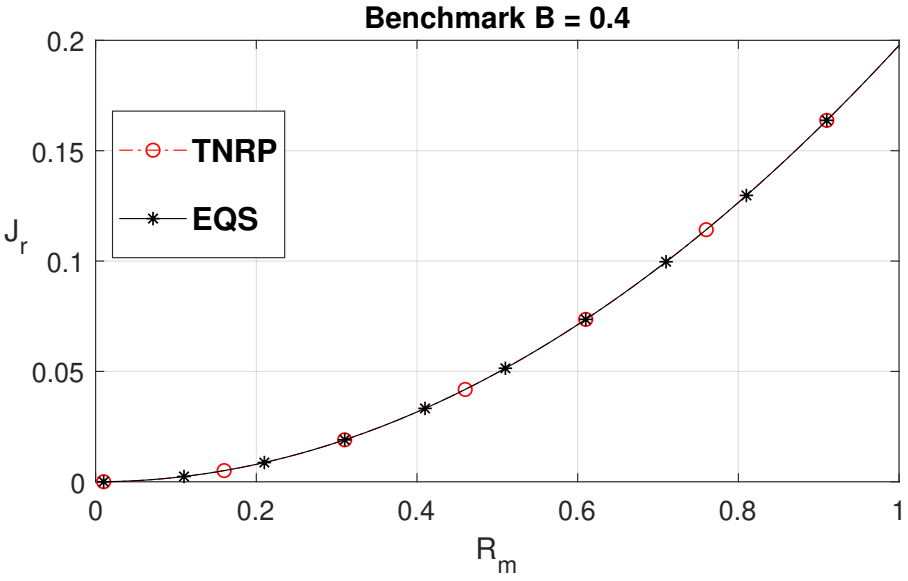

Figure 3.9: RF jammer producing identical impact on the two routing paths.

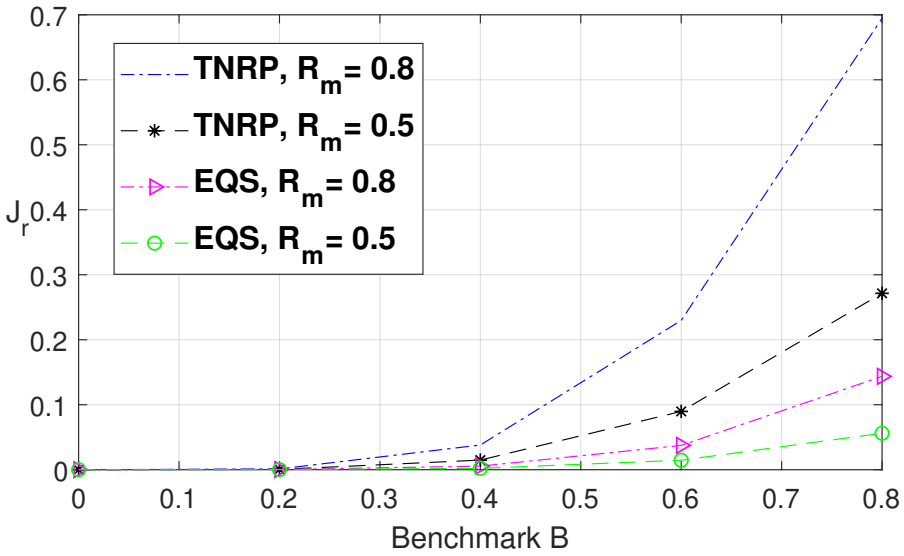

Figure 3.10: RF-jamming risk J_r achieved by the EQS scheme and the TNRP algorithm for different benchmark values at $R_m = 0.5$ and 0.8.

Chapter 4

RAM: Risk-Averse Multi-RAT Connectivity for Traffic Allocation in HetNets

4.1 Introduction

Multiple–radio-access technology (multi-RAT) networking is a promising technique to meet the pressing demand imposed on cellular networks to provide extremely high network availability and increased data rates. By employing multi-RAT connectivity, capacity can be leveraged from surrounding heterogeneous networks (HetNets) by transmissions between base station(s) (BS(s)) and connected user equipment (UE), concurrently using more than one radio interface per BS/UE link. Moreover, there is a recent trend followed by mobile network operators toward integrating WLAN (prominently WiFi) technologies within cellular networks, to harvest more capacity from the scarce spectrum resource [44].

In this chapter, we consider the problem of source-data rate allocation using multi-RAT connectivity in HetNets, while taking *risk* into account. (In the context of this chapter, risk refers to the throughput dropping below a specified benchmark; the benchmark here is measured in bits per second (bps).) To account for this risk, we develop a risk-averse scheme for data-source allocation to the available RATs. In this chapter, we introduce our new risk-averse multi-RAT connectivity (RAM) algorithm.

Fig. 4.1 depicts our system model. The figure illustrates the concept of multi-RAT connectivity, and how it distributes source data over the involved RATs at the BS side in HetNet environments and aggregates traffic at the UE side. We obtain the traffic allocation decision vector in Fig. 4.1 by solving an optimization problem. This optimization problem involves trading off throughput for risk in the form of throughput semivariance.

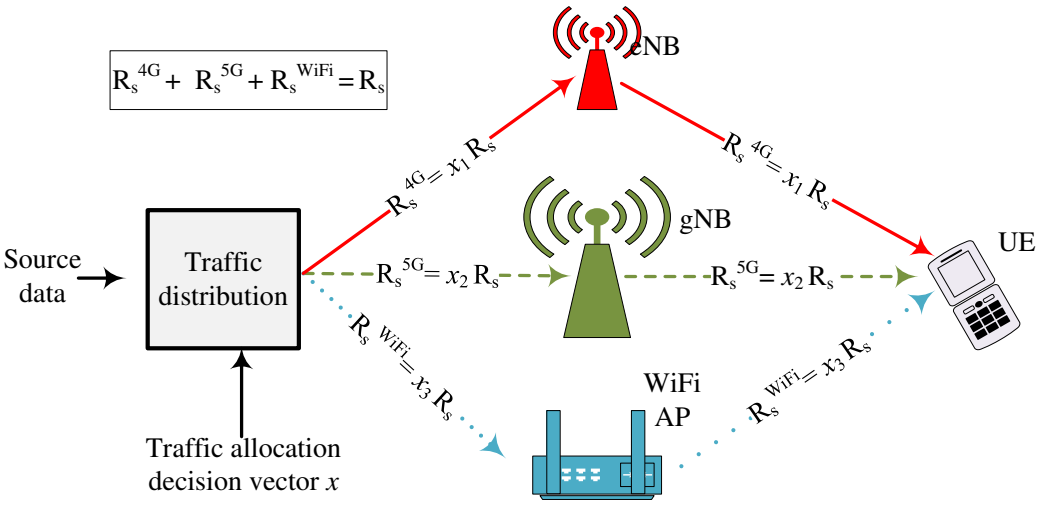

Figure 4.1: A schematic of the system model. The figure illustrates how source data traffic is distributed across the involved RATs in HetNet environments, and how traffic is aggregated at the UE. We limit our scope to the downlink. However, our approach can also be applied in the uplink.

We also introduce a new performance metric, the *risk-adjusted throughput*. We define our new metric, the *risk-adjusted throughput*, in a fashion similar to the *risk-adjusted return* from the literature of finance and economics with some modifications. In finance and economics, risk-adjusted return is defined in many ways. One of the earliest notable definitions of the risk-adjusted return is the *Sharpe ratio* (named after William F. Sharpe [71]). The Sharpe ratio is a term originally used in portfolio theory; it is defined as return per unit volatility, where volatility is expressed by the standard deviation of portfolio return . Another definition of the risk-adjusted return is the *Sortino ratio*, named after F. A. Sortino, that defines the risk-adjusted return as return per unit of downside volatility, where downside volatility is expressed in terms of the semideviation of portfolio return [72], [21]. Semideviation is the square root of semivariance. For now, we define semivariance as a measure of throughput volatility below a given benchmark. In Section 4.3.1, we provide rigorous mathematical definitions of the semivariance and other related concepts.

In the context of wireless communication, the authors of [9] define the *risk-adjusted throughput* as throughput per unit volatility of total throughput from different communication paths, where volatility is expressed in terms of the standard deviation of this total throughput.

In our definition of the risk-adjusted throughput, we only take volatility below the benchmark into account. Hence, we define the *risk-adjusted throughput* in our work as throughput divided by *semideviation* of total throughput from different communication links involved in the multi-RAT connectivity. We use risk-adjusted throughput as a performance metric to evaluate the performance of our algorithm and two other schemes. In Section 3.6, we provide a mathematical definition of the risk-adjusted throughput.

We summarize the prime motivations of our work as follows:

- The requirements of coexistence—set by the 3rd Generation Partnership Project (3GPP)—between technologies from different cellular generations and WLAN. Our work on multi-RAN connectivity is in line with these requirements.

- Availability of architectures that support source-data fragmentation over multi-RATs. These architectures make multi-RAT schemes, including ours, applicable in real network environments.

- Diverse use cases and the emergence of network slicing. Varied use cases lead to different throughput requirements. Our solution allows users/applications to specify their throughput requirements. Network slicing enables dynamic resource allocation that can adapt to these user preferences varying over both time and space.

- Edge computing enables implementing distributed algorithms at the BS(s), i.e., eNB(s), gNB(s), and integrated WiFi access point(s) (WiFi AP(s)) (given that WiFi is adequately integrated and managed under unified HetNet control architectures).

- Our work is motivated by the absence of risk-aversion studies in multi-RAT connectivity. Our work is a first step in the direction of risk-averse traffic allocation in multi-RAT/HetNet environments.

In this chapter, we propose a unified approach to leverage capacity through cellular/WiFi multi-RAT connectivity. We suggest a framework based on semivariance optimization. Our scheme mitigates risk and enhances risk-adjusted throughput by allocating user traffic to diversified network

connections, provided through cellular/WiFi multi-RAT connectivity. We formulate the problem of user traffic allocation through the diversified connections as a semivariance optimization problem.

Our main contributions are as follows:

- Our work contributes to the efforts that aim at throughput maximization without retransmission requests (which lead to latency that can violate the quality of service (QoS) for delay-sensitive applications).
- We formulate the problem of multi-RAT connectivity as a semivariance optimization problem.
- We introduce a unified framework for the multi-RAT connectivity problem
- Our work is the first to take a risk-averse view of the source-data fragmentation decision making in the context of multi-RAT connectivity.
- We introduce a new traffic allocation performance metric, the *risk-adjusted throughput*.
- We follow 3GPP specifications for throughput calculation in our simulation. We develop an algorithm that is amenable to practical implementation in real scenarios of network control and provisioning, with only minor modifications to match deployment specificities.

The rest of this chapter is organized as follows. In Section 4.2, we overview efforts that address multi-RAT connectivity. In Section 4.3, we introduce our formulation of the multi-RAT connectivity problem as semivariance optimization. We start by reviewing semivariance optimization in its original framework, portfolio selection. We also study the issues of using semivariance and survey approximations that address these problems. In Section 4.4, we explain how we use semivariance approximation to develop our algorithm. We introduce our simulation results in Section 4.5. We conclude the chapter in Section 4.6.

4.2 Related Work

The efforts in [44], [45], [12], and [73] propose various architectures to enable concurrent connections through multi-RAT in HetNets. For example, the work in [45] suggests a radio network architecture for tight integration of multi-RAT connectivity. More specifically, the authors of [45] propose a common user plane and control plane across different RATs to optimize traffic aggregation from and to different sources. Among others, the goals of this tight integration are to increase throughput and improve reliability.

The authors of [13] propose a dynamic spectrum re-allocation scheme for spectrum sharing across different 3GPP networks. Specifically, the authors consider the problem of using LTE in GSM bands to enhance the capacity of the network with GSM/LTE co-existence and inter-RAT interference coordination. The authors of [13] show the capacity gains of their scheme through simulation of a GSM and LTE network compared to fixed spectrum allocation among multi-RAT networks, which cannot make optimal use of the available spectrum.

The work in [14] proposes an algorithm to jointly optimize resource allocation for a cellular network based on OFDAM and CDMA technologies. The authors of [14] introduce their joint optimization algorithm in the context of "spectrum refarming." Spectrum refarming is a process that allows different generations of cellular networks to operate in the same radio spectrum. Because of its capability to alleviate the spectrum scarcity problem, spectrum refarming has been receiving significant attention in recent years. Simulation results in [14] show the effectiveness of the proposed scheme to increase OFDMA throughput in the proposed OFDMA/CDMA spectrum refarming system.

The efforts in [74] consider resource allocation in HSPA/LTE multi-RAT HetNets with carrier aggregation in an integrated 5G environment. The authors provide a scheme for joint resource reallocation within the context of spectrum refarming. The authors test the performance of their algorithm through simulation. The results show that when resource allocation is performed jointly between the involved RATs, throughput increases for all HSPA and LTE users in the HetNet.

The authors of [75] build a prototype using multiple Android cell phones. The default Android operating system allows the cell phone to connect to only one network at a time. So the authors build their prototype by modifying the operating system (Android) code on these cell phones. The prototype allows multiple networks to be used concurrently. The authors then use these phones to run a number of experiments. They call this set of experiments "Stitching Networks for Throughput." To test the performance, the authors stream data while varying the number of interfaces, and measure throughput at the application layer. The interfaces in this experiment are WiFi, WiMaX, CDMA, and HSPA links from different operators. The reported results show a significant increase in throughput with more RATs, at negligible control overhead and delay.

The efforts in [46] extend the work in [75]. In [46], the authors introduce a packet scheduling scheme that allows users and applications to specify which RAT(s) to connect to, to save cost and increase throughput.

The authors of [47] formulate the problem of multi-RAT connectivity in HetNets as a network utility maximization problem to maximize throughput while providing proportional fairness between users.

Many of the papers mentioned above consider the problem of throughput maximization using concurrent transmissions across the available multiple radio interfaces in HetNets. However, none of these papers view the problem from the perspective of risk. Additionally, none of the papers above explicitly account for the correlation between the throughput of the radio interfaces.

Our work here considers the tradeoff between throughput and associated risk. Our work also accounts for correlation between throughput of the different RATs (more specifically, *semicorrelation*) through the quantification of *semivariance*. In [76], we present a preliminary version of parts of this chapter. However, our scheme in [76] requires knowledge of the source-data rate and does not consider capacity constraints of the links involved in the multi-RAT system model. Here we extend our previous work [76] in several ways. Importantly, we introduce a new scheme that does not require knowledge of the source-data rate. We also impose new capacity constrains to account for the capacities of the involved wireless links.

Often, return-risk–tradeoff problems are formulated as mean-variance optimization. The work in [9] considers the problem of source-data allocation in wireless–multi-path–routing networks. The authors of [9] develop an algorithm based on variance-based portfolio selection. They use historical records of packet delivery ratios through the available routing paths, and use these records to calculate risk in the form of throughput variance. While the work in [9] solves a problem somewhat similar to ours, there are two key differences. First, our work provides a different measure of risk based on throughput semivariance (or semideviation, which is the square root of semivariance) instead of variance. Second, our work addresses the problem of multi-RAT connectivity in HetNets, while [9] addresses the problem of traffic allocation in multipath-routing networks.

4.3 Problem Formulation

In this chapter, we formulate the problem of multi-RAT connectivity as a semivariance-optimization problem, inspired by methods for portfolio selection. Consider a number of available RATs. The problem is to optimize the allocation of source data in the downlink (DL) direction of the communication link. We limit the scope of this chapter to the frequency-division duplexing (FDD) scenario. However, the framework is equally applicable to the case of time-division duplexing (TDD).

The fundamental tradeoff in this framework is between throughput and downside risk. That is, to maximize throughput while minimizing risk in terms of throughput semivariance. We proceed by reviewing semivariance optimization in the context of portfolio selection. Then, we introduce our formulation of multi-RAT connectivity as a semivariance-optimization problem. We provide some basic definitions and define a new metric, the *risk-adjusted throughput*.

4.3.1 Review of the semivariance risk framework

Semivariance optimization has its roots in portfolio selection. Hence, to facilitate the explanation and discussion of semivariance optimization, we review semivariance optimization in the context of portfolio selection, following the treatments in [21] and [19] (in a separate unpublished

paper [77], we are also exploring jamming risks using semivariance). Originally, Markowitz [19] introduced semivariance optimization as a risk-averse portfolio-selection approach in finance and economics.

Portfolio-selection problems take four standard forms:

- Minimizing the risk of a portfolio;
- Minimizing the risk of a portfolio subject to a target return;
- Maximizing the return of a portfolio subject to a target level of risk;
- Maximizing the risk-adjusted return of a portfolio.

In this chapter, we consider the last form of the problem: Maximizing the risk-adjusted return of a portfolio. We measure the portfolio risk in terms of its semivariance $\Sigma^2_{pB}(x)$ (defined precisely below), which represents only downside variance. Let $\bar{R}(x)$ be the mean return of the portfolio. Consider a collection of n assets, indexed by $i = 1, \ldots, n$. Let m_i be the expected value of return from asset i. Let $x_i \in \mathbb{R}, i = 1, \ldots, n$ be the relative amount to be invested in asset i (x_i is the decision variable of the optimization problem). Denote the Markowitz semicovariance between assets i and j by $S_{ijB}(x)$ (defined precisely later). The portfolio-optimization problem can be written as

$$\begin{aligned} f^*(x) &= \max_{x_1,\ldots,x_n} \left[\bar{R}(x) - \Sigma^2_{pB}(x) \right] \\ &= \max_{x_1,\ldots,x_n} \left[\sum_{i=1}^{n} x_i m_i - \sum_{i=1}^{n} \sum_{j=1}^{n} x_i x_j S_{ijB}(x) \right], \\ &\quad \text{subject to } \sum_{i=1}^{n} x_i = 1, \end{aligned} \tag{4.1}$$

where the superscript $*$ signifies the maximum value and the mean return $\bar{R}(x) = \sum_{i=1}^{n} x_i m_i$. Note that the variables x_i can take negative values in general because of the possibility of short sales.

For the sake of completeness, it is worth mentioning that there is a version of portfolio-selection theory that uses variance as a measure of risk (e.g., [9], [19]). One of the main disadvantages of

the variance-based approach is that it treats and penalizes upside and downside volatilities in the same way. Obviously, this often does not properly reflect the notion of risk from the perspective of a reasonable investor, who is concerned with the return being *lower* than desired but is happy with the return being *higher* than desired. For this reason, semivariance is commonly accepted as a better measure of risk; it treats upside and downside volatilities differently.

In our work, we adopt semivariance as a measure of risk for two reasons. First, as mentioned above, the semivariance-based approach is more a plausible measure of risk. Second, there are many semivariance approximations in the literature (specifically, in the field of finance) that alleviate the computational problems of semivariance optimization. Later, we will show how to overcome these semivariance computational issues and develop a scheme based on one of these semivariance approximations.

In his celebrated work [19], Markowitz introduced modern portfolio theory based on mean-variance optimization. Part of his book [19] was dedicated to introducing the notion of semivariance (Markowitz defined the semivariance and discussed—in contrast to variance—the pros and cons of measuring portfolio risk in terms of semivariance). Here, we use the terms *Markowitz semivariance* and *Markowitz semicovariance* to distinguish the original definitions—by Markowitz—from other notions of semivariance and semicovariance, such as the notion of *symmetric semivariance* defined later in this section. The *Markowitz semivariance* $\Sigma^2_{pB}(x)$ is defined as

$$\begin{aligned} \Sigma^2_{pB}(x) &= E[(R(x) - B)^2 \cdot \mathbb{1}_{\{R(x) < B\}}] \\ &= \sum_{i=1}^{n} \sum_{j=1}^{n} x_i x_j S_{ijB}(x), \end{aligned} \tag{4.2}$$

where $x = (x_1, \ldots, x_n)$, R_i is a random variable representing return of asset i, $R(x) = \sum_{i=1}^{n} x_i R_i$, B is an investor-specified parameter called the *benchmark*, $\mathbb{1}_{\{R(x) < B\}}$ is the indicator function of the event $\{R(x) < B\}$, and $S_{ijB}(x)$ is called the *Markowitz semicovariance* between R_i and R_j. The definition of the *Markowitz semicovariance* $S_{ijB}(x)$ is

$$
\begin{aligned}
S_{ijB}(x) &= E[(R_i - B)(R_j - B) \cdot \mathbb{1}_{\{R(x) < B\}}] \\
&\approx \frac{1}{T} \sum_{t=1}^{T} (R_{it} - B)(R_{jt} - B) \cdot \mathbb{1}_{\{R_t(x) < B\}},
\end{aligned}
\tag{4.3}
$$

where T is the total number of data samples, $\{R_{it} : t = 1, \ldots, T\}$ are samples of R_i, and $R_t(x) = \sum_{i=1}^{n} x_i R_{it}$. Note that in general $S_{ijB}(x)$ depends on the vector x. The benchmark parameter B specifies the level of *risk aversion*. A larger value of B reflects a higher level of risk aversion (or, correspondingly, a lower level of risk tolerance). In the context of wireless networks, we suggest that with the emergence of network slicing architectures (e.g., in 3GPP Release 15 and 16), users can subscribe to "slices of the network" for different user-specified benchmarks. In such scenarios, higher values of B might require a prime subscription and probably users would be charged more because service providers would spend more to provide the required (higher) data rates.

4.3.2 Formulation of the multi-RAT connectivity problem as semivariance optimization

We seek to maximize the total downlink throughput—aggregated from all available RATs—and minimize the risk in the form of total throughput semivariance. As a first step, we express this problem in a form that is identical to the portfolio-selection problem:

$$
\begin{aligned}
f^*(x) &= \max_{x_1, \ldots, x_n} \left[\bar{R}(x) - \Sigma^2_{pB}(x) \right] \\
&= \max_{x_1, \ldots, x_n} \left[\sum_{i=1}^{n} x_i m_i - \sum_{i=1}^{n} \sum_{j=1}^{n} x_i x_j S_{ijB}(x) \right], \\
&\quad \text{subject to } \sum_{i=1}^{n} x_i = 1,
\end{aligned}
\tag{4.4}
$$

where $x_i \in \mathbb{R}, i = 1, \ldots, n$, is now the *traffic* allocation decision variable (i.e., the *relative* source-data rate to be allocated to RAT_i), and m_i is the expected throughput over RAT_i. Recall that the Markowitz semicovariance between paths i and j with respect to a benchmark B is denoted by $S_{ijB}(x)$. This is the standard (Markowitz) form of the semivariance-based allocation problem.

While this standard formalism works well for many applications in finance and economics, it does not exactly serve our purpose. Thus, we must deviate from this standard formalism of the problem. For instance, when short sales are allowed in portfolio optimization, the decision variables can have negative values. In our application, we need to impose the non-negativity constraint $x_i \geq 0$ $\forall\ i$ on the decision variables because a negative allocation of source-data rate is not feasible. In addition, we introduce link capacity constraints in terms of the throughput mean and standard deviation. Let σ_i be the standard deviation of the throughput over RAT_i and c_i be the capacity of RAT_i defined as the maximum rate that can be supported by RAT_i while maintaining reliable communication. Specifically, we write our capacity constraint as $x_i(m_i + \delta \cdot \sigma_i) \leq c_i\ \forall\ i$, where $\delta \geq 0$ is a "tuning parameter"; the higher the value of δ, the more conservative the traffic allocation strategy. On the other hand, if we set $\delta = 0$, we have the case of average capacity constraints, which can compromise the QoS because of possible "overallocation" of traffic to a given wireless link. Overallocation comes at the expense of underutilization of possible available capacity from other wireless links involved in the multi-RAT architecture. Our capacity constraints are similar to those imposed in [9] with the exception that we use the standard deviation σ_i instead of variance.

Introducing these constraints, and changing the meaning of some of the variables in the problem, the multi-RAT connectivity problem based on the semivariance risk framework can be written as

$$\begin{aligned} f^*(x) &= \max_{x_1,\ldots,x_n} \left[\bar{R}(x) - \Sigma^2_{pB}(x)\right] \\ &= \max_{x_1,\ldots,x_n} \left[\sum_{i=1}^{n} x_i m_i - \sum_{i=1}^{n}\sum_{j=1}^{n} x_i x_j S_{ijB}(x)\right], \\ &\text{subject to } \sum_{i=1}^{n} x_i = 1, \\ &\qquad 0 \leq x_i \leq \frac{c_i}{m_i + \delta \cdot \sigma_i}, i = 1, \ldots, n, \end{aligned} \tag{4.5}$$

where again x_i is the traffic allocation decision variable, $\bar{R}(x)$ is the mean throughput of the allocation x, $S_{ijB}(x)$ is the semicovariance between the throughputs of RAT i and j, and m_i is the

expected throughput of RAT_i. We assume that $\sum_{i=1}^{n} c_i/(m_i + \delta \cdot \sigma_i) > 1$, which is necessary and sufficient for the existence of a feasible solution to (4.5). The benchmark parameter B in the multi-RAT connectivity problem still reflects risk aversion: A large value of B reflects a high level of risk aversion. Users express their risk-aversion benchmark B in Mbps.

4.3.3 The Markowitz semivariance: Issues and solutions

So far, we have formulated the problem of multi-RAT connectivity as a semivariance-optimization problem. However, we still need to address issues that arise when using semivariance. Note that to find $f^*(x)$, we need to plug the *Markowitz semivariance* $\Sigma^2_{pB}(x)$—defined in (4.3)—into (4.5). The empirical formula in (4.3) has one main disadvantage. The problem is that to compute the semicovariance, one needs to know the time periods in which the portfolio underperforms the benchmark (i.e., those t such that $R_t(x) < B$). This limits the practicality of this empirical calculation; it has elements that economists call "endogenous" [21]. The term endogenous in this context means the following: The values of the semicovariance depend on the allocation vector x. This makes the Markowitz semivariance difficult to calculate and even more difficult to optimize.

4.3.4 Portfolio-semivariance approximations

To overcome the issues mentioned above, many solutions have been proposed, with varying levels of complexity and applicability [21]. Many researchers have introduced solutions to these problems from different points of view. For example, the work in [20] presents a method to approximate the semicovariance $S_{ijB}(x)$ between asset returns R_i and R_j. This approximation $\Sigma^{\text{asym}}_{ijB} \approx S_{ijB}(x)$ is given by

$$\Sigma^{\text{asym}}_{ijB} = E[(R_i - B) \cdot \min(R_j - B, 0)]. \tag{4.6}$$

We use the superscript *asym* in equation (4.6) to indicate that this definition of the semicovariance is asymmetric: In general, $\Sigma^{\text{asym}}_{ijB} \neq \Sigma^{\text{asym}}_{jiB}$. This can be disadvantageous: It is not clear how assets i and j contribute to the risk of the portfolio. Another disadvantage of the definition of $\Sigma^{\text{asym}}_{ijB}$ in [20]

is that it was limited to the case where $B = R_f$, and R_f is the risk-free rate (the return of a risk-free asset, such as U.S. treasury bills). In this case, the approach does not account for individual investor's perception of risk [21]. The work in [69] suggests a non-parametric approach to calculate and optimize the semivariance. The work in [70] proposes a definition of the semivariance that lends the problem of mean-semivariance optimization to parametric quadratic programming. However, [70] limits the benchmark to the mean. Thus, this approach does not express individual investors' preferences regarding the measure of risk.

To cope with the problems mentioned above, Estrada [21] suggests yet another approximation to the semicovariance. Denoting this approximation by $\Sigma^{\text{sym}}_{ijB} \approx S_{ijB}(x)$, it is defined by

$$\begin{aligned} \Sigma^{\text{sym}}_{ijB} &= E[\min(R_i - B, 0) \cdot \min(R_j - B, 0)] \\ &\approx \frac{1}{T} \sum_{t=1}^{T} [\min(R_{it} - B, 0) \cdot \min(R_{jt} - B, 0)]. \end{aligned} \tag{4.7}$$

The approximation of the semicovariance $\Sigma^{\text{sym}}_{ijB}$ in (4.7) is symmetric and *exogenous*: It does not depend on x. We use the superscript *sym* to signify that this approximation is symmetric. Plugging Σ^{sym}_{ij} into equation (4.2), we get the following approximation of the portfolio semivariance:

$$\hat{\Sigma}^2_{pB}(x) = \sum_{i=1}^{n} \sum_{j=1}^{n} x_i x_j \Sigma^{\text{sym}}_{ijB}. \tag{4.8}$$

The approximation $\hat{\Sigma}^2_{pB}(x)$ in (4.8) using $\Sigma^{\text{sym}}_{ijB}$ overcomes the problems associated with S_{ijB} and $\Sigma^{\text{asym}}_{ijB}$.

4.4 The RAM Algorithm

In this section, we introduce our RAM algorithm. As mentioned above, the benchmark B, introduced by Markowitz [19] and modified by Estrada [21], allows individual investors to express their preferences regarding risk. In our algorithm, the user/application specifies the risk-aversion benchmark B in terms of minimum acceptable throughput, in bps.

Our algorithm works by finding an approximate solution to the multi-RAT connectivity optimization problem. Specifically, we use the semivariance approximation $\hat{\Sigma}^2_{pB}(x)$ in (4.8). Plugging $\hat{\Sigma}^2_{pB}(x)$ from (4.8) into (4.5), we get

$$\begin{aligned}\hat{f}^*(x) &= \max_{x_1,\ldots,x_n} \left[\bar{R}(x) - \hat{\Sigma}^2_{pB}(x)\right] \\ &= \max_{x_1,\ldots,x_n} \left[\sum_{i=1}^{n} x_i m_i - \sum_{i=1}^{n}\sum_{j=1}^{n} x_i x_j \Sigma^{\text{sym}}_{ijB}\right], \\ &\quad \text{subject to } \sum_{i=1}^{n} x_i = 1, \\ &\qquad 0 \le x_i \le \frac{c_i}{m_i + \delta \cdot \sigma_i}, i = 1, i = 1, \ldots, n.\end{aligned} \tag{4.9}$$

Because the constraints in (4.9) are the same as those in (4.5), the assumption that $\sum_{i=1}^{n} c_i/(m_i + \delta \cdot \sigma_i) > 1$ is still needed here: This assumption is necessary and sufficient for the existence of a feasible solution to (3.10). Notice that the problem in (4.9) is the same as in (4.5) with only one change: We replace $S_{ijB}(x)$ with the approximation $\Sigma^{\text{sym}}_{ijB}$, which does not depend on x. In conclusion, our strategy is that by solving the optimization problem in (4.9), we obtain an approximate solution to the original problem in (4.5). In the next section, we show the efficacy of our algorithm through simulation.

4.5 Simulation

We consider the system illustrated in Fig. 4.1. This system model is a representation of multi-RAT connectivity in HetNets and consists of two cellular links, 4G LTE and 5G NR links, plus a WiFi link.

Without loss of generality, we simulate the DL of an FDD-based HetNet; however, our approach is equally applicable to cases involving TDD based networks. The applicability of multi-RAT connectivity in the UL is, in general, subject to strict battery constraints. Hence, the applicability of our scheme to the UL case is also limited by these constraints.

In our simulation, we evaluate the performance of three schemes. The first is a scheme that allocates all traffic to the RAT that has the maximum expected throughput. We refer to this scheme as *maxOne*; it is a baseline to evaluate the improvement in performance when we concurrently employ multiple air interfaces. In maxOne, $x_i = 0$ for all i except for one component in the allocation vector x that has $x_i = 1$:

$$x_i = \begin{cases} 1 & \text{if } m_i = \max(m) \\ 0 & \text{otherwise,} \end{cases} \tag{4.10}$$

where $m = \{m_1, \ldots, m_n\}$, and $\max(m)$ indicates the maximum value of the vector m. If more than one RAT satisfies $m_i = \max(m)$, then maxOne sets $x_i = 1$ for only one of them according to some predefined tie-breaking criterion (but this situation is practically unlikely). The second scheme is a scheme that maximizes throughput. We refer to this scheme as *maxThroughput*. (We implement maxThroughput by setting the quadratic term—i.e., the semivariance approximation—in (4.9) to zero.) The third scheme is our algorithm—the RAM scheme—which accounts for risk in addition to throughput.

In our simulation, we conduct three experiments:

- The first experiment involves 4G LTE and 5G NR RATs only.
- The second experiment involves 4G LTE, 5G NR, and WiFi RATs.
- The third experiment again involves 4G LTE, 5G NR, and WiFi RATs. However, in the third experiment, we examine the performance of the two schemes under improved WiFi throughput relative to the WiFi throughput in the second experiment.

We run each of these three experiments twice. First, we run each experiment for the tuning parameter value $\delta = 1$; then, we repeat for $\delta = 2.5$. In practice, the values of δ can be tuned to match real network conditions and QoS preferences in terms of acceptable bit error rate and/or delay.

For convenience, we refer to the 4G LTE RAT, the 5G NR RAT, and the WiFi RAT as RAT_1, RAT_2, and RAT_3, respectively. We then simulate the throughput of each RAT independently. In the case of the cellular RATs, we calculate the peak throughput achievable under certain values of LTE and NR parameters, following 3GPP throughput calculation procedures for 4G LTE and 5G NR [78], [79]. For the WiFi throughput, we use the peak throughput value of WiFi 4 based on IEEE 802.11n specifications [80], [81] (2.4 GHz band only), as detailed below.

We proceed by calculating these throughput values required in our simulation. As mentioned above, we assume the DL of an FDD-based HetNet. Hence, we follow the 3GPP specifications for DL throughput calculation in 4G LTE and 5G NR based on FDD. A full explanation of these specifications is beyond the scope of this chapter. However, below, we introduce detailed examples of such calculations to illustrate our approach.

4.5.1 Throughput of 4G LTE and 5G NR based on 3GPP specifications

Consider this example of throughput calculation for the case of 4G LTE DL based on FDD (the procedure, formula, and tables used in this example are given by 3GPP release 8 for 4G LTE). To calculate the throughput, we need the formula (4.11), Table 4.1, and Table 4.2. The 3GPP formula for calculating the throughput $R_{4\text{G}}$ (in bps) for this case is given as

$$R_{4\text{G}} = u \cdot \text{TBS}, \tag{4.11}$$

where u is the number of MIMO layers and TBS is the transport block size (transport block is the PHY layer payload).

Typically, operators of cellular networks divide the "span" of channel quality into a number of levels. Each of these levels is assigned a unique channel quality indicator (CQI) that is mapped to a modulation and coding scheme index (I_{MCS}). This mapping however is not standardized. It depends on vendor implementation.

Now to determine the transport block size TBS, we use Table 4.1 and Table 4.2. Table 4.1 shows part of the 3GPP MCS index (I_{MCS}) table for the physical downlink shared channel (PDSCH) for

Table 4.1: Modulation and coding index table for PDSCH for 4G LTE

MCS index I_{MCS}	Modulation order Q_m	TBS index I_{TBS}
0	2	0
1	2	1
⋮	⋮	⋮
27	6	25
28	6	26
29	2	Reserved
30	4	Reserved
31	6	Reserved

Table 4.2: Transport block size for 4G LTE

I_{MCS}	N_{PRB}				
	...	97	98	99	100
0	...	2728	2728	2728	2792
...					
25	...	61664	61664	63776	63776
26	...	7112	71112	73712	75376

4G LTE. First, given a modulation and coding scheme index (I_{MCS}) in Table 4.1, we determine the TBS index (I_{TBS}). Then, given I_{TBS} and the number of physical resource blocks N_{PRB}, we use Table 4.2 to find the TBS. We substitute this value in (4.11) to get the throughput $R_{4\text{G}}$. The TBS values in Table 4.2 are given assuming 25% control and signaling overhead.

If an ICQ value is mapped to $I_{\text{MCS}} = 28$, then using Table 4.1, we get $I_{\text{TBS}} = 26$. If we assume a bandwidth of 20 MHz, then the number of physical resource blocks $N_{\text{PRB}} = \frac{20\text{ MHz}}{180\text{ kHz}} \approx 100$. Using Table 4.2, for $I_{\text{TBS}} = 26$ and $N_{\text{PRB}} = 100$, we get TBS = 75376. If we substitute TBS = 75376 in (4.11), assuming $u = 2$ (2×2 MIMO), we get $R_{4\text{G}} = 150.752$ Mbps. This is the peak throughput for most of the 4G LTE UEs currently on the market, which support up to 64-QAM in the DL. Newer UE device categories are expected to support up to 256-QAM in the DL.

Now consider another example of throughput calculation for the case of 5G NR DL based on FDD (the procedure, formula, and tables used in this example are given by 3GPP release 15 for 5G

NR). We first introduce the term "numerology" according to its use in 3GPP documents. Referring to Table 4.3, in 3GPP terminology, a numerology μ is a value that determines the subcarrier spacing and the symbol duration, mainly in 5G NR. In 5G NR there are five values that μ can take. In 4G LTE however, there is only one numerology that corresponds to a subcarrier spacing of 15 kHz. To calculate the throughput, we need the formula (4.12), Table 4.3, and Table 4.4. The 3GPP formula for calculating the throughput R_{5G} (in bps) for this case is given as

$$R_{5G} = \sum_{i=1}^{K^{CA}} \left[v^i \cdot Q_m^i \cdot f_s(i) \cdot r \cdot \frac{N_{PRB}^{BW(i),\mu} \cdot 12}{T_s^\mu} \cdot (1 - OH^i) \right], \tag{4.12}$$

where K^{CA} is the number of aggregated carriers, v^i is the number of multiple-input–multiple-output (MIMO) layers, Q_m^i is the modulation order, $f_s(i)$ is a scaling factor that depends on UE capabilities, r is the target rate that depends on the type of error correction code, $N_{PRB}^{BW(i),\mu}$ is the number of physical resource blocks for given bandwidth $BW(i)$ and numerology μ, T_s^μ is the OFDM symbol duration for the given numerology μ, and OH is the fraction of control and signaling overhead. The values of OH in 5G NR specifications for the DL are 0.14 and 0.18 for frequency range 450–600 MHz (a.k.a FR1), and frequency range 24250–52600 (a.k.a FR2), respectively.

Table 4.3: 5G NR numerology

Numerology μ	Subcarrier spacing $\Delta f = 2^\mu \cdot 15$ [kHz]	Symbol duration $T_s^\mu = \frac{1000}{14.2^\mu}$ [μs]
0	15	71.43
1	30	35.71
2	60	17.86
3	120	8.93
4	240	4.46

As in the case of 4G LTE, operators of cellular networks divide the "span" of channel quality into a number of levels. Each of these levels has a unique CQI. This unique CQI value is mapped

to a modulation and coding scheme index (I_{MCS}). Again, this mapping is not standardized. It depends on vendor implementation.

Table 4.4 shows part of the 3GPP MCS index (I_{MCS}) table for the PDSCH. Note that there are multiple possible tables in the 3GPP specifications depending on the highest modulation order configuration. Table 4.4 shows the case when this configurations is 256-QAM. The coding type used in 5G NR is low density parity check (LDPC) codes. The maximum coding rate of LDPC in 5G NR is $r = \frac{k_{\max}}{1024} = \frac{948}{1024} = 0.9258$. As shown in Table 4.4, in this configuration, there are 28 I_{MCS} values, $0 \leq I_{\text{MCS}} \leq 27$. The values $28 \leq I_{\text{MCS}} \leq 31$ are reserved for other purposes. Now using unreserved values from the range $0 \leq I_{\text{MCS}} \leq 27$, we determine the modulation order Q_m^i and coding rate r. Then, we calculate throughput using (4.12).

Table 4.4: Modulation and coding index table for PDSCH for 5G NR

MCS index I_{MCS}	Modulation order Q_m	Target code rate $r \times [1024]$ k
0	2	120
1	2	193
⋮	⋮	⋮
18	4	822
19	6	873
⋮	⋮	⋮
26	8	916.5
27	8	948
28	2	Reserved
29	4	Reserved
30	6	Reserved
31	8	Reserved

For more details, the reader is referred to 3GPP releases 8–14—specification series 36 for 4G LTE, and 3GPP release 15 and beyond—specification series 38 for 5G NR. We follow 4G LTE and 5G NR procedures to calculate the theoretical throughput values assuming the availability of channel state information (CSI).

To simulate 4G LTE and 5G NR throughput measurements, we generate two time series using these throughput values, together with probability distributions as detailed below. A summary of the simulation parameters for 4G LTE (RAT_1) and 5G NR (RAT_2) is given in Table 4.5.

Table 4.5: Simulation Parameters

Parameter	Value
Number of aggregated carriers	1 (no carrier aggregation)
Numerology μ	0
Duplex mode	FDD
4G and 5G bandwidth	20 MHz
WiFi bandwidth	40 MHz
Subcarrier spacing Δf	15 kHz
Resource block bandwidth	$12 \cdot 15 = 180$ kHz
Number of MIMO layers v[1]	2 spatial streams (2×2 MIMO)
4G highest modulation order	6 (64-QAM configuration)
5G highest modulation order	8 (256-QAM configuration)
$N_{\text{PRB}}^{\text{BW}(1)}$	$\frac{20 \text{ MHz}}{180 \text{ kHz}} \approx 100$
Symbol duration T_s^{μ}	$71.43\mu s$
4G overhead	0.25
5G overhead OH[1]	0.14 (band 450–600 MHz)
Scaling factor $f_s(i)$	1
Tuning parameter δ	$\delta = 1$, $\delta = 2.5$
4G capacity c_1 in Mbps	150.752 (peak rate at 64-QAM)
5G capacity c_2 in Mbps	226 (peak rate at 256-QAM)
WiFi 4 capacity c_3 in Mbps	300 ((peak rate at 64-QAM))

Now, to simulate the throughput over the two cellular RATs—4G LTE and 5G NR—we model the throughput in our simulation by two truncated Gaussian distributions. By truncation, we mean that we apply hard limits to Gaussian samples so that our throughput samples lie between certain values. Specifically, in our simulation, we create a set of samples $\{R_{it} : t = 1, \ldots, T\}$ to represent the throughput samples over time across RAT_i at time instants $t = 1, \ldots, T$. Each sample R_{it} for (RAT_i) is generated as follows:

$$R_{it} = \max(R_i^{\text{Lower}}, (\min(R_i^{\text{Upper}}, \bar{R}_{it}))), \quad \bar{R}_{it} \sim \mathcal{N}(\bar{m}_i, \bar{\sigma}_i^2),$$
$$i = 1, \ldots, n, \quad t = 1, \ldots, T, \tag{4.13}$$

where $\bar{R}_{it}$ is the sample from the underlying Gaussian distribution that corresponds to R_{it}, $\bar{m}_i$ and $\bar{\sigma}_i$ are the mean and standard deviation of this underlying Gaussian distribution of the throughput samples across RAT_i, and R_i^{Lower} and R_i^{Upper} are the truncation limits. We set $\bar{\sigma}_i = 30\% \cdot (R_i^{\text{Upper}} - \bar{m}_i)$. We generate 1000 samples of R_{it} ($T = 1000$) for each of RAT_1 (4G LTE) and RAT_2 (5G NR).

For RAT_1, we set the values of mean and truncation limits at $\bar{m}_1 = 100$ Mbps (LTE rate at 16-QAM), $R_1^{\text{Lower}} = 50$ Mbps (LTE rate at QPSK), and $R_1^{\text{Upper}} = 150.752$ Mbps (peak LTE rate at 64-QAM). We set the variance $\bar{\sigma}_1 = 30\% \cdot (R_1^{\text{Upper}} - \bar{m}_1)$.

For RAT_2, we set the values of mean and truncation limits at $\bar{m}_2 = 170$ Mbps (NR rate at 64-QAM), $R_2^{\text{Lower}} = 0$ (e.g., severe interference), and $R_2^{\text{Upper}} = 226$ Mbps (peak NR rate at 256-QAM). We set the variance $\bar{\sigma}_2 = 30\% \cdot (R_2^{\text{Upper}} - \bar{m}_2)$. (All these values are for NR numerology $\mu = 0$.)

4.5.2 Throughput of WiFi 4 based on 802.11n specifications

For the WiFi link, we consider the 802.11n—a.k.a WiFi 4—standard (we only consider the 2.4 GHz band although some versions of WiFi are dual-band and can deliver data over the WiFi 5 GHz band). We consider WiFi 4 because of its ubiquitous coverage compared to the newer WiFi 5 and WiFi 6 at the time of this work.

To simulate the throughput over RAT_3 (WiFi 4, 2.4 GHz band), we first calculate the peak theoretical throughput of WiFi 4. For a channel of 40 MHz, the peak throughput (at 64-QAM, with code rate of $\frac{5}{6}$) is 150 Mbps for one spatial stream. If we assume 2×2 MIMO, then the peak throughput is 300 Mbps for the WiFi AP.

As in the case of the cellular throughput values, the throughput of 300 Mbps is a theoretical peak that is subject to the assumptions here. In practice, however, the throughput drops because of many factors, such as the number of users and/or applications sharing the same WiFi AP, interfer-

ence from poorly shielded microwave ovens or neighboring WiFi APs, denial-of-service attacks, etc. We capture such time-varying throughput as described next.

To simulate the throughput over the WiFi link, we generate a set of samples $\{R_{it} : t = 1, \ldots, T\}$ to represent the throughput samples over time across RAT_3 at time instants $t = 1, \ldots, T$. We generate 1000 samples of R_{it} ($T = 1000$). Each sample R_{it} for RAT_3) is generated as follows:

$$R_{it} = \begin{cases} R_{\text{High}}, & 1 \leq t \leq 600 \\ R_{\text{Low}}, & 601 \leq t \leq 1000, \end{cases} \tag{4.14}$$

where R_{High} and R_{Low} are two throughput values such that $R_{\text{High}} > R_{\text{Low}}$. We create two scenarios using (4.14). In the first scenario, we set $R_{\text{High}} = 300$ and $R_{\text{Low}} = 30$. In the second scenario, we keep $R_{\text{High}} = 300$ and set $R_{\text{Low}} = 60$.

4.5.3 Performance metric: The risk-adjusted throughput

As mentioned earlier, the performance in this chapter is measured in terms of the *risk-adjusted throughput* versus benchmark values in Mbps. The definition of our metric given by (4.15) below is based on the *risk-adjusted return* and *risk-adjusted throughput* introduced in [71], [72], [9], and [21] (as discussed earlier in Section 2.1), in addition to the subsequent definitions and explanations introduced throughout this chapter. We define our risk-adjusted throughput $R'(x)$ as follows:

$$R'(x) = \frac{\bar{R}(x)}{\Sigma_{pB}(x)} \approx \frac{\frac{1}{T}\sum_{t=1}^{T} R_t(x)}{\sqrt{\Sigma_{pB}^2(x)}}, \tag{4.15}$$

where $\bar{R}(x)$ is the mean throughput (as defined earlier in Section 3.4), $R_t(x), t = 1, \ldots, T$ is the sample of the throughput of the allocation x at time t, and $\Sigma_{pB}(x)$ is the semideviation (square root of the semivariance as shown in (4.15)). Note that we use $\Sigma_{pB}^2(x)$, which is the Markowitz semivariance in (4.2), because we want to measure the Markowitz risk exactly and not through an approximation of the semivariance.

4.5.4 Simulation results

Having explained our simulation setup and defined the performance metric, we now discuss our three experiments. Our simulation results are shown in Figs. 4.2–4.4. These figures show the performance of our algorithm (RAM), the maxOne scheme, and the maxThroughput algorithm.

Fig. 4.2 (a and b) shows the results of the first experiment. Here, we consider the DL of the system with cellular RATs only, i.e., RAT_1 (4G LTE) and RAT_2 (5G NR).

In Fig. 4.2a we introduce the results for the tuning parameter value $\delta = 1$. We can see in this figure that the RAM algorithm outperforms the maxOne and the maxThroughput algorithms in the range of the benchmark between 100 to 150 Mbps. As expected, we see a decline in the risk-adjusted throughput as the value of the benchmark increases, e.g., above 150 Mbps. We also notice that there is no significant difference in performance between maxOne and maxThroughput. This is because we set $\delta = 1$, which leads to relatively large upper bounds on the allocation variables (see the capacity constraints in (4.9)); hence, the allocation vector of maxThroughput is almost the same as that of the maxOne.

On the other hand, as the benchmark value is decreased, the risk becomes smaller. As a result, the risk-adjusted throughput increases accordingly. We can see from the figure that at some point, the performance of the RAM algorithm and the maxThroughput (and the maxOne according to our discussion above) becomes almost identical. This is because as risk decreases, its effect becomes negligible; hence, decision making (choice of decision variables in the allocation vector x) becomes dominated by throughput maximization.

In addition, we notice that at the benchmark value of 98 Mbps, there is a non-smooth change in the risk-adjusted throughput. This is because the number of active constraints in (4.9) changes at 98 Mbps. For the same reason, we can see non-smooth variations of the risk-adjusted throughput at 98 Mbps given in the second and third experiments below for the case of $\delta = 1$.

In Fig. 4.2b we now introduce the results of the first experiment for the tuning parameter value of $\delta = 2.5$. We can see in this figure that the RAM algorithm outperforms the maxOne and the maxThroughput algorithms in the range of the benchmark between 100 to 150 Mbps. As before,

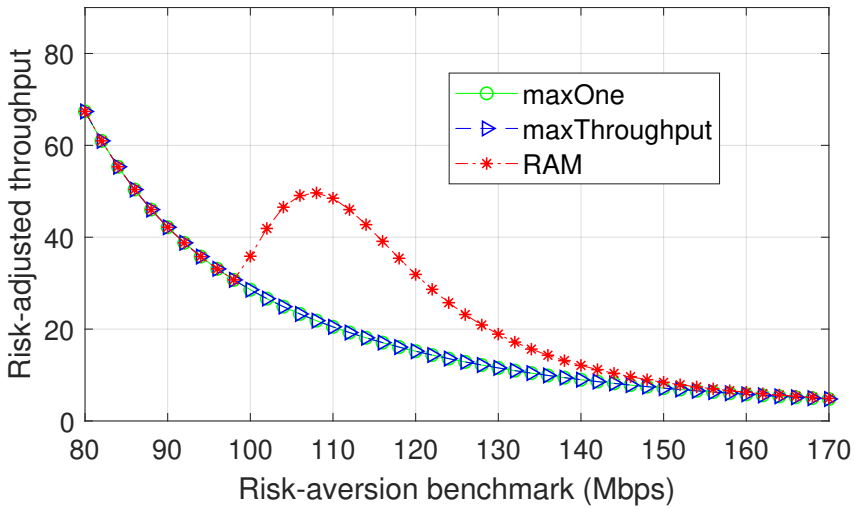

(a)

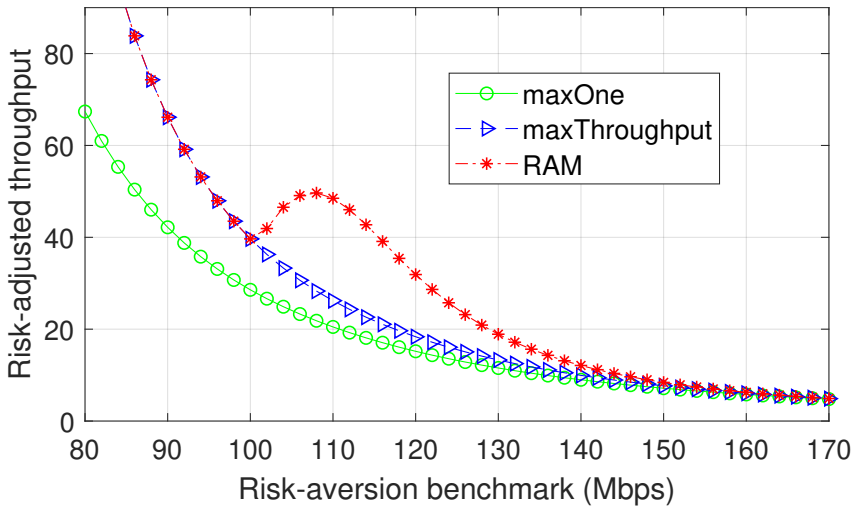

(b)

Figure 4.2: Risk-adjusted throughput for 4G LTE and 5G NR multi-RAT connectivity for two different values of the tuning parameter δ: (a) $\delta = 1$, (b) $\delta = 2.5$.

we see a decline in the risk-adjusted throughput as the value of the benchmark increases, e.g., above 150 Mbps. Now, if we compare the results of this case, i.e, for $\delta = 2.5$ with that for $\delta = 1$ at given values of the benchmark, we notice that there is a significant improvement in the performance of our algorithm and maxThroughput compared to the maxOne scheme, which does not benefit from the available capacity from the other RATs. This improvement relative to the case of $\delta = 1$ is because when we set $\delta = 2.5$, the upper bounds on the allocation variables become smaller; hence, this limits the possibility of traffic overallocation to specific wireless link(s) and the corresponding underutilization of the potential capacity available from other RAT(s). Just like in Fig. 4.2a, when the benchmark value is decreased in Fig. 4.2b, the risk becomes smaller. As a result, the risk-adjusted throughput increases accordingly. We can see from the figure that at the benchmark of 100 Mbps, the performance of the RAM algorithm and the maxThroughput algorithm becomes almost identical; however, now we notice significant improvements in the performance of RAM and maxThroughput relative to the maxOne scheme because of the change in δ that leads to better exploitation of the link capacities in this scenario.

In Fig. 4.2b we also notice that there is a non-smooth change in the risk-adjusted throughput. However, this non-smooth change here happens at 100 Mbps. This is because there is a change in the number of active constraints in (4.9) now at 100 Mbps. For the same reason, we can see non-smooth variations of the risk-adjusted throughput at 100 Mbps in the second and third experiments below for the case of $\delta = 2.5$.

Referring to Fig. 4.3 (a and b), we now discuss the results of the second experiment. In this experiment, we consider three RATs, namely, 4G LTE, 5G NR, and WiFi. We use the same throughput values for 4G LTE and 5G NR as in the first experiment. For the WiFi link, we use throughput values of $R_{\text{High}} = 300$ and $R_{\text{Low}} = 30$ Mbps. We can see from both Fig. 4.3a and Fig. 4.3b that the performance of the RAM algorithm improves with respect to the first experiment. At the same time, we can see that the performance of the maxThroughput drastically (and perhaps surprisingly) worsens. It might be less surprising that the performance of maxOne declines despite having more RATs to choose from.

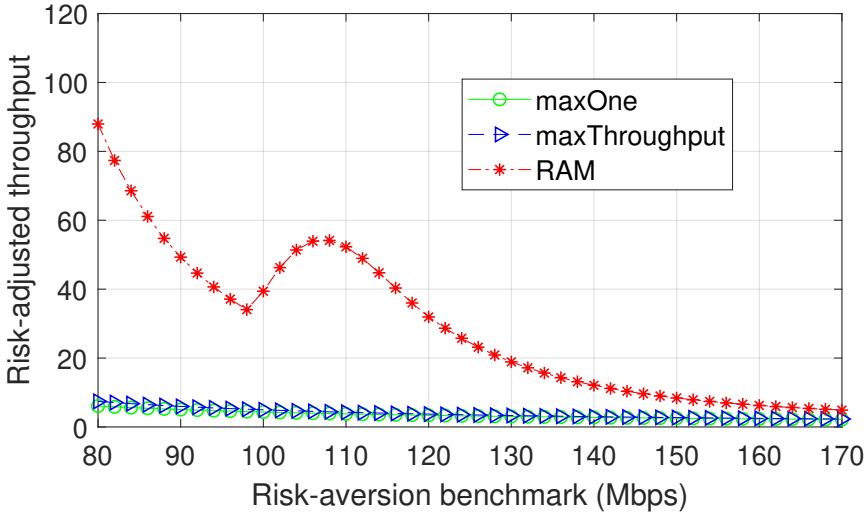

(a)

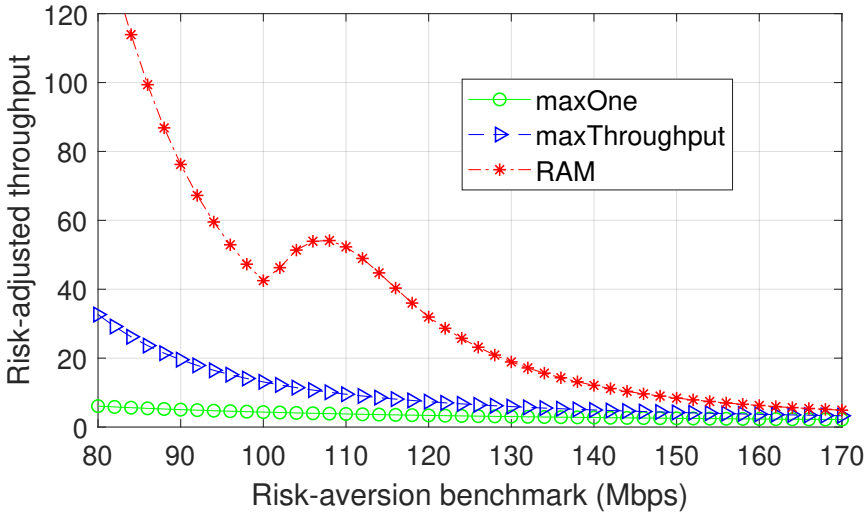

(b)

Figure 4.3: Risk-adjusted throughput for 4G LTE, 5G NR, and WiFi 2.4 GHz multi-RAT connectivity. The minimum WiFi throughput in this scenario is fixed at 30 Mbps. We show our results for two different values of the tuning parameter δ: (a) $\delta = 1$, (b) $\delta = 2.5$.

Although it might be more expected to witness performance improvement with increased resources, this is not always the case. Recall that maxThroughput allocates source data based on maximizing expected throughput, without regard to risk. Hence, even with the availability of additional communication resources in the form of the WiFi link, the allocation is suboptimal in the sense of risk-adjusted throughput. The additional WiFi link provides high expected throughput, but at high risk with respect to the benchmark values (recall that we use $R_{\text{High}} = 300$ and $R_{\text{Low}} = 30$ Mbps in this experiment). The performance of the maxOne scheme declines because now maxOne connects through the WiFi link, which provides the highest mean throughput but at a much higher risk, as mentioned above.

In the third experiment, we also consider three RATs similar to the case in the second experiment. However, here we set $R_{\text{Low}} = 60$ Mbps. We can see from Fig. 4.4 (a and b) that the performance of the RAM algorithm improves. This improvement is more obvious in the range of the benchmark between 98 to 130 Mbps in Fig. 4.4a, and 100 to 130 Mbps in Fig. 4.4b. We can also see an improvement in the performance of maxThroughput. This is because the additional communication resources, the WiFi link, has higher expected throughput, but also lower risk. As expected, both RAM and maxThroughput perform better than maxOne in this experiment as well.

From these observations, we can see that in all of the three experiments, the RAM algorithm performs better than maxOne and maxThroughput. Another observation is that adding more air interfaces is not a guarantee of performance improvement (e.g., maxOne and maxThroughput in the second experiment). In addition, we notice that the choice of the tuning parameter δ has a significant impact on the performance of the two multi-RAT schemes evaluated in this chapter. Overall, our simulation shows the potential gains of our algorithm in all the considered experiments.

4.6 Conclusion

In this chapetr, we studied the problem of multi-RAT connectivity in HetNets; we considered the problem from a risk perspective. We formulated the problem as a semivariance optimization.

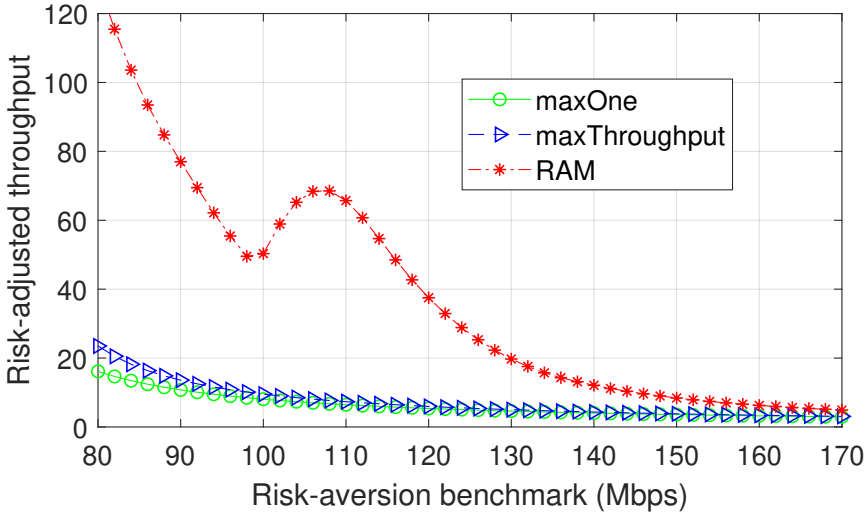

(a)

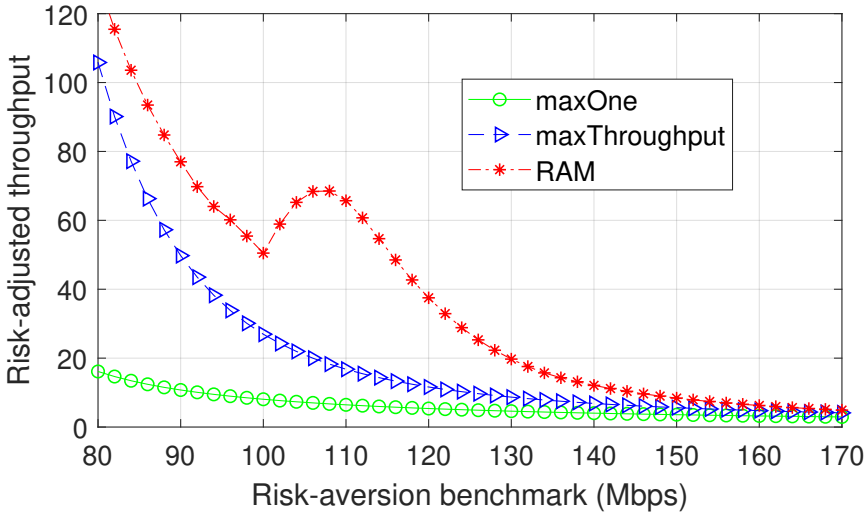

(b)

Figure 4.4: Risk-adjusted throughput for 4G LTE, 5G NR, and WiFi 2.4 GHz multi-RAT connectivity. We evaluate the performance at higher WiFi throughput. The minimum WiFi throughput in this scenario is fixed at 60 Mbps. We show our results for two different values of the tuning parameter δ: (a) $\delta = 1$, (b) $\delta = 2.5$.

Because of the computational issues associated with using the semivariance, we developed a new algorithm based on a semivariance approximation.

Our scheme provides a tool for risk-averse data-source allocation for multi-RAT connectivity in HetNets. We defined a new metric, the risk-adjusted throughput, and evaluated the performance of our algorithm through simulation in a HetNet environment; we considered 4G LTE, 5G NR, and WiFi radio-access technologies. We designed our simulation experiments based on 3GPP specifications for 4G LTE and 5G NR throughput calculations. Simulation results show the effectiveness of our algorithm.

We envision extending our work in many directions. For example, because our algorithm improves throughput by exploiting the inherent transmission diversification in multi-RAT, it can provide an alternative to retransmission schemes and their associated delay. Hence, we plan to investigate the possibility of applying our algorithm for the use case of ultra-reliable-low-latency communication (URLLC), and to evaluate its reliability-delay performance versus that of schemes based on retransmission. Also, in the context of URLLC, we plan to use our approach for delay minimization by minimizing semivariance above a given delay benchmark.

Chapter 5

Conclusion and Future Work

In this dissertation, we considered three resource allocation problems in wireless communication. We formulated problems based on the MDP and semivariance-optimization frameworks, and developed computationally efficient algorithms to solve them.

In Chapter 2, we introduced our design of an MDP-based algorithm for BS control. We designed an algorithm that allows fast adaptation to user location in the network to provide more energy savings, while providing QoS guarantees. For efficient implementation, we employed the rollout algorithm as an approximation method for MDP. The simulation results show the potential of our proposed solution by fostering significant energy savings without sacrificing QoS. An important feature of the suggested solution is scalability (for multi-user multi-ON scenarios). We started by introducing our solution to the smallest version of this problem (one-user one-ON). We presented a systematic and modular algorithm design that allows "plugging in" new models and features. We then scaled up our proposed solution to solve the problem for the multi-user multi-ON scenario.

Possible future extensions to the work in Chapter 2 are to consider information about user destination, and to use our algorithm with maps of real roads and highways. This increases the potential of using the algorithm and allows customizing its design. The performance of the algorithm can also be augmented by the utilization of the available support of location prediction in LTE networks. As there is a growing interest in implanting sensor fusion in 5G networks, we envision the possibility of incorporating sensor fusion in our BS control action selection, with location information coming from different sources. It is possible to borrow some best practices form fleet management in location-based services as well.

In Chapter 3, we considered the problem of RF-jamming mitigation for multipath routing. We formulated the problem as a portfolio-selection problem. We introduced the Markowitz semivariance as a new and appropriate cost function to measure RF-jamming risk. Because the original

Markowitz semivariance has some issues, we adopted an approximation method from economics and finance: This approximation method resolves these semivariance issues. We developed a new jamming-mitigation scheme based on this semivariance approximation. We evaluated the performance of our algorithm by considering multiple scenarios for different user-specified risk aversion and packet rate requirements. The simulation results show the potential gains of using our proposed jamming-mitigation solution. In some cases, the performance of our solution is multiple times that of the benchmarking scheme.

In Chapter 4, we studied the problem of multi-RAT connectivity in HetNets. We considered 4G LTE, 5G NR, and WiFi radio-access technologies and approached the problem from a risk perspective. In this chapter, we also formulated the problem as a semivariance optimization. However, the objective function and the set of constraints we considered here are different from those in Chapter 3. Specifically, the objective function is based on a different standard form of portfolio selection, and the set of constraints includes stochastic constraints that specifically account for the 4G LTE, 5G NR, and the WiFi wireless links. Our scheme provides a tool for risk-averse data-source allocation for multi-RAT connectivity in HetNets. We defined a new metric, the risk-adjusted throughput, which is the ratio between throughput mean and throughput semideviation (where semideviation is the square root of semivariance) and evaluated the performance of our algorithm through simulation in a HetNet environment. We designed our simulation experiments based on 3GPP specifications for 4G LTE and 5G NR throughput calculations. Simulation results show the effectiveness of our algorithm.

We envision extending our work in Chapter 4 in many directions. Because the RAM algorithm improves throughput by exploiting the inherent transmission diversification in multi-RAT, it can provide an alternative to retransmission schemes and their associated delay. Hence, we plan to investigate the possibility of applying our algorithm for the use case of ultra-reliable-low-latency communication (URLLC), and to evaluate its reliability-delay performance versus that of schemes based on retransmission. Also, in the context of URLLC, we plan to investigate the possibility to

apply semivariance optimization to develop a delay "mitigation" scheme by minimizing semivariance *above* a given delay benchmark.

Further extensions of the multi-RAT connectivity are in the field of transportation. More specifically, we suggest applications in the filed of vehicle-to-everything (V2X) communication technology. In the United States and Europe, the current V2X technology relies on the dedicated short-range communications (DSRC) technology, which is based on the 802.11p standard. Recently, 3GPP has released standards for cellular-based V2X (C-V2X) technology. We plan to examine the possible performance improvements by combining the C-V2X and DSRC/IEEE 802.11p technologies into one multi-RAT–V2X system.

In the context of 6G zero-touch networks, we introduce two possible future extensions. The first possible extension is based on the work in Chapter 2, where we formulated an MDP problem and solved it using rollout (recall that rolluot is not a machine learning algorithm and is typically based on domain knowledge). We plan to formulate potential problems based on MDP and exploiting user location/mobility information, and possibly solve them using reinforcement learning (reinforcement learning is used to solve many MDP problems involving mobility). The second possible extension is to use artificial intelligence and machine learning algorithms for traffic classification. Based on the type of traffic, we can automate the choice of the risk-aversion benchmark and use it to yield optimal control.

Overall, in this dissertation, we considered resource allocation problems in terrestrial wireless networks. We envision developing new algorithms for common resource management in future four-tier (satellite-air-terrestrial-underwater) network environments.

Bibliography

[1] Zhengquan Zhang, Yue Xiao, Zheng Ma, Ming Xiao, Zhiguo Ding, Xianfu Lei, George K Karagiannidis, and Pingzhi Fan. 6G wireless networks: Vision, requirements, architecture, and key technologies. *IEEE Vehicular Technology Magazine*, 14(3):28–41, 2019.

[2] Walid Saad, Mehdi Bennis, and Mingzhe Chen. A vision of 6G wireless systems: Applications, trends, technologies, and open research problems. *IEEE network*, 2019.

[3] Jeffrey G Andrews, Stefano Buzzi, Wan Choi, Stephen V Hanly, Angel Lozano, Anthony CK Soong, and Jianzhong Charlie Zhang. What will 5g be? *IEEE J. Sel. Areas Commun.*, 32(6):1065–1082, 2014.

[4] Marc Lichtman, Roger Piqueras Jover, Mina Labib, Raghunandan Rao, Vuk Marojevic, and Jeffrey H Reed. Lte/lte-a jamming, spoofing, and sniffing: threat assessment and mitigation. *IEEE Commun. Mag.*, 54(4):54–61, 2016.

[5] Marc Lichtman, Raghunandan Rao, Vuk Marojevic, Jeffrey Reed, and Roger Piqueras Jover. 5g nr jamming, spoofing, and sniffing: threat assessment and mitigation. pages 1–6. IEEE, 2018.

[6] Hanif Rahbari and Marwan Krunz. Secrecy beyond encryption: obfuscating transmission signatures in wireless communications. *IEEE Commun. Mag.*, 53(12):54–60, 2015.

[7] Opeyemi Osanaiye, Attahiru S Alfa, and Gerhard P Hancke. A statistical approach to detect jamming attacks in wireless sensor networks. Multidisciplinary Digital Publishing Institute, 2018.

[8] Diksha Singhal, Ritu Prasad, and Praneet Saurabh. Secure multipath routing for efficient load balancing and jamming attack protection. In *Soft Computing for Problem Solving*, pages 705–716. Springer, 2020.

[9] Patrick Tague, Sidharth Nabar, James A Ritcey, and Radha Poovendran. Jamming-aware traffic allocation for multiple-path routing using portfolio selection. *IEEE/ACM Transactions on Networking (TON)*, 19(1):184–194, 2011.

[10] Petar Popovski, Čedomir Stefanović, Jimmy J Nielsen, Elisabeth De Carvalho, Marko Angjelichinoski, Kasper F Trillingsgaard, and Alexandru-Sabin Bana. Wireless access in ultra-reliable low-latency communication (urllc). *IEEE Transactions on Communications*, 67(8):5783–5801, 2019.

[11] Khaled B Letaief, Wei Chen, Yuanming Shi, Jun Zhang, and Ying-Jun Angela Zhang. The roadmap to 6G: Ai empowered wireless networks. *IEEE Communications Magazine*, 57(8):84–90, 2019.

[12] Icaro Da Silva, Gunnar Mildh, Johan Rune, Pontus Wallentin, Jari Vikberg, Paul Schliwa-Bertling, and Rui Fan. Tight integration of new 5G air interface and lte to fulfill 5G requirements. In *2015 IEEE 81st Vehicular Technology Conference (VTC Spring)*, pages 1–5. IEEE, 2015.

[13] Zhou Guohua, Deng Tianle, and Yang Li. A dynamic spectrum re-allocation scheme in gsm and lte co-existed networks. In *2014 International Symposium on Wireless Personal Multimedia Communications (WPMC)*, pages 595–600. IEEE, 2014.

[14] Shiying Han, Ying-Chang Liang, and Boon-Hee Soong. Joint resource allocation in ofdma/cdma spectrum refarming system. *IEEE Wireless Communications Letters*, 3(5):469–472, 2014.

[15] Edwin K P Chong, Christopher M Kreucher, and Alfred O Hero. Partially observable markov decision process approximations for adaptive sensing. *Discrete Event Dynamic Systems*, 19(3):377–422, 2009.

[16] Dimitri Bertsekas. *Dynamic Programming and Optimal Control, Vol. I*. Athena Scientific, 2005.

[17] Dimitri Bertsekas. *Dynamic Programming and Optimal Control, Vol. II*. Athena Scientific, 2014.

[18] H.M. Markowitz. *Portfolio Selection: Efficient Diversification of Investments*. John Wiley & Sons. INC., 1959.

[19] H.M. Markowitz. *Portfolio Selection: Efficient Diversification of Investments*. Blackwell Publisher, 1991.

[20] William Hogan and James M Warren. Toward the development of an equilibrium capital-market model based on semivariance. *Journal of Financial and Quantitative Analysis*, 9(1):1–11, 1974.

[21] Javier Estrada. Mean-semivariance optimization: A heuristic approach. 2015.

[22] JQ James and Victor OK Li. Base station switching problem for green cellular networks with social spider algorithm. In *Proc. IEEE Cong. on Evolutionary Computation (CEC), Beijing, China, Jul. 2014*, pages 2338–2344.

[23] Wei-Te Wong, Ya-Ju Yu, and Ai-Chun Pang. Decentralized energy-efficient base station operation for green cellular networks. In *Proc. IEEE GLOBECOM*, pages 5194–5200, 2012.

[24] Tamer Beitelmal and Halim Yanikomeroglu. A set cover based algorithm for cell switch-off with different cell sorting criteria. In *Proc. IEEE ICC, Jun. 2014*, pages 641–646.

[25] Kyuho Son, Hongseok Kim, Yung Yi, and Bhaskar Krishnamachari. Base station operation and user association mechanisms for energy-delay tradeoffs in green cellular networks. *IEEE J. Sel. Areas Commun.*, 29(8):1525–1536, 2011.

[26] Jianchao Zheng, Yueming Cai, Xianfu Chen, Rongpeng Li, and Honggang Zhang. Optimal base station sleeping in green cellular networks: A distributed cooperative framework based on game theory. *IEEE Trans. Wireless Commun.*, 14(8):4391–4406, 2015.

[27] Stefan Videv, John S Thompson, and Harald Haas. Exploiting user movement patterns to enhance energy efficiency in wireless networks. In *Symp. Personal Indoor and Mobile Radio Communications (PIMRC), IEEE 24th*, pages 2596–2600, 2013.

[28] Gong Jie, Zhou Sheng, and Niu Zhisheng. A dynamic programming approach for base station sleeping in cellular networks. *IEICE Transactions on Communications*, 95(2):551–562, 2012.

[29] Jian Wu, Sheng Zhou, and Zhisheng Niu. Traffic-aware base station sleeping control and power matching for energy-delay tradeoffs in green cellular networks. *IEEE Trans. Wireless Commun.*, 12(8):4196–4209, 2013.

[30] Nuo Yu, Yuting Miao, Lan Mu, Hongwei Du, Hejiao Huang, and Xiaohua Jia. Minimizing energy cost by dynamic switching on/off base stations in cellular networks. *IEEE Trans. Wireless Commun.*, 15(11):7457–7469, 2016.

[31] Hatem Abou-Zeid and Hossam S Hassanein. Predictive green wireless access: Exploiting mobility and application information. *IEEE Wireless Commun.*, 20(5):92–99, 2013.

[32] R.S. Campos. Evolution of positioning techniques in cellular networks, from 2g to 4g. *Wireless Communications and Mobile Computing*, 2017, 2017.

[33] Robert Margolies, Richard Becker, Simon Byers, Supratim Deb, Rittwik Jana, Simon Urbanek, and Chris Volinsky. Can you find me now? evaluation of network-based localization in a 4g lte network. In *INFOCOM 2017-IEEE Conference on Computer Communications, IEEE*, pages 1–9. IEEE, 2017.

[34] Anthony D Wood, John A Stankovic, and Gang Zhou. Deejam: Defeating energy-efficient jamming in ieee 802.15. 4-based wireless networks. In *Proc. IEEE SECON*, pages 60–69. IEEE, 2007.

[35] Abid Hussain and Nazar Abbas Saqib. Protocol aware shot-noise based radio frequency jamming method in 802.11 networks. In *Proc. IEEE WOCN*, pages 1–6. IEEE, 2011.

[36] Marc Lichtman, Thaddeus Czauski, Sean Ha, Paul David, and Jeffrey H Reed. Detection and mitigation of uplink control channel jamming in lte. In *Proc. IEEE MILCOM*, pages 1187–1194. IEEE, 2014.

[37] Jerry T Chiang and Y-C Hu. Dynamic jamming mitigation for wireless broadcast networks. In *Proc./ IEEE INFOCOM*, pages 1211–1219. IEEE, 2008.

[38] Kui Wu and Janelle Harms. On-demand multipath routing for mobile ad hoc networks. In *Proc. EPMCC*, pages 1–7, 2001.

[39] Kui Wu and Janelle Harms. Performance study of a multipath routing method for wireless mobile ad hoc networks. pages 99–107. IEEE, 2001.

[40] Hossen A Mustafa, Xin Zhang, Zhenhua Liu, Wenyuan Xu, and Adrian Perrig. Short paper: Jamming-resilient multipath routing leveraging availability-based correlation. In *Proc. ACM Conf. WiSec*, pages 41–46. ACM, 2011.

[41] Hossen Mustafa, Xin Zhang, Zhenhua Liu, Wenyuan Xu, and Adrian Perrig. Jamming-resilient multipath routing. *IEEE Trans. Depend. Secure Comput.*, 9(6):852–864, 2012.

[42] Xin Zhang and Adrian Perrig. Correlation-resilient path selection in multi-path routing. In *Proc./ IEEE Globecom*, pages 1–6. IEEE, 2010.

[43] Manfred Gilli, Evis Këllezi, and Hilda Hysi. A data-driven optimization heuristic for downside risk minimization. *Swiss Finance Institute Research Paper*, (06-2), 2006.

[44] Sergey Andreev, Mikhail Gerasimenko, Olga Galinina, Yevgeni Koucheryavy, Nageen Himayat, Shu-Ping Yeh, and Shilpa Talwar. Intelligent access network selection in converged multi-radio heterogeneous networks. *IEEE wireless communications*, 21(6):86–96, 2014.

[45] Subramanya Chandrashekar, Andreas Maeder, Cinzia Sartori, Thomas Höhne, Benny Vejlgaard, and Devaki Chandramouli. 5G multi-rat multi-connectivity architecture. In *2016 IEEE International Conference on Communications Workshops (ICC)*, pages 180–186. IEEE, 2016.

[46] Kok-Kiong Yap, Te-Yuan Huang, Yiannis Yiakoumis, Sandeep Chinchali, Nick McKeown, and Sachin Katti. Scheduling packets over multiple interfaces while respecting user preferences. In *Proc. 9th CoNEXT*, pages 109–120. ACM, 2013.

[47] Sarabjot Singh, Shu-ping Yeh, Nageen Himayat, and Shilpa Talwar. Optimal traffic aggregation in multi-rat heterogeneous wireless networks. In *2016 IEEE International Conference on Communications Workshops (ICC)*, pages 626–631. IEEE, 2016.

[48] Kande Archana, Linugtla Laxmi, and A Govardhan. Maximizing efficiency of multiple–path source routing in presence of jammer. *IOSR–JCE*, 11(3):10–16, 2013.

[49] C.-L. I, Corbett Rowell, Shuangfeng Han, Zhikun Xu, Gang Li, and Zhengang Pan. Toward green and soft: A 5G perspective. *IEEE Commun. Mag.*, 52(2):66–73, 2014.

[50] H. Zhang J. Wu, S. Rangan. *Green Communications: Theoretical Fundamentals, Algorithms and Applications*. CRC Press, 2012.

[51] F. Richter, A. J. Fehske, and G. P. Fettweis. Energy efficiency aspects of base station deployment strategies for cellular networks. In *Proc. IEEE 70th Veh. Technol. Conf. Fall (VTC-Fall), Sep. 2009*, pages 1–5.

[52] Albrecht Fehske, Gerhard Fettweis, Jens Malmodin, and Gergely Biczok. The global footprint of mobile communications: The ecological and economic perspective. *IEEE Commun. Mag.*, 49(8), 2011.

[53] Sheng Zhou, Jie Gong, Zexi Yang, Zhisheng Niu, and Peng Yang. Green mobile access network with dynamic base station energy saving. In *Proc. ACM MobiCom*, volume 9, pages 10–12, 2009.

[54] Gunther Auer et al. How much energy is needed to run a wireless network? *IEEE Wireless Communications*, 18(5), 2011.

[55] Eunsung Oh and Bhaskar Krishnamachari. Energy savings through dynamic base station switching in cellular wireless access networks. In *Proc. IEEE GLOBECOM*, pages 1–5, 2010.

[56] Eunsung Oh, Kyuho Son, and Bhaskar Krishnamachari. Dynamic base station switching-on/off strategies for green cellular networks. *IEEE Trans. Wireless Commun.*, 12(5):2126–2136, 2013.

[57] Chaoming Song, Zehui Qu, Nicholas Blumm, and Albert-László Barabási. Limits of predictability in human mobility. *Science*, 327(5968):1018–1021, 2010.

[58] Lan Zhang, Gang Feng, Shuang Qin, Wei Jiang, and Yao Sun. Energy efficient sleep strategy for decoupled uplink/downlink access in hetnets. In *WCNC*, pages 1–6. IEEE, 2017.

[59] L. Zhang, F. Gang, S. Qin, and W. Nie. A comparison study of coupled and decoupled uplink-downlink access in heterogeneous cellular networks. In *Proc. IEEE Global Commun. Conf.*, pages 1–7. IEEE, 2015.

[60] Ying He and Edwin K P Chong. Sensor scheduling for target tracking: A monte carlo sampling approach. *Digital Signal Processing*, 16(5):533–545, 2006.

[61] Dimitri P Bertsekas and David A Castanon. Rollout algorithms for stochastic scheduling problems. *J. Heuristics*, 5(1):89–108, 1999.

[62] T. Han, Z. Zhang, M. Hu, G. Mao, X. Ge, Q. Li, and L. Wang. Energy efficiency of cooperative base station sleep scheduling for vehicular networks. In *IEEE 79th VTC Spring*, pages 1–5. IEEE, 2014.

[63] Theodore S Rappaport et al. *Wireless communications: principles and practice*, volume 2. prentice hall PTR New Jersey, 1996.

[64] Abid Hussain, Nazar A Saqib, Usman Qamar, Muhammad Zia, and Hassan Mahmood. Protocol-aware radio frequency jamming in wi-fi and commercial wireless networks. *J. Commun. Netw.*, 16(4):397–406, 2014.

[65] R. M. Rao, Sean, V. Marojevic, and Jeffrey H Reed. Lte phy layer vulnerability analysis and testing using open-source sdr tools. In *Proc. IEEE MILCOM*, pages 744–749. IEEE, 2017.

[66] Roger Piqueras Jover, Joshua Lackey, and Arvind Raghavan. Enhancing the security of lte networks against jamming attacks. *EURASIP Journal on Information Security*, 2014(1):7, 2014.

[67] Ghada Alnifie and Robert Simon. A multi-channel defense against jamming attacks in wireless sensor networks. In *Proceedings of the 3rd ACM workshop on QoS and security for wireless and mobile networks*, pages 95–104. ACM, 2007.

[68] Stephen Mueller, Rose P Tsang, and Dipak Ghosal. Multipath routing in mobile ad hoc networks: Issues and challenges. In *International Workshop on Modeling, Analysis, and Simulation of Computer and Telecommunication Systems*, pages 209–234. Springer, 2003.

[69] Gustavo M de Athayde. Building a mean-downside risk portfolio frontier. In *Managing downside risk in financial markets*, pages 194–211. Elsevier, 2001.

[70] Enrique Ballestero. Mean-semivariance efficient frontier: A downside risk model for portfolio selection. *Applied Mathematical Finance*, 12(1):1–15, 2005.

[71] John B Caouette, Jack B Caouette, Edward I Altman, and Paul Narayanan. *Managing credit risk: the next great financial challenge*, volume 2. John Wiley & Sons, 1998.

[72] V. Mohan, J. G. Singh, and W. Ongsakul. Sortino ratio based portfolio optimization considering evs and renewable energy in microgrid power market. *IEEE Transactions on Sustainable Energy*, 8(1):219–229, 2017.

[73] Azad Ravanshid, Peter Rost, Diomidis S Michalopoulos, Vinh V Phan, Hajo Bakker, Danish Aziz, Shreya Tayade, Hans D Schotten, Stan Wong, and Oliver Holland. Multi-connectivity functional architectures in 5G. In *2016 IEEE international conference on communications workshops (ICC)*, pages 187–192. IEEE, 2016.

[74] Apostolus Galanopoulos, Fotis Foukalas, and Apostolos Xenakis. Multi-rat spectrum reallocation including carrier aggregation for 5G networks. In *Proceedings of the 22nd Pan-Hellenic Conference on Informatics*, pages 22–27. ACM, 2018.

[75] Kok-Kiong Yap, Te-Yuan Huang, Masayoshi Kobayashi, Yiannis Yiakoumis, Nick McKeown, Sachin Katti, and Guru Parulkar. Making use of all the networks around us: a case study in android. *ACM SIGCOMM Computer Communication Review*, 42(4):455–460, 2012.

[76] Fateh Elsherif and E. K. P Chong. Risk-averse mult- RAT connectivity in HetNets. In *2020 IEEE 10th Annual Computing and Communication Workshop and Conference (CCWC)*. Accpeted for publication.

[77] Fateh Elsherif and E. K. P Chong. Wireless jamming-mitigation for multipath routing using semivariance risk measures. *Submitted for publication*, 2019.

[78] 3GPP specification series. Accessed on: Nov. 15, 2019.

[79] 3GPP specification series. Accessed on: Nov. 16, 2019.

[80] 802.11ac wireless throughput testing and validation guide. Accessed on: Nov. 16, 2019.

[81] Eng Hwee Ong, Jarkko Kneckt, Olli Alanen, Zheng Chang, Toni Huovinen, and Timo Nihtila. IEEE 802.11 ac: Enhancements for very high throughput WLANs. In *2011 IEEE 22nd International Symposium on Personal, Indoor and Mobile Radio Communications (PIMRC)*, pages 849–853. IEEE, 2011.

Appendix A

License

Green Communication and Security in Wireless Networks Based on Markov Decision Process and Semivariance Optimization

by Fateh Elsherif – 2019